CORROSION RESISTANCE OF SILVER THIN FILMS ON TITANIUM NITRIDE AND TANTALUM SUBSTRATES

David Turcio-Ortega

B.S. National Autonomous University of Mexico, Mexico, 1995

A thesis presented to the faculty of the

Oregon Graduate Institute of Science and Technology

in partial fulfillment of the requirements for the degree

Masters of Science

in

Materials Science and Engineering

January 2000

This thesis titled "Corrosion Resistance of Silver Thin Films on Titanium Nitride and Tantalum Substrates" by David Turcio-Ortega had been examined and approved by the following Examination Committee:

Dr. Margaret Ziomek-Moroz, Thesis Advisor
Associate Professor

Dr. Donald D. Danielson
Intel Corporation

Dr. David E. Alman
U.S. Department of Energy
Albany Research Center

Dr. Lemmy Meekisho
Associate Professor

Dr. Henrikas Cesiulis
Vilnius University
Physical Chemistry Department

Acknowledgments

I would like to thank my thesis advisor Dr. Margaret Ziomek-Moroz for her academic guidance and all the help that I have received from her. Special thanks to Dr. Donald D. Danielson of Intel Corporation for his help with this thesis and for the time he took to review the manuscript. I am grateful to Dr. David Alman of the U.S. Department of Energy, and Dr. Lemmy Meekisho of the MSE Department at OGI for reviewing the manuscript. I owe a lot to Dr. Henrikas Cesiulis, who has been patient helping me with some electrochemical experiments. This research is supported by the Research Council/National Science Foundation and Intel Corporation. I also would like to express my deep appreciation to the professors and all the students in the Department of Materials Science and Engineering at Oregon Graduate Institute of Science and Technology.

I would like to thank my wife, Lupita, my grandma, my parents and my brothers for their support.

Table of Contents

List of Tables

List of Figures

Abstract

Corrosion Resistance of Silver Thin Films on Titanium Nitride and Tantalum Substrates

David Turcio-Ortega

M.S., Oregon Graduate Institute of Science and Technology

January 2000

Thesis Advisor: Dr. Margaret Ziomek-Moroz

Currently, aluminum and its alloys are the most common materials used for interconnections in both VLSI and ULSI. As the dimensions of devices decrease, the high resistance and poor electromigration of aluminum interconnects become problematic. Based on the electrical and corrosion properties, copper and silver are recognized as potential replacements for aluminum interconnects in these devices. The aim of this thesis is to investigate the corrosion behavior of silver and silver thin film on TiN and Ta substrates using electrochemical methods. The electrochemical methods included potentiodynamic, potentiostatic, and open-circuit measurements. The experiments were performed in hydrochloric acid (HCl), phosphoric acid (H_3PO_4), sulfuric acid (H_2SO_4), a mixture of sulfuric acid and hydrogen peroxide (H_2SO_4 and H_2O_2), sodium borate ($Na_2B_4O_7$), and tetramethylammonium hydroxide ((CH_3)$_4$NOH). TiN and Ta passivate in the investigated solutions. Ag and Ag thin films exhibit active, active-passive, and passive behavior in HCl, H_3PO_4, H_2SO_4, and in the H_2SO_4 + H_2O_2 mixture. The mechanical passivation of Ag occurs in HCl and H_3PO_4. Other materials undergo chemical passivation.

Chapter 1

Introduction

1.1 Application of Silver and Silver Thin Films

As device dimensions continue to shrink and chip speeds increase, transmission delays through interconnects connecting active devices, has become a major contributing factor to the overall delay of any circuit. Silver has potential benefits in electrical and mechanical performance, useful properties in the solution of actual problems in the Semiconductor Industry, for example in ultra-large scale integration (ULSI) [1].

Silver has a room temperature bulk resistivity of 1.59 $\mu\Omega$-cm, compared to 1.67 $\mu\Omega$-cm for copper, 2.65 $\mu\Omega$-cm for aluminum and 5.5 $\mu\Omega$-cm for tungsten [2]. Further, silver has distinct advantage in terms of its low residual stress due to a combination of its modulus and coefficient of thermal expansion [1].

Silver is widely used in contacts that remain closed for long period of time, and as coating connecting plugs and sockets. It is also used in contacts subject to occasional sliding, such as in rotary switches, and to a limited extent for low-resistance sliding contacts such as slip rings. Silver contacts are used instead of copper because it exhibits better oxidation resistance in contact with the air [3].

The electrical and thermal conductivities of silver are the highest of all metals at room temperature, and as a result, silver will carry high currents without excessive

heating. Although good thermal conductivity is desired, once the silver contact is in service, the conductivity increases the difficulty of assembly welding. In contact with materials like phenol fiber and under electrical potentials, silver can migrate through the insulation and degrade its dielectric strength [3].

Silver has been used in different areas, and for different applications:

Photographic materials: conventional photographic emulsions contain face-centered cubic (FCC) silver bromide (AgBr) and silver chloride (AgCl), and may contain up to 10 wt % hexagonal silver iodide (AgI). Their primary sensitivity to light is amplified up to 10^{11} times when the emulsions are developed [4]. Photographic emulsions are prepared by the reaction between silver nitrate and sodium or potassium chloride, in the presence of a colloidal substance which adsorbs on to the crystallite surfaces to prevent their coalescence. Precise control of the crystallite size is achieved by controlling the conditions of precipitation and average sizes is as small as 0.04 µm. One mole of silver bromide will yield 10^{18} crystallites of this size. Such crystals are very insensitive to light although they can resolve extremely fine detail. The speed of the photographic film is achieved by growing the crystals; the growth of the crystals is promoted by having present in the suspending medium a complexing agent for the silver halide. Only light absorbed by the crystallites is utilized in producing a "latent image" . A typical and particularly useful ripening agent is ammonia, which forms the complex $[Ag(NH_3)_2]^+$ [6].

Electronic products: silver paints are of two types: the air drying paints are used on wood, paper, plastics, etc, and those that must be fired are used on ceramics, mica, glass, and other refractory materials. Silver paints are used for producing electrically conducting surfaces on non-conductors, solder bonding to non-conductors and non-metallic surfaces, and decorating porcelain or glass [4].

Batteries: silver batteries include silver oxide-potassium hydroxide-zinc secondary batteries and silver oxide-potassium hydroxide-zinc, and silver chloride-seawater-magnesium primary batteries [4].

Brazing Alloys and Solders: with respect to modern brazing alloys, silver is present in five of the seven copper-phosphorous alloys, all of the seventeen silver-copper alloys, and four of the six silver-copper vacuum-tube alloys [4].

Catalyst: Silver catalyst are used most frequently in oxidation reaction, e.g., the production of formaldehyde from methanol and air by means of silver screens or crystallites, these crystallites contains 99.95 wt % minimal of silver and no zinc or any element of the fifth and sixth groups. A tubular reaction chamber filled with silver is used in the production of ethylene oxide from ethylene and air; also, the production of glyoxal from the oxidation of ethylene glycol in an air-nitrogen mixture over finely dispersed silver or silver oxide or a blend of the two is another example of the use of silver as a catalyst [4].

Mirrors: mirrors are silver-coated by reducing $AgNO_3$ solutions with reducing solutions on glass, that is pretreated with stannous chloride. The reducing solutions include sugar, rochelle salts, or formaldehyde [4].

Dental Amalgam: The comminuted product that is supplied to the dentist is basically the intermetallic epsilon silver-tin phase, which contains 67-70 wt % Ag, 25.3-27.7 wt % Sn, 0-5.2 wt % Cu, and 0-1.2 wt % Zn. The mix between this product and mercury (5:8) produce the dental amalgam. The low expansion of this alloy that occurs when it sets is one of its chief advantages for tooth fillings [5].

Antiseptic: Water stored in silver vessels, or less than 10 ppm $AgNO_3$ in aqueous solution destroys bacteria in the water. Silver nitrate is also used as an antiseptic but it is quite caustic. Colloidal solutions of AgI (Neo-Silvol) and strong-to-mild silver proteins, e.g., Protargol (strong) and Argyrol (mild), are effective and are much less caustic [4].

Jewerly: Silver is widely used to make jewerly. Also, silver wire can be encrusted on the surface of iron, steel, bronze, or brass by the damascene process [6].

1.2 Occurrence, Physical and Chemical Properties of Silver

1.2.1 Occurrence

Silver is widely distributed in inanimate nature and is a major component of a wide range of minerals. It also occurs in smaller quantities in very many base metal ores. Sea-water contains an estimated 0.01 ppm and the overall terrestrial concentration is considered to be ~0.1 ppm. Silver appears to be non-essential to life but is nevertheless found in trace quantities in a wide range of living organisms, e.g. in the liver (0.005 – 0.001 %) of cattle and in Pacific marine organisms. Silver is found native, usually associated with silver ores in the upper portions of the silver-bearing veins. In these environs native silver is of secondary origin, formed chemically in past ages by reduction of a portion of the ore body. The basic processes that have been used in the extraction of silver from its ores are the amalgamation process, the cyanide process, and the flotation process [7].

1.2.2 Physical Properties

Silver is classified as a transition metal in the Copper Group I-B of copper, silver and gold, in increasing order of atomic weight and density, as is showed in Figure 1.1. Table 1.1 lists some of the physical properties of silver.

Table 1.1 Physical properties of silver

Atomic weight	107.87
Atomic number	47
Melting point ($^\circ$C)	960.8
Boiling point ($^\circ$C)	2212
Density (g/cm^3)	10.5
Thermal conductance (cal/sec)(cm^2)(C/cm) 0°C	0.999
Specific heat (cal/g) 25°C	0.056
Latent heat of fusion (cal/g)	25
Heat of vaporization (cal/g)	565
Electronegativity (Pauling's)	1.9
Covalent radius (Å)	1.34
Ionic radius (Å)	1.26
Coefficient of linear thermal expansion (x10^{-6} $^\circ$C)	19.68
Electrical resistivity ($\mu\Omega$-cm) 20°C	1.59
Elastic modulus (psi x 10^6) 30°C	10.6
Tensile strength (psi – annealed)	25.000
Vapor pressure (mm Hg), 735-960 $^\circ$C	$\log P = -1.4580\text{x}10^4/T(^\circ\text{Abs}) + 9.22$
Hardness (Mohs – scratch)	2.5 – 3
Crystal structure (isometric – normal)	(100) cube, fcc
Color (solid)	Silver-white

d transition elements

III A	IV A	V A	VI A	VII A	VIII A			I B	II B
21 2.99 **Sc** 44.956	22 4.51 **Ti** 47.88	23 6.09 **V** 50.942	24 7.19 **Cr** 51.996	25 7.47 **Mn** 54.938	26 7.87 **Fe** 55.847	27 8.8 **Co** 58.933	28 8.91 **Ni** 58.69	29 8.93 **Cu** 63.546	30 7.13 **Zn** 65.39
39 4.48 **Y** 88.906	40 6.51 **Zr** 91.224	41 8.58 **Nb** 92.906	42 10.22 **Mo** 95.94	43 11.50 **Tc** (97.907)	44 12.36 **Ru** 101.07	45 12.42 **Rh** 102.906	46 12.00 **Pd** 106.42	47 10.5 **Ag** 107.87	48 8.65 **Cd** 112.41
57 6.17 **La*** 138.91	72 13.28 **Hf** 178.49	73 16.67 **Ta** 180.95	74 19.25 **W** 183.85	75 21.02 **Re** 186.21	76 22.58 **Os** 190.2	77 22.55 **Ir** 192.22	78 21.44 **Pt** 195.08	79 19.28 **Au** 196.97	80 - **Hg** 200.59
89 **Ac**** (227.03)	104 **Unq** (261.11)	105 **Unp** (262.11)	106 **Unh** (262.12)						

-----Atomic Number
----Density (g/cm^3)
----Element
----Atomic weight (amu)

Figure 1.1 *d* Transition Elements in the Periodic Table

1.2.3 Chemical Properties

As we can see from Table 1.2 (EMF series), silver is more noble than copper, somewhat less noble than palladium and platinum, and less noble than gold [8]. However, silver reacts with sulfur, nitrogen, and halogen compounds, their reactions are shown in Figure 1.2 [9].

Table 1.2 EMF series (From *Handbook of Chemistry and Physics*, 71st ed., CRC press, 1991).

active↑	$Cu^{2+} + 2e^- = Cu$	0.342 V vs. SHE
	$Ag^+ + e^- = Ag$	0.799 V vs. SHE
	$Pd^{2+} + 2e^- = Pd$	0.951 V vs. SHE
noble↓	$Pt^{2+} + 2e^- = Pt$	1.118 V vs. SHE

$$Ag_2S$$

$$\uparrow \quad \begin{array}{c} S \\ heat \end{array}$$

$$K[AgF_4] \qquad\qquad Ag \qquad\qquad AgF$$

$$\uparrow \begin{array}{c} F_2 \text{ and } KF \\ heat \end{array} \qquad \begin{array}{c} \text{450 K} \\ HNO_3 \end{array} \qquad \begin{array}{c} HF \text{ aq} \\ \end{array} \uparrow$$

$$AgX \xleftarrow[\text{(X = Cl, Br, I)}]{X^- \text{ aq}} AgNO_3 \xrightarrow{OH^- \text{ aq}} Ag_2O \xrightarrow[\text{360 K}]{S_2O_8{}^{2-} \text{ aq}} AgO$$

$$\downarrow NH_3 \qquad\qquad\qquad\qquad \downarrow \text{excess of OH}^-$$

$$[Ag(NH_3)_2]X \qquad\qquad\qquad [Ag(OH)_2]^-$$
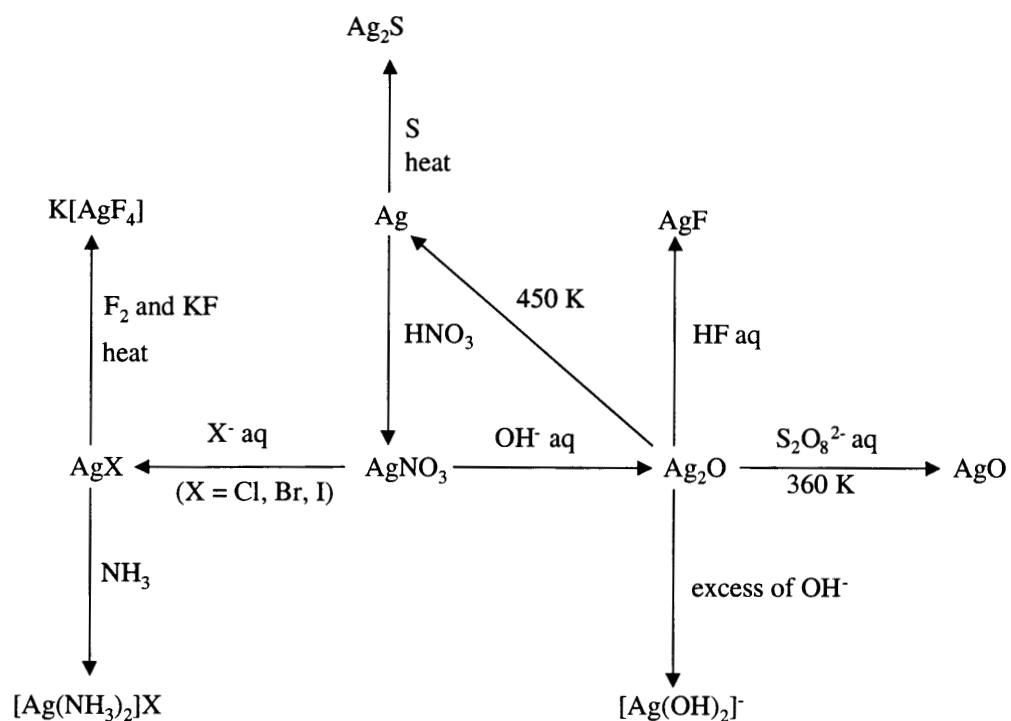
Figure 1.2 Reactions of Silver

Silver is dissolved by alkali metal cyanide solutions as the anode or in the presence of oxygen to form $NaAg(CN)_2$ or $KAg(CN)_2$ [4]:

$$2Ag + 4NaCN \rightarrow 2NaAg(CN)_2 + 2Na^+ + 2e^- \qquad \text{anodic} \qquad (1)$$

$$\tfrac{1}{2}H_2O + \tfrac{1}{2}O_2 + 2e^- \rightarrow 2OH^- \qquad\qquad \text{cathodic} \qquad (2)$$

$$2Ag + 4NaCN + H_2O + \tfrac{1}{2}O_2 \rightarrow 2NaAg(CN)_2 + 2NaOH \qquad (3)$$
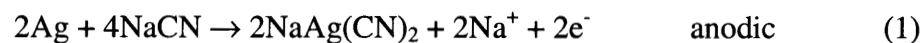
These reactions are of commercial importance in electroplating and have been used to extract silver from its ores.

At elevated temperatures, silver and the halogens react quickly with liberation of heat. Thus, molten silver chloride is prepared for use in batteries by the direct reaction of chlorine gas on silver at above 445° C, when is the melting point of AgCl (batteries and cells).

The reaction of silver with nitric acid is as follows [4]:

$$4Ag + 6HNO_3 \rightarrow 4AgNO_3 + NO + NO_2 + 3H_2O \tag{4}$$
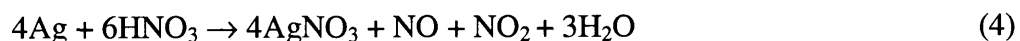
Nitric acid attacks silver at all concentrations, but the reaction usually employs concentrations 50:50 hot, HNO_3:H_2O. The silver nitrate solution produced is the starting material for most other chemical compounds of silver. For the dilute acid the reaction is [5]:

$$3Ag + 4H^+ + NO_3^- \rightarrow 3Ag^+ + NO + 2H_2O \tag{5}$$
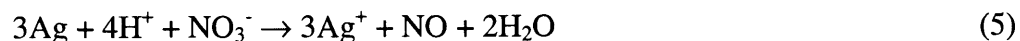
Silver is rapidly darkened (tarnished) by exposure to even low concentrations of hydrogen sulfide in air, owing to the formation of black sulfide Ag_2S. The presence of oxygen is necessary for the sulfide to form [5]:

$$2Ag + H_2S + \tfrac{1}{2}O_2 \rightarrow Ag_2S + H_2O \tag{6}$$

Sulfur dioxide also reacts with silver at elevated temperatures, forming both silver sulfate and silver sulfide [5]:

$$4Ag + 2SO_2 \rightarrow Ag_2SO_4 + Ag_2S \tag{7}$$

In the presence of sufficient oxygen, and at temperatures below 1085° C, only the sulfate is formed [5]:

$$2Ag + SO_2 + O_2 \rightarrow Ag_2SO_4 \tag{8}$$

All of the halogens react with silver forming the corresponding silver halides. The rate of reaction is slow at room temperature but becomes more rapid as the temperature is increased [5]:

$$2Ag + 2HCl + \tfrac{1}{2}O_2 \rightarrow 2AgCl + H_2O \tag{9}$$

Hot concentrated sulfuric acid dissolves silver readily, forming the moderately soluble silver sulfate and evolving sulfur dioxide [5]:

$$2Ag + 2H_2SO_4 \rightarrow Ag_2SO_4 + SO_2 + H_2O \tag{10}$$
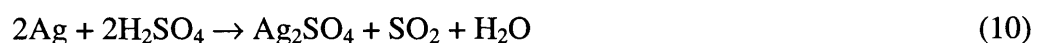
Silver dissolves to a moderate extent in concentrated sodium chloride solution if atmospheric oxygen is available. Silver Chloride is formed [5]:

$$2Ag + 2Cl^- + H_2O + \tfrac{1}{2}O_2 \rightarrow 2AgCl + 2OH^- \tag{11}$$
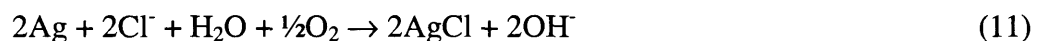
The possibility of oxidation/reduction of the Ag^+/Ag^{2+} couple is possible, even though Ag^{2+} ions are uncommon and unstable. In acidic solution, the process is [10]:

$$Ag^+ + O_3 \rightarrow AgO^+ + O_2 \tag{12}$$
$$AgO^+ + H_2O \rightarrow Ag^{2+} + OH^- + OH^- \tag{13}$$

Once Ag^{2+} is generated, it can react with H_2O_2 by the process [10]:

$$Ag^{2+} + H_2O_2 \rightarrow Ag^+ + H^+ + H_2O^- \tag{14}$$

Hydrogen peroxide is at least present in indoor air, is highly soluble in water, and can reacts with silver surfaces to produce free radical species [10]:

$$Ag(s) + H_2O_2 \rightarrow Ag^+ OH^- + OH^- \tag{15}$$

Silver has the ability to reduce $CuCl_2$ and $HgCl_2$. Iron (III) chloride is similarly reduced by silver to iron (II) chloride. Silver is to some extent soluble in iron (III) sulfate solution owing to a reversible reduction of the Fe^{3+} salt and the coincident formation of silver sulfate [5]:

$$Ag + Fe^{+3} = Ag^+ + Fe^{++} \tag{16}$$

1.3 Corrosion of Silver in Specific Environments

1.3.1 Low pH Solutions, Neutral Solutions, Alkaline Solutions

Low pH solutions

Silver exhibits corrosion resistance to dilute HCl at room temperature, de-aerated HF at low temperature, H_3PO_4 at room temperature, H_2SO_4 at room temperature (reaction 10), and it is also resistant to hot, concentrated organic acids such as acetic, formic, citric, lactic, fumaric, phtalic, and benzoic acids, fatty acids, and phenol. Silver is not resistant to concentrated HCl at high temperature (reaction 9), aerated HF at high temperature, dilute HNO_3 at room temperature (reaction 5), concentrated H_3PO_4 at high temperature, and concentrated H_2SO_4 at high temperature.

Neutral solutions

Silver is corrosion resistant in most non-oxidizing salts and $KMnO_4$ at room temperature. It is not corrosion resistant in oxidizing salts (e.g. $K_2S_2O_8$, $FeCl_3$, $CuCl_2$, and $HgCl_2$) and in complexing salts (e.g. cyanides, polysulphides, thiosulphates, and ammonium salts).

Alkaline solutions

Silver is resistant in LiOH, NaOH, KOH at all concentrations up to boiling point. It is not resistant to NH_4OH due to formation of complexes. Silver is attacked by Na_2S, and NaCN (reaction 1).

1.3.2 Atmospheric Corrosion

Atmospheric corrosion of silver occurs only in the presence of moisture. Silver corrosion increases with increasing relative humidity. The crucial role of the water layer on the metal surface is to provide a medium for the absorption of atmospheric gases and the subsequent dissolution of solid silver. The oxidation step for the dissolution can be expressed as [10]:

$$Ag(s) \rightarrow Ag^+ + e^- \tag{17}$$

This reaction is balanced in acid solution by:

$$O_2 + 4H^+ + 4e^- \rightarrow 2H_2O \tag{18}$$

And:

$$4H^+ + \frac{1}{2}O_2 + 2e^- \rightarrow 2H_2O + H_2\uparrow \tag{19}$$

In neutral solution:

$$2H_2O + 2e^- \rightarrow H_2\uparrow + OH^- \qquad \text{deareated} \tag{20}$$

$$O_2 + 2H_2O + 4e^- \rightarrow 4OH^- \qquad \text{areated} \tag{21}$$
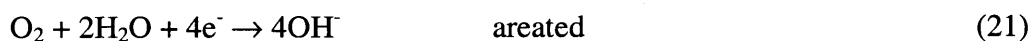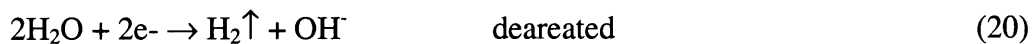
Dry silver does not form a significant surface oxide at ambient temperature and pressure. Based on the Purbaix diagram for Ag-water showed in Figure 1.3, Ag_2O is soluble at biggest values of pH than 8.5 [11].

Atmospheric carbon dioxide is quite abundant, and will dissolve in aqueous surface layers on silver to produce weakly acidic solutions. Silver carbonate is soluble, but is expected only in strongly alkaline solutions.

The principal constituent of corrosion layers on silver is Ag_2S. The formation of silver sulfide is related to the presence of reduced sulfur in the indoor atmosphere. Silver is very sensitive to the presence of hydrogen sulfide (H_2S) and carbonyl sulfide (COS), and about an order of magnitude less sensitive to SO_2. Silver sulfate can be formed by contact with SO_2 in moist air, but only at SO_2 concentrations two to three orders of magnitude higher than typical of ambient environments [10].

Silver is quite sensitive to molecular chlorine and exhibits some degree of sensitivity to gaseous HCl in moist air.

Silver is known to be resistant to corrosion in organic acids present in the atmosphere.

Hydrogen peroxide is sometimes present in indoor air, and it is highly soluble in water reacting with silver surfaces to produce free radical species (reaction 15) [10].

1.4 Potential Applications of Silver in ULSI circuitry

The development of ULSI requires higher integration density with smaller submicrometer design rules. Aluminum, aluminum copper alloys, and copper have been used as metallization materials. But for the ULSI application, the electrical resistivities of these Al alloys are relatively high, and they are also susceptible to failures caused by electromigration and stress migration [12].
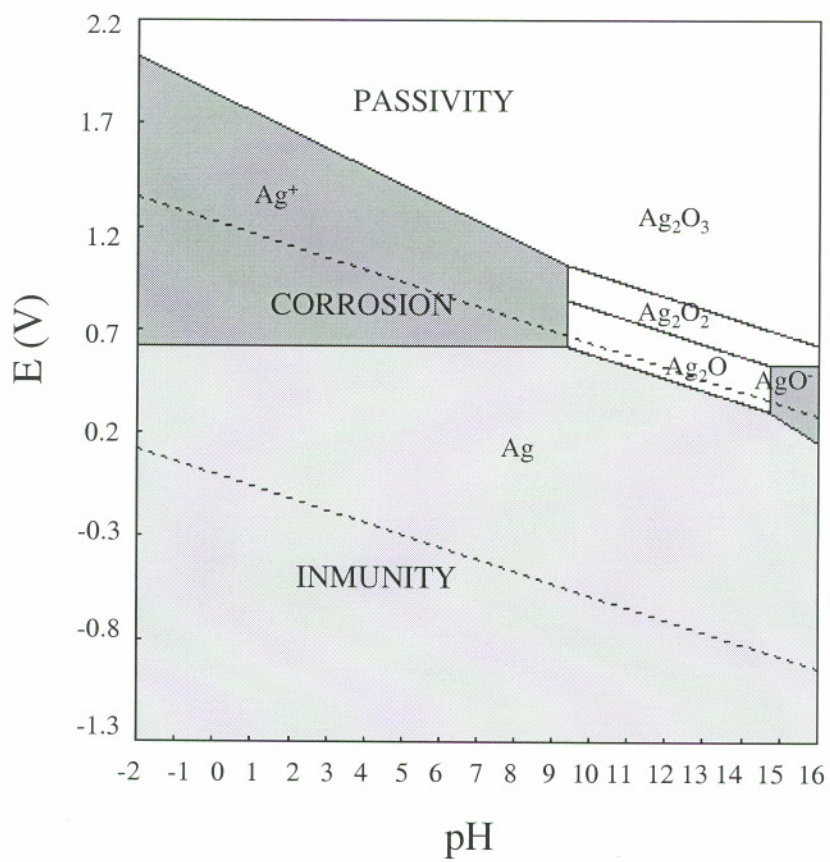
Figure 1.3 Potential-pH equilibrium diagram for the system silver-water, at 25° C

Silver has better conductivity than Cu. However, this Ag thin films can diffuse through an insulator material; hence, a diffusion barrier is necessary between the silver layer and Si substrate. Figure 1.4 shows a cross-section of a complementary metal-oxide semiconductor (CMOS) transistor.

The requirements for such barriers layer are low contact resistance, good adhesion to both the deposited film and the underlying contact configuration, and prevention of interdiffusion at processing temperatures and under operating conditions. In addition, the barrier material has to be resistant against corrosion and must be easy to etch.

Titanium Nitride (TiN), and Tantalum (Ta) have been used successfully as barrier materials for copper interconnections.
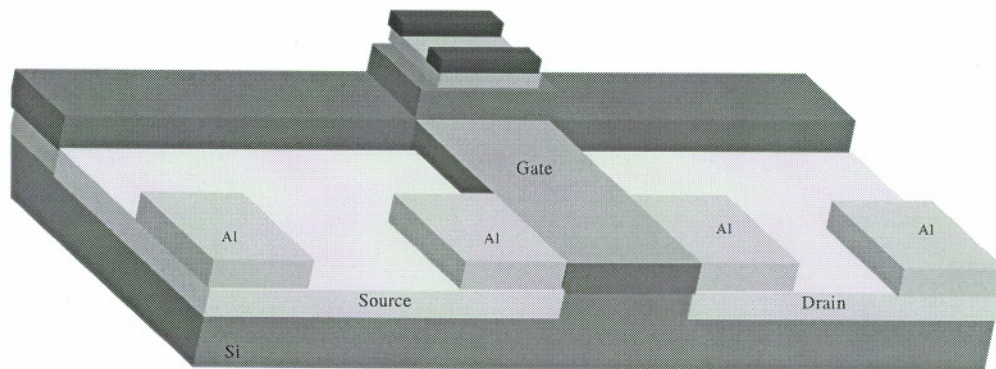
Figure 1.4 CMOS Transistor

1.5 Physical and Chemical Properties of TiN and Ta

Some of the physical properties of this materials are shown in Table 1.3.

Table 1.3 Physical properties of TiN and Ta [13]

	TiN	Ta
Atomic weight	61.9	73
Melting point ($^\circ$C)	3220	2696
Density (g/cm^3)	5.3	16.6
Hardness (Mohs-scratch)	5 – 7	6-6.5
Color	Bronze-red/gold	Grey/silver (yellowish)

Table 1.4 and 1.5 show the etchant solutions for TiN and Ta, respectively.

Table 1.4 TiN etchants [13]

$HF:HNO_3:H_2O$	(1:27.5:10) at room temperature
$HF:HNO_3:H_2O_2$	(10:45:45)
$HF:NH_4F:H_2O$	(1:5) at hot temperature
$HF:HNO_3:H_2O$	(1:27.5:10) at 60°C
$EDTA:H_2O_2:H_2O:NH_4OH$	(2.8 g:60 ml :120 ml :5 ml) at 60°C
$HF:NH_4F:H_2O$	(134 ml: 452 g: 625 ml) at room temperature

Table 1.5 Ta etchants [13]

$HF:HNO_3:H_2O$	(1:1:2) at room temperature
$HF:HNO_3:H_2O$	(1:2:1)
$H_2SO_4:HNO_3:H_2O$	(5:2:2) at room temperature
$HF:HN_3F$	(1:1)
$HNO_3:NH_4F$	(20 ml:10 ml) at 60°C
H_2SO_4 (electrolytic)	90 % concentrated
$KOH:H_2O_2$	(9:1)

1.6 Deposition Methods of TiN and Ta

TiN films can be deposited by chemical vapor deposition (CVD) or by physical vapor deposition (PVD).

Typical TiN CVD process parameters are [14]:

- Temperature: greater than 800° C and typically up to 2000° C
- Pressures: less than 1 atm and as low as 10^{-6} torr
- Precursors: these include reactive gases such as metal halides and carbonyls, reducing gases such as H_2, inert gases such as Ar, or N_2; and other gases such as CH_4, CO_2, NH_3 and other hydrocarbons.

In the TiN CVD process, a chemical reaction occurring between the titanium compound and reactive gases leads to the formation and depositon of TiN on substrates in a closed reactor. Plasma-assisted CVD (PACVD) and laser-assisted CVD (LACVD) are variations of this technique.

PVD techniques require a relative low coating temperature (approximately 500° C or less). Evaporation, sputtering, and ion-plating, constitute the three main classes for PVD processes [14]:

Evaporation: for high melting-point compounds, a high power density is required to obtain appreciable and economical evaporation rates, leading to operational problems with the source for extended run periods. Non-stoichiometric films can result due to partial dissociation of compounds. As a result, non-uniform films can be obtained because this process works with to much heat.

Sputtering: TiN is deposited by reactive sputter deposition of a Ti target in the presence of nitrogen, typically by using an Ar/N_2 mixture; gas-phase nitrogen is consumed by the reaction of molecular N_2 with Ti [15] :

$$2\text{Ti} + \text{N}_2 = 2\text{TiN} \tag{22}$$

Nitrogen bound as TiN is liberated by Ar^+ or N_2^+ ion bombardment.

TiN films deposited into high aspect ratio contact holes have been observed to be substantially nitrogen-deficient ($\text{TiN}_{0.75}$) at the bottom relative to the stoichiometric TiN on the field, but a postdeposition thermal anneal in N_2 (e.g. 30 min at $450^\circ\,\text{C}$) has been found sufficient to restore the composition of the in-depth depleted films to near-stoichiometric TiN [16]. Sputter ion plating (SIP) and magnetron sputtering (MS) are variations of the sputtering process [14].

Ion plating: in this process it is possible to deposit an initially molten target material on to a preheated substrate. The substrate is pre-heated by ion bombardment to raise it to the required deposition temperature. Melting of the target is accomplished by an electron-beam gun. Various modifications of the ion plating technique include, among others, activated reactive ion plating (ARIP) and cathodic arc plasma deposition (CAPD) [14].

Ta films can be deposited by chemical vapor deposition (CVD) or by physical vapor deposition (PVD) [17].

In the sputter deposition of Ta, ions of the Ta target are liberated by bombardment by Ar gas ions, and attracted to the workpiece [17].

Ta films can be deposited by chemical vapor deposition (CVD). The main source for this deposition is the tantalum chloride (TaCl_5). The Ta films obtained by the use of TaCl_5 are very pure. The deposition process rates are 1,000 nm/min using hydrogen as a reducing agent. Tantalum deposition has also been attempted from tantalum carbonate (Ta(CO)_5), but those films contained 5-10 % impurities. Table 1.6 shows several conditions for the Ta CVD [16].

Table 1.6 Tantalum Chemical Vapor Deposition Conditions

Precursor	Substrate	T substrate °C	Carrier Gas	Purity	Rate nm/min
$TaCl_5$	Mo	650-110	H_2, N_2	high	50-100
$TaCl_5$	Stainless steel	900-1050	H_2	>99 %	2000
$TaCl_5$	SiO_2, Al_2O_3	800-1500	H_2, N_2	high	30
$TaCl_5$	Al_2O_3	up to 1500	Ar, H_2	high	---
$TaCl_5$	Steel	1000	H_2, N_2	high	2000
$TaCl_5$	Cu, Fe, Ni, Mo	600-1400	H_2, N_2	high	125
$Ta(CO)_5$	Cu	450-600	H_2	90-95 %	---
TaF_5	Si, SiO_2	250-400	none	high	---

1.7 Deposition Methods of Al and Cu in ULSI

Aluminum can be deposited by CVD technique. The most extensively Al precursor studied is tri-isobutyl-Al, $(C_4H_9)_3Al$ or TIBA. The chemistry is a three-step decomposition [18]:

$$TIBA + H_2 \rightarrow DIBAH + C_4H_8 \qquad (40\text{-}50^{\circ}C) \qquad (26)$$

$$DIBAH + H_2 \rightarrow AlH_3 + 2C_4H_8 \qquad (150\text{-}300^{\circ}C) \qquad (27)$$

$$AlH_3 \rightarrow Al + 3/2H_2 \qquad (28)$$

DIBAH: di-isobutyl Al hydride, or $(C_4H_9)_2AlH$

The Al deposited by this process do not contain hydrocarbon residue and exhibit good conductivity. The disadvantage of this process is the low utilization of the precursor TIBA, less than 15% of the molecular weight is from Al.

Copper can be deposited by PVD, CVD, laser induced reflow, electroless deposition and electroplating techniques [19]. Plating techniques such as electroless deposition and electroplating have the advantages of low tool cost and low processing temperature as well as high quality deposits and good via/trench filling capability [20].

In Cu CVD, the most commonly used Cu precursor is bis-hexafluoroacetyl-acetonate-Cu (II) or $(CF_3COCHCF_3CO)_2Cu$ [16]. This compund is solid at room temperature and sublimes at low heat (35-130° C). Higher deposition rates and better quality films are achieved by hydrogen reduction:

$$Cu(hfac)2 + H2 \rightarrow Cu + 2H(hfac) \tag{29}$$

To prevent corrosion and Cu diffusion into Si, a cladding layer (e.g., TiN or Ta) is needed .

Silver that shows lower resistivity than copper is being investigated as a potential replacement of Cu in ULSI applications. Therefore, corrosion behavior of thin films of Ag is of importance.

Chapter 2
Research objectives

The aim of this study is to investigate the corrosion behavior of silver and silver thin film on TiN and Ta substrates using electrochemical methods.

Chapter 3
Experimental Procedures

3.1 Materials

The materials used in this research were: Ag, TiN, and Ta. For the electrochemical experiments, silver wire was protected against corrosion by Teflon tape (Figure 3.1a). The bottom and the top of the wire were uncovered for the following reasons: the top side for electrical contact while the other side was immersed in the solution.

Figure 3.1.b shows a schematic view of TiN, and Ta specimens. The TiN and Ta specimens were mounted in epoxy after the piece was first welded to a copper wire to achieve electrical contact. Conductive lacquer was used between the specimen and the copper wire. In the next step, the Cu wire was sheathed in Nalgene tubing, and then the assembly was mounted in epoxy. After the epoxy hardened, these specimens were wet polished using 600-grit SiC paper.

In addition to the above materials, silver thin films were used in this research. The films were deposited onto TiN specimen by electroless deposition. The Ag deposition process consists of the following steps [21]:

1. 14.8 N Ammonium hydroxide (NH_4OH) was added to silver nitrate ($AgNO_3$) 6.25 %.
2. The next step was the addition of 12.28 % potassium hydroxide (KOH) to the above solution.

3. When 6.1 % of dextrose ($C_6H_{12}O_6$) was added to the mix, silver began the deposit on the electrode surface.

4. The silver thin film was rinsed with distilled water. The silver deposition process usually takes 5-10 min. This process was performed at 18°C.

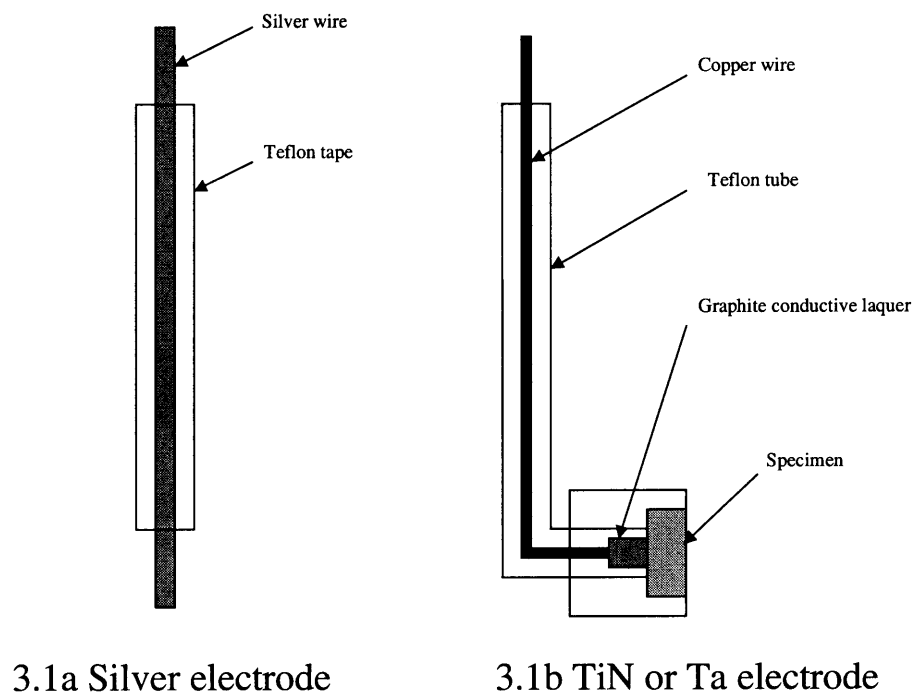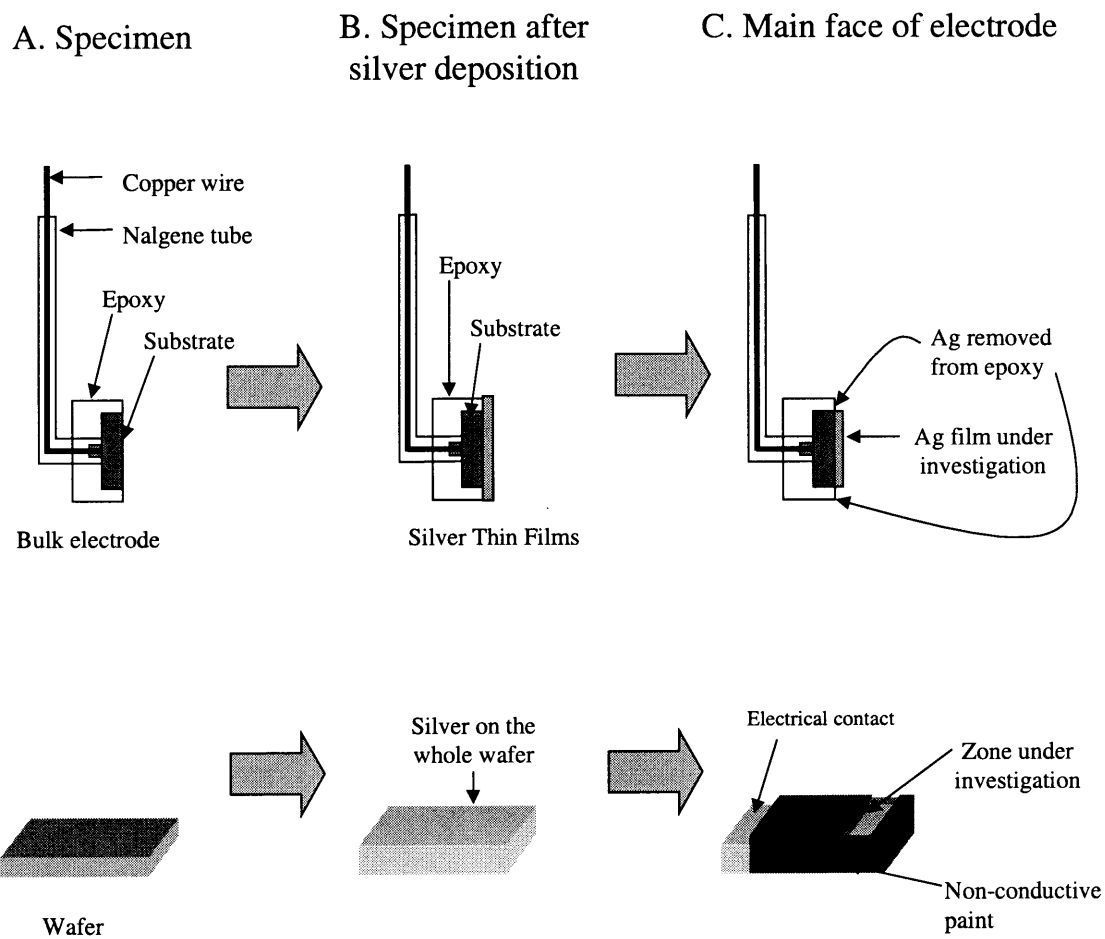3.1a Silver electrode   3.1b TiN or Ta electrode

Figure 3.1. Schematic Electrochemical Specimens

The silver thin film was deposited onto TiN, and wafers. Figure 3.2 illustrates thin film electrodes. The bulk materials and the wafers covered with silver thin films were used as working electrodes in potentiodynamic, potentiostatic, and open-circuit potential test.

A. Specimen

B. Specimen after silver deposition

C. Main face of electrode

Copper wire

Nalgene tube

Epoxy

Substrate

Bulk electrode

Epoxy

Substrate

Silver Thin Films

Ag removed from epoxy

Ag film under investigation

Silver on the whole wafer

Electrical contact

Zone under investigation

Non-conductive paint

Wafer

3.2 Construction of Ag Thin Film Electrode

3.2 Electrolyte Preparation

The electrolytes and concentrations used are shown in table 3.1. Aqueous solutions of hydrogen peroxide, hydrochloric and sulfuric acids, were prepared from certified ACS grade concentrated solutions and deionized water. Sodium borate and tetramethylammonium hydroxide were prepared from Aldrich products.

Table 3.1 Electrolytes

Electrolyte	Chemical formula	Concentration
Hydrochloric acid	HCl	0.1 N 0.01 N
Phosphoric acid	H_3PO_4	0.1 N
Sulfuric acid	H_2SO_4	0.1 N
Sulfuric acid + Hydrogen peroxide	$H_2SO_4 + H_2O_2$	0.1 N + 0.1 N
Sodium borate	$Na_2B_4O_7$	0.1 N
Tetrametylammonium hydroxide	$(CH_3)_4NOH$	0.1 N

3.3 Experimental Set-up

Electrochemical experiments were generated using an EG & G Princeton Applied Research Potentiostat / Galvanostat Model 273A, which is connected to a PC to collect data. All data were plotted by the use of Microsoft Excel. A three electrode setup was used, with a platinum mesh counter electrode and a Saturated Calomel Electrode (SCE) reference electrode. A schematic diagram of the three-electrode electrochemical cell is shown in Figure 3.3. All test were performed at room temperature, in static, non-deareated solutions.
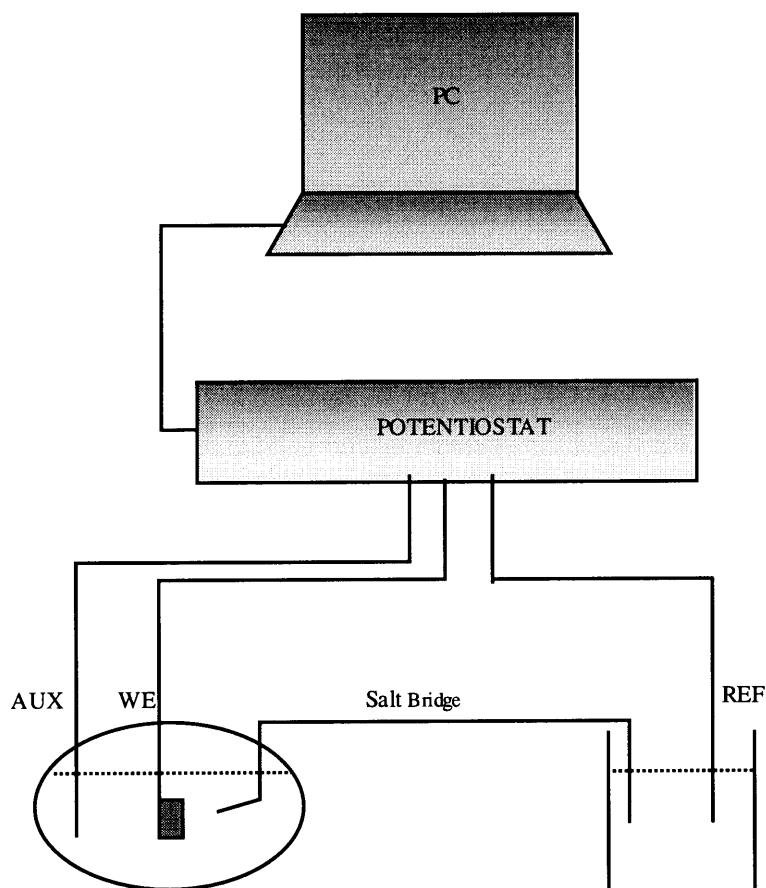

Figure 3.3 Schematic Diagram of the Three-Electrode Electrochemical Cell

3.4 Electrochemical experiments

Electrochemical experiments were conducted in order to understand the corrosion behavior of silver and silver thin films on the electrolytes listed in Table 3.1. These experiments were: open circuit potential, potentiodynamic, and potentiostatic polarization.

3.4.1 Potentiodynamic experiments

Potentiodynamic experiments were conducted in order to develop polarization curves. These experiments determine active, active-passive, and passive regions. The experiments were carried out at several scan rates between 2 and 50 mV/sec. Potentiodynamic scans began at –0.25 V below the open circuit potential, and continued to 2.0 V. Experiments with tetrametylammonium hydroxide as electrolyte were performed when the solution was fresh. A schematic polarization curve for an active-passive metal is shown in Figure 3.4.1. The polarization curves provides the next information [22]:

- Presence or absence of an active (etching) range of potentials
- Range of passive potentials
- Presence or absence of a transpassive region
- Stability of the passive region

The measured potentials depend on the solution chemistry, temperature and in some cases, agitation, and the alloying elements in the material.

The information from the polarization curves can be used to define the behavior of the specimen by the type of passivity. Chemical passivity appears on passivating metals like the transition metals. Some transition metals like titanium show this type of passivity. During the chemical pasivation process, a thin and semiconducting oxide film

is formed on the metal surface. Examples of this type of passivity are metals from the iron and platinum groups, as well as chromium, molybdenum, tungsten and zirconium. Mechanical passivity may occur on almost all metals in environments where the conditions are favorable to the precipitation of solid salts on the metal surface. The cause of the strongly reduced corrosion rate is a thick salt layer. This salt layer could be porous and in most of the cases non-conductive. Examples of this type of passivity are lead in sulfuric acid, magnesium in water or fluoride solutions, silver in chloride solutions, etc. [23].
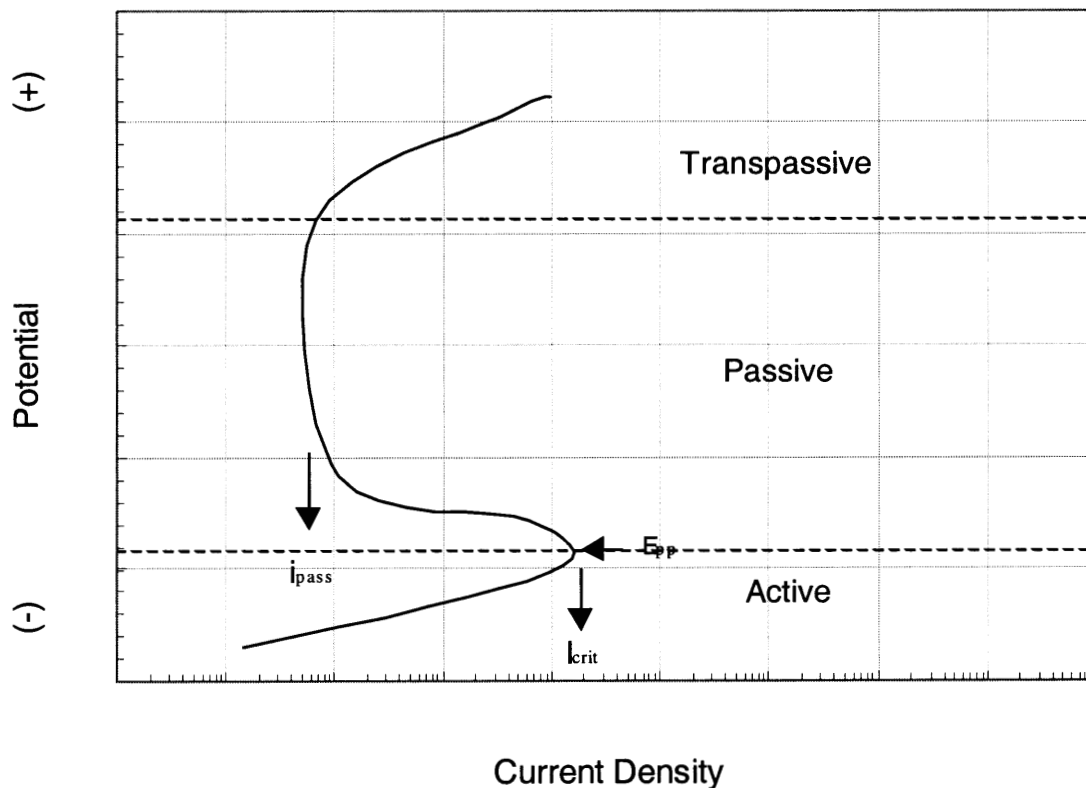
Figure 3.4.1 Schematic Polarization Curve for an Active-Passive Metal

E_{pp} = Primary passivation potential

I_{crit} = Critical current

i_{pass} = Passive current

3.4.2 Potentiostatic experiments

Potentiostatic experiments allow the study of parameters affecting formation and growth of passive films and passivity. The specimen was held at a constant potential for 20 seconds at $25°$ C, and the change in current density with time was monitored during the experiments. Figure 3.4.2 shows a schematic potentiostatic curve. A decrease in current with the time represents the passivation of the material. A current decreasing linearly indicates that the formation of a passive film is in progress. A slight increase in current or no change in current with time indicates the dissolution of the material.
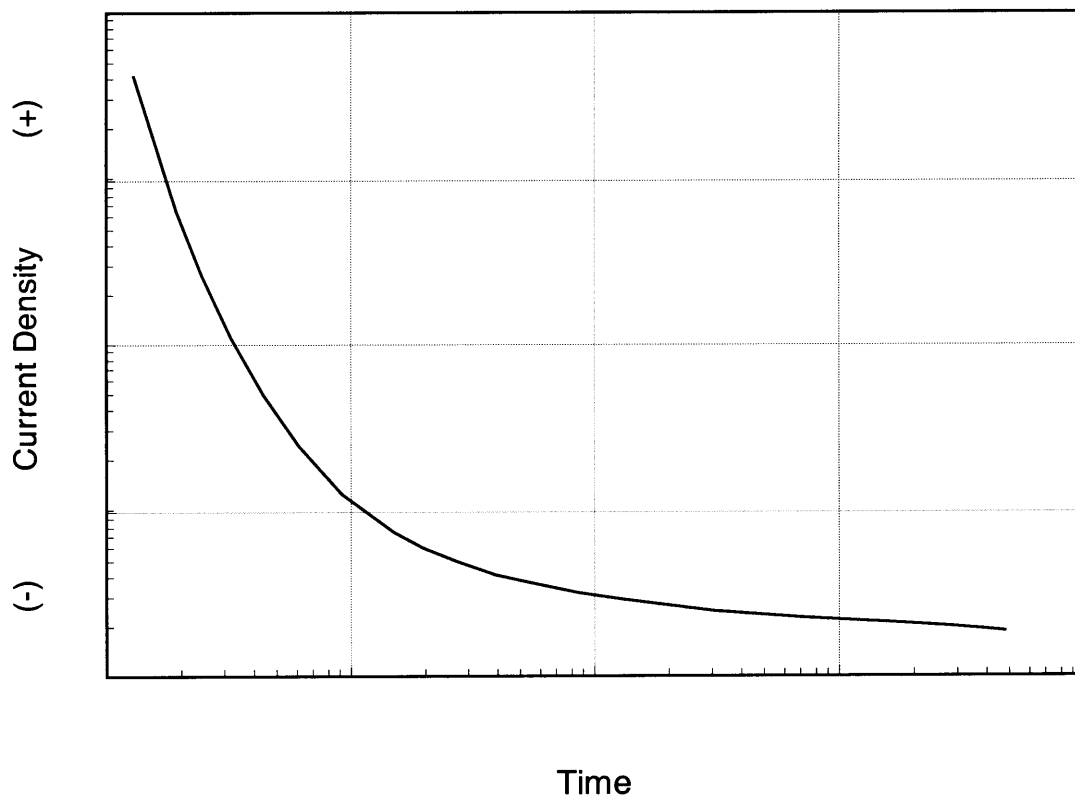
Figure 3.4.2 Schematic Potentiostatic Curve

3.4.3 Open circuit potential

The open circuit potential determines if current values stay in the active or passive state described in the potentiodynamic experiments. The experiments were carried out for 6 hours. An example of open circuit potential is showed in Figure 3.4.3.
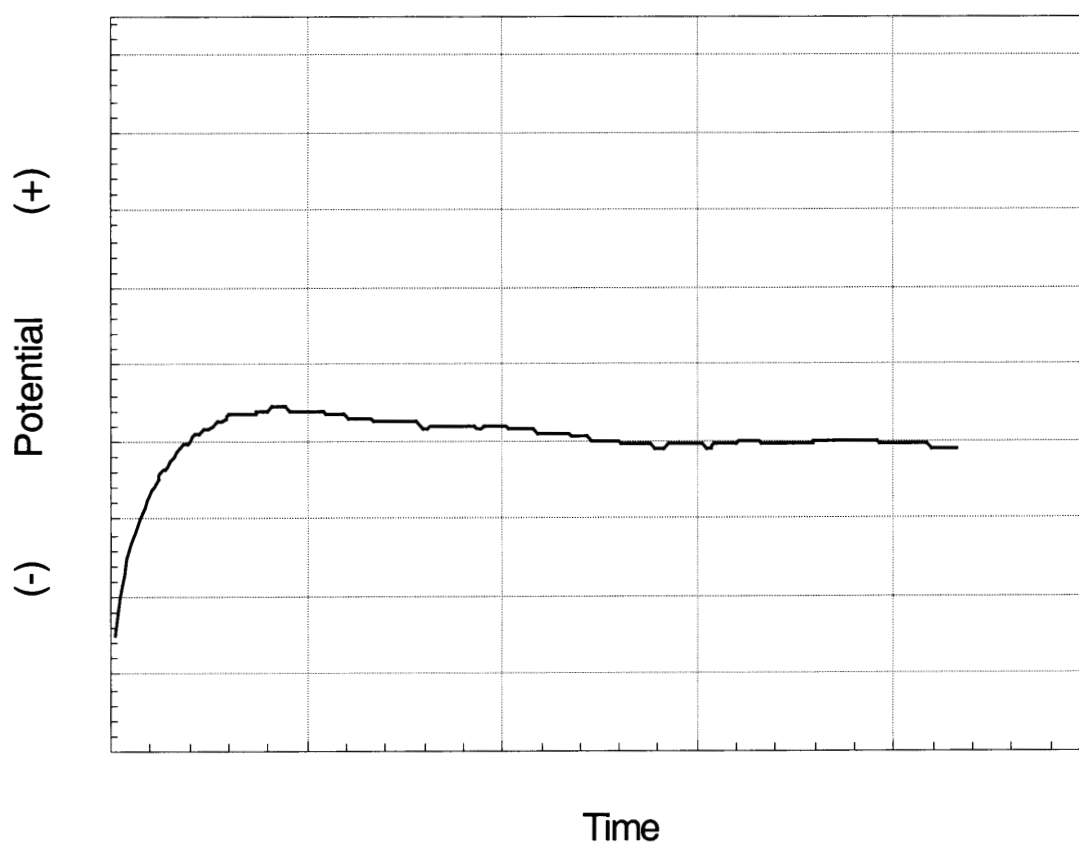

Figure 3.4.3 Schematic Open Circuit Potential

3.5 Microscopic Investigations

Figure 3.5.1 shows a SEM picture of Ag Thin Film on Si/SiO$_2$/TiN wafer at 100X. The Ag thin film is uniform and continuous, but very rough.
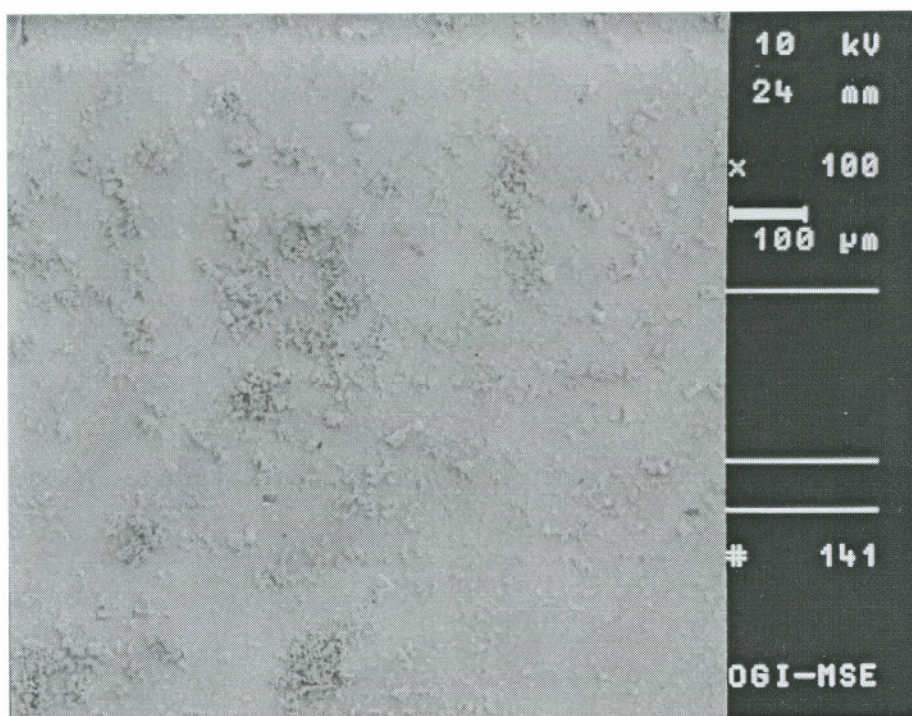
Figure 3.5.1 Ag Thin Film on Si/SiO$_2$/TiN wafer

Also, the film's thickness was approximately 0.5 μm as shown in Figure 3.5.2. (SEM picture courtesy of Mr. Gary Harris).
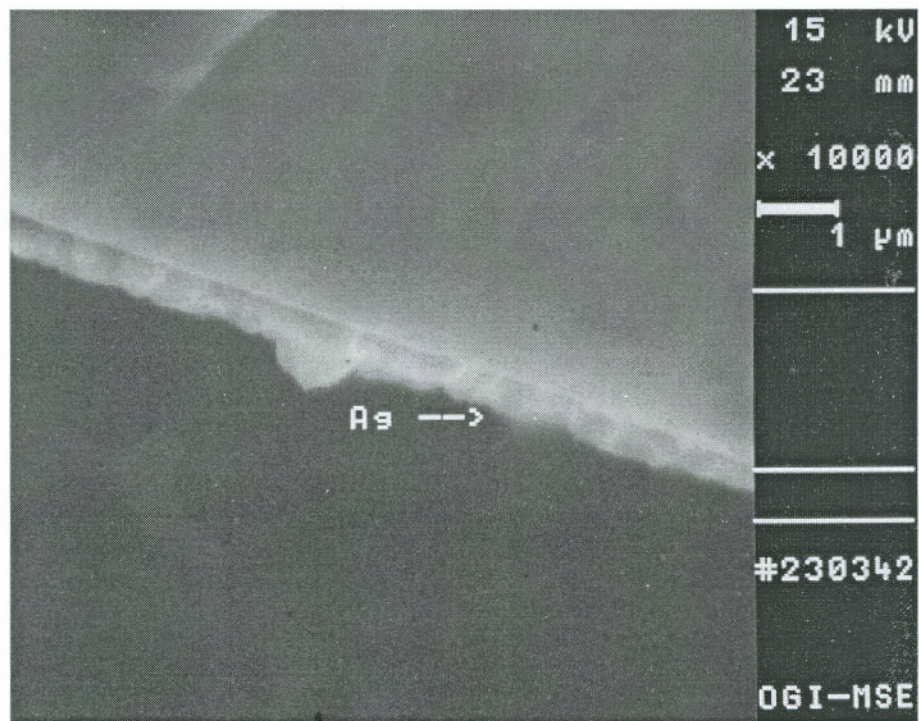

Figure 3.5.2 Ag Thin Film on Si/SiO$_2$/TiN wafer

Chapter 4

Results and Discussion

4.1 Potentiodynamic experiments for Silver, TiN, Silver Thin Films on TiN, and Ta

4.1.1 Aqueous Inorganic Solutions

HCl

Figure 4.1.1.1 shows the anodic polarization curves for Ag, TiN, Ag thin films on TiN (Ag/TiN), and Ta in 0.01 N HCl. Ag shows active and passive states. TiN shows active, active-passive, and passive states. Ag/TiN shows active, and active-passive states. Ta shows passive state. Passive current densities are lower for TiN than for Ag.

For Ag, the current in the passive region is approximately 3×10^{-3} A/cm^2 at the potentials between 0.2 and 2.0 V.

TiN reaches $I_{critical}$ of 3×10^{-5} A/cm^2 at 0.15 V. The current in the passive region starts at 3×10^{-6} A/cm^2 and at the potential value of 0.3 V. An increase in current density is observed at potential values higher than 0.9 V; this behavior could be associated with the transformation of the passive film.

Ag/TiN reaches $I_{critical}$ of 4×10^{-3} A/cm^2 at 0.5 V. A decrease in current density is observed between 0.5 to 1.3 V, which corresponds to the active passive behavior. Above
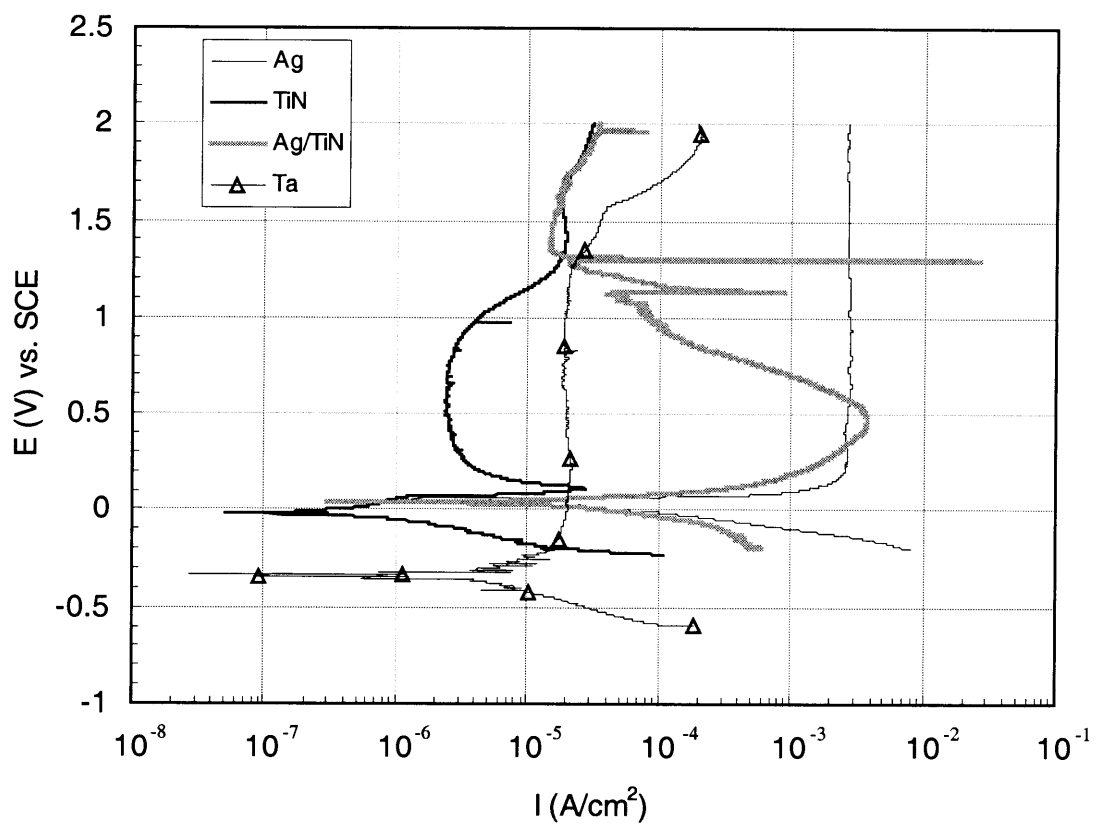
32

Figure 4.1.1.1 Anodic Polarization Curves for Ag, TiN, Ag/TiN, and Ta in 0.01 N HCl.
Scan rate: 2 mV/sec.

1.3 V, the current density of Ag/TiN is similar to that of TiN. This indicates that there is not Ag present on the TiN substrate and the current density values correspond to the passive behavior of TiN.

For Ta, the passive state starts at approximately 2×10^{-5} A/cm^2 and –0.2 V. An increase in current density is observed at potential values higher than 1.3 V; this behavior could be associated with the transformation of the passive film.

Figure 4.1.1.2a shows the anodic polarization curves for Ag, TiN, Ag/TiN, and Ta in 0.1 N HCl. The behavior of the investigated materials is similar to the results in 0.01 N HCl. Ag reaches $I_{critical}$ of 4×10^{-3} A/cm^2 at 0.2 V. The active-passive behavior is observed between 0.2 and 3.5 V. The passive region starts at a potential of 0.35 V, and current density is 5×10^{-3} A/cm^2.

TiN reaches $I_{critical}$ of 2×10^{-4} A/cm^2 at 0.1 V. The passive region start at 0.25V, and the current density is 3×10^{-6} A/cm^2. An increase in current density is observed at potential values higher than 0.9 V. This behavior could be associated with the transformation of the passive film.

Ag/TiN reaches $I_{critical}$ of 2.5×10^{-3} A/cm^2 at approximately 0.2 V. A decrease in current density is observed between 0.3 and 0.9 V, which corresponds to the active-passive behavior. Above 0.9 V, the current density of Ag/TiN is similar to the current density of TiN. This indicates that there is not Ag present on the TiN substrate and the current density values correspond to the passive behavior of TiN.

Ta shows passive state between –0.2 and 1.3 V, at 3×10^{-5} A/cm^2. Above 1.3 V, an increase in current density is observed. This behavior could be associated with the transformation of the passive film.

Figure 4.1.1.2b shows the effect of scan rate for Ag/TiN in 0.1 N HCl. The values of E_{pp} and $I_{critical}$ increase with increasing in a scan rate. Above E_{pp}, values of current
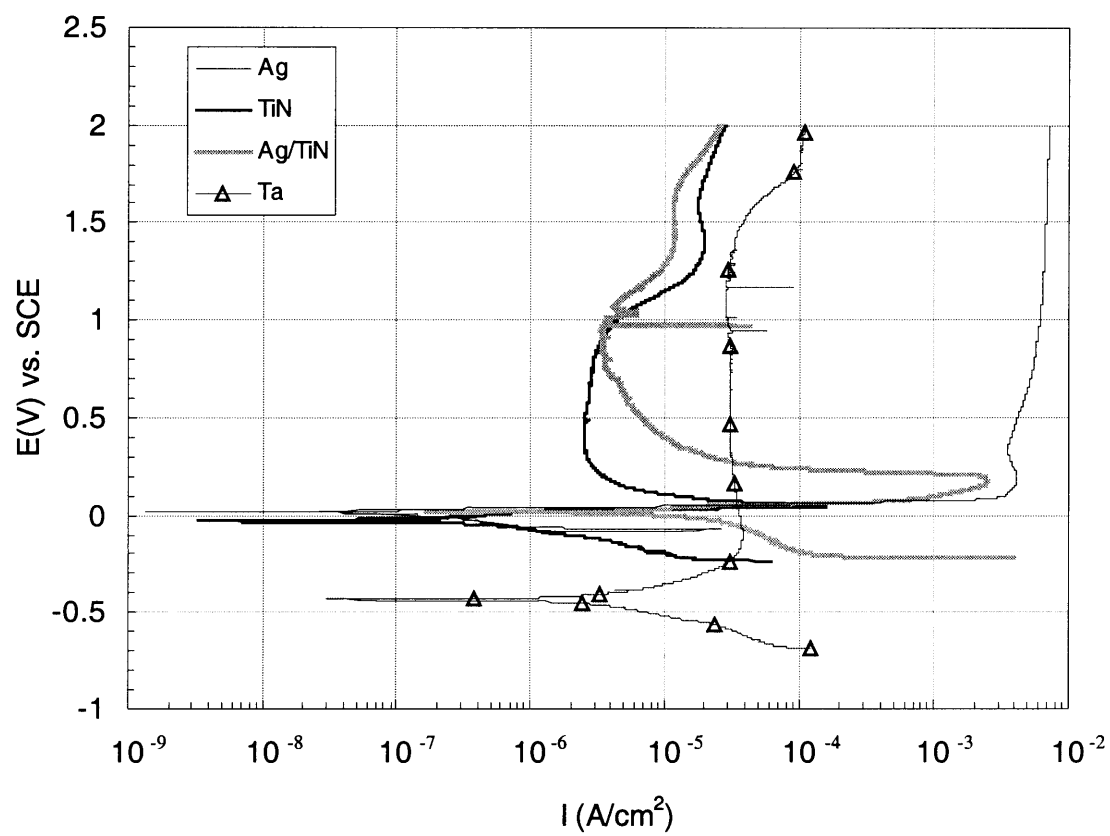
Figure 4.1.1.2a Anodic Polarization Curves for Ag, TiN, Ag/TiN, and Ta in 0.1 N HCl.
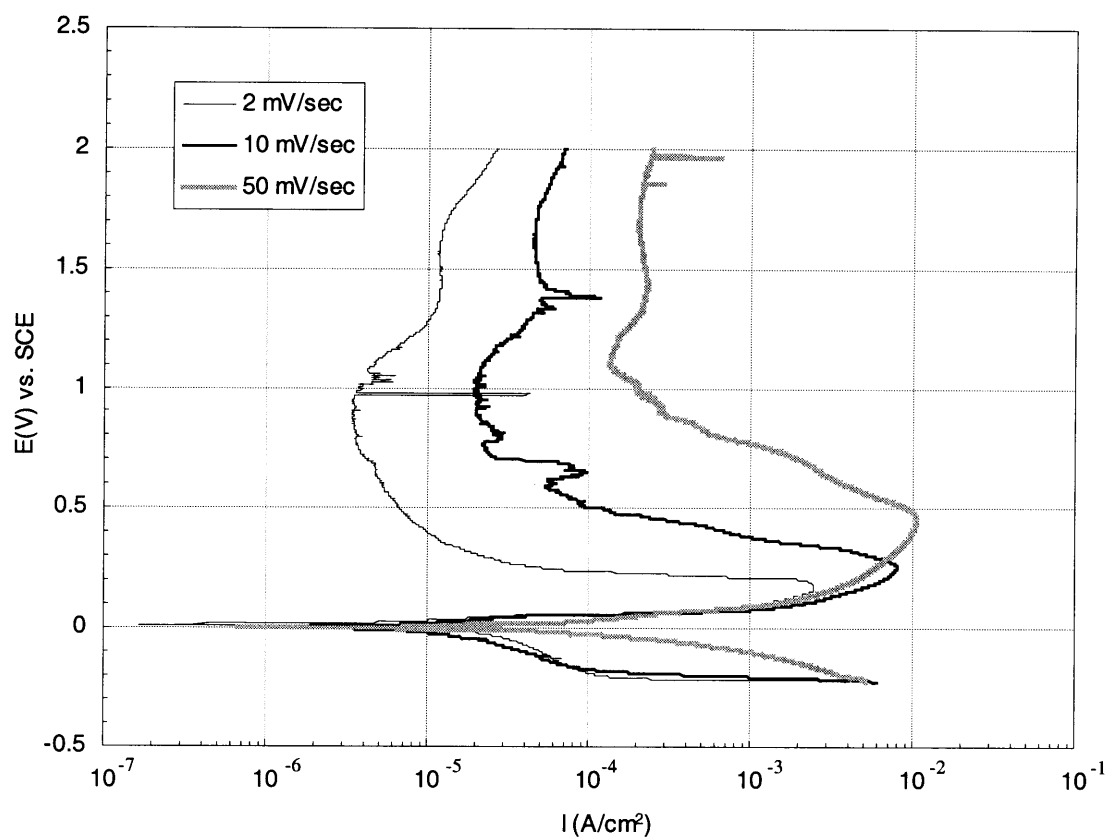Scan rate: 2 mV/sec.

Figure 4.1.1.2b Anodic Polarization Curves for Ag/TiN in 0.1 N HCl at different scan rates.

density increase in the order: 2 mV/sec < 10 mV/sec < 50 mV/sec. This indicates that the passivation process is controlled by diffusion.

H_3PO_4

Figure 4.1.1.3a shows anodic polarization curves for Ag, TiN, Ag/TiN, and Ta in 0.1 N H_3PO_4. Ag/TiN, Ag and TiN show active, active-passive, and passive states. Ta shows passive state.

Ag reaches $I_{critical}$ of 0.5 x 10^{-2} A/cm^2 at 0.7 V. Above 0.75 V, oscillations are observed in the passive region. Relatively high current values may indicate that a mechanical passivation occured.

For the TiN specimen, $I_{critical}$ is 8 x 10^{-6} A/cm^2 at 0.2 V. The current in the passive region is approximately 3 x 10^{-6} A/cm^2 at the potential value of 0.3 V. An increase in current density is observed at potential values higher than 0.9 V; this behavior could be associated with the transformation of the passive film.

Ag/TiN reaches $I_{critical}$ value of 3 x 10^{-3} A/cm^2 at approximately 0.3 V. An active-passive state is observed between 0.3 and 0.9 V. Above 0.9 V, Ag/TiN shows similar values of current density to TiN. However, the presence of oscillations indicates that some silver is still present on the TiN surface.

Ta displays passive behavior between –0.1 and 1.5 V, at 3 x 10^{-5} A/cm^2. Above 1.5 V, an slight increase in current density is observed. This behavior could be associated with the transformation of the passive film.

Figure 4.1.1.3b shows the effect of scan rate for Ag/TiN in 0.1 N H_3PO_4. Above E_{pp}, at any applied potential, current densities increase with increasing scan rates,
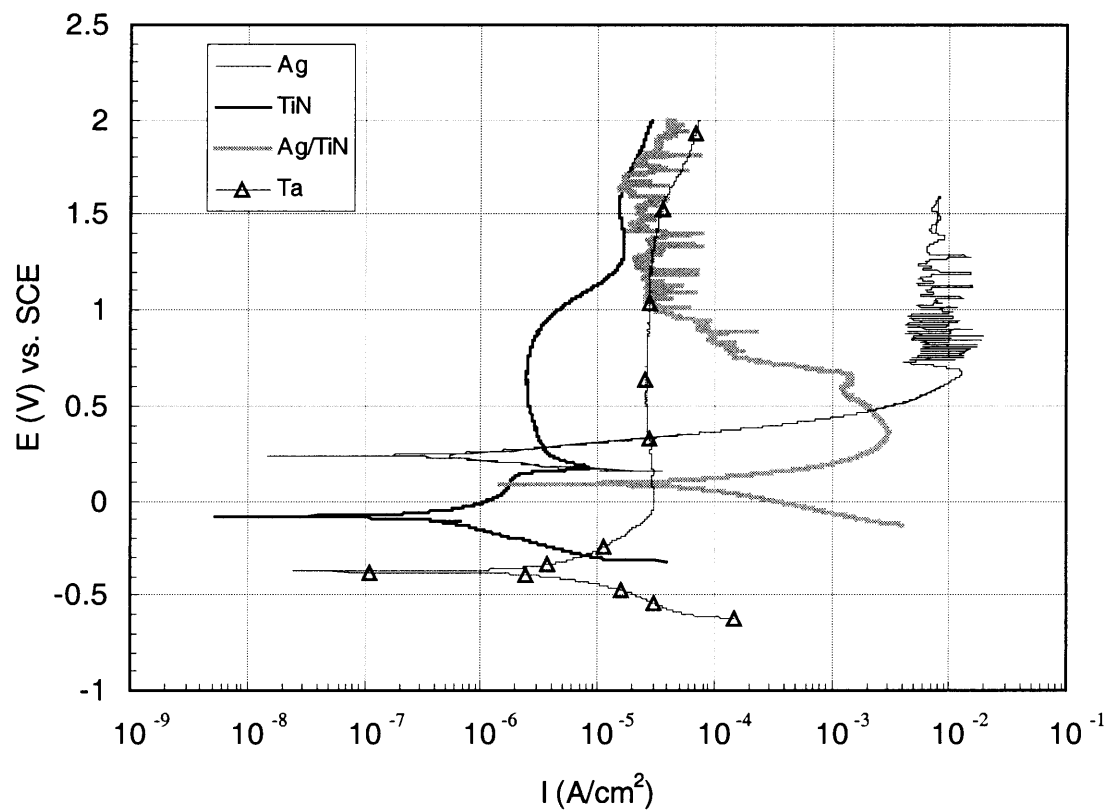
Figure 4.1.1.3a Anodic Polarization Curves for Ag, TiN, Ag/TiN, and Ta in 0.1 N H_3PO_4.
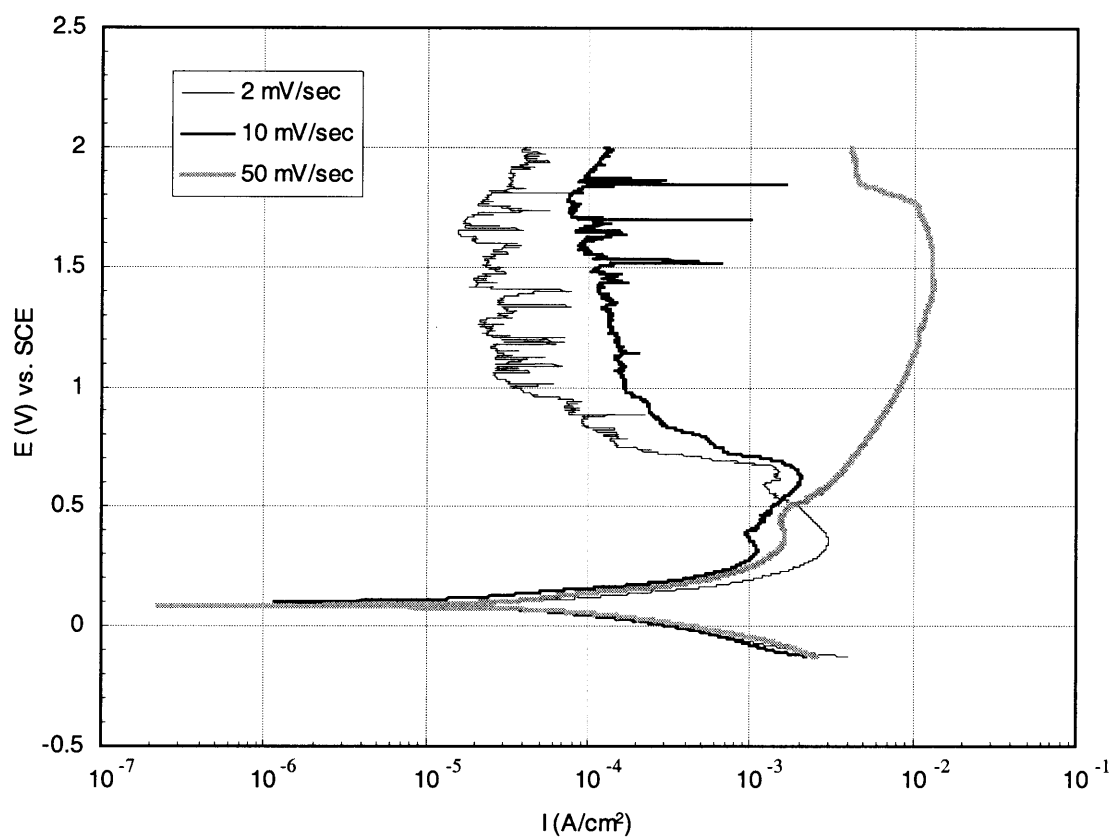Scan rate: 2 mV/sec.

Figure 4.1.1.3b Anodic Polarization Curves for Ag/TiN in 0.1 N H_3PO_4 at different scan rates.

namely: 2 mV/sec < 10 mV/sec < 50 mV/sec. At each scan rate, Ag/TiN shows active, active-passive, and passive behavior.

H_2SO_4

Figure 4.1.1.4a shows the results of the potentiodynamic experiments for Ag, TiN, Ag/TiN, and Ta in 0.1 N H_2SO_4. Ag and Ag/TiN show active, active-passive, and passive behavior. TiN shows active-passive behavior at any applied potential. Ta shows passive state in a wide range of potentials.

Figure 4.1.1.4b, Figure 4.1.1.4c, and Figure 4.1.1.4d show the effect of scan rate for Ag, TiN, and Ta respectively in 0.1 N H_2SO_4. For Ag, high $I_{critical}$ at high E_{pp} are reached with an increment in scan rate. In the case of TiN the values of the passive current density increase when the scan rate increases at the potentials values between 0.1 and 1.0 V. After 1.0 V at all scan rates, an increasing in current density is observed, such increment could be associated with the transformation of the passive film. For Ta, the passive current densities start at approximately -0.3 V for 2, 10, and 50 mV/sec. An increase in the passive current density is observed with increasing scan rate.

$H_2SO_4 + H_2O_2$

Figure 4.1.1.5 shows the results of anodic polarization curves for Ag, TiN, Ag/TiN, and Ta in 0.1 N $H_2SO_4 + H_2O_2$. Ag and Ag/TiN show active, active-passive, and passive behavior. TiN does not have an active-passive state. Ag/TiN exhibits an active state and a similar value of E_{pp} to that for Ag. Ta shows passive behavior.

Ag reaches $I_{critical}$ value of 2 x 10^{-2} A/cm^2 at 0.7 V. Current density in the passive region starts at 5 x 10^{-3} A/cm^2 at the potential value of 0.8 V. Between 0.7 and 0.9 V reactivation of Ag is observed.
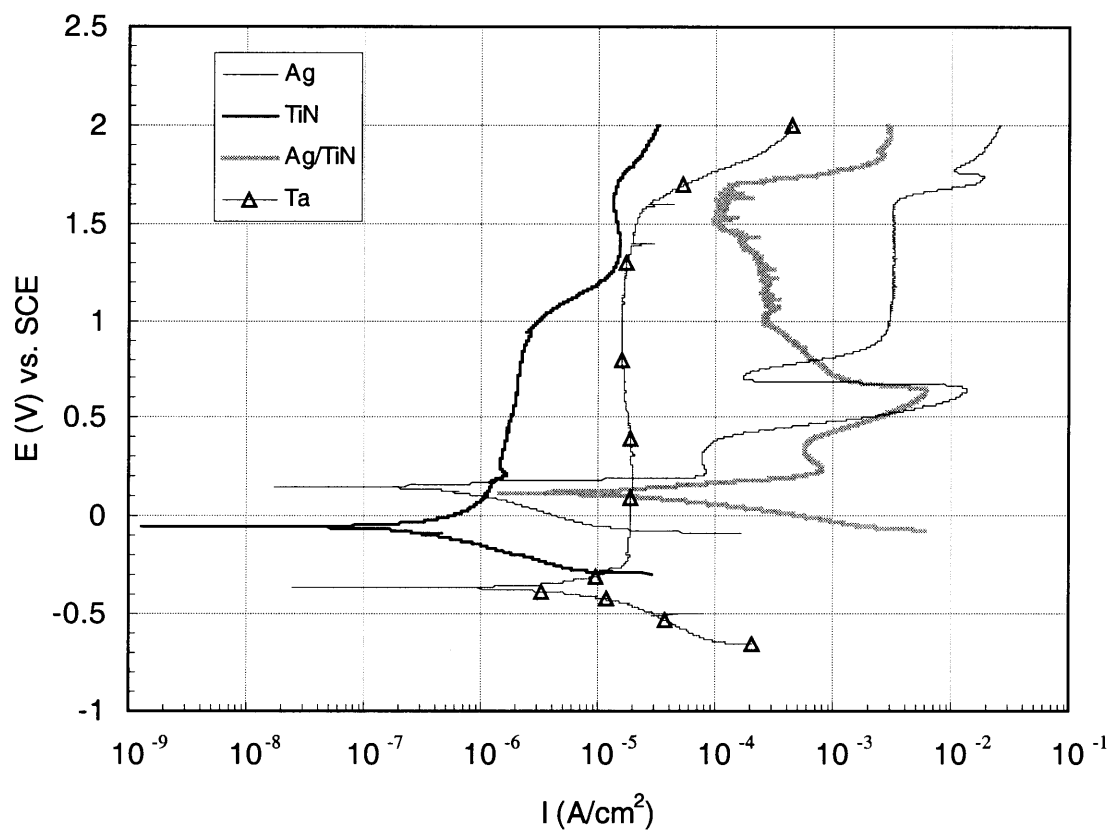
Figure 4.1.1.4a Anodic Polarization Curves for Ag, TiN, Ag/TiN, and Ta in 0.1 N H_2SO_4.
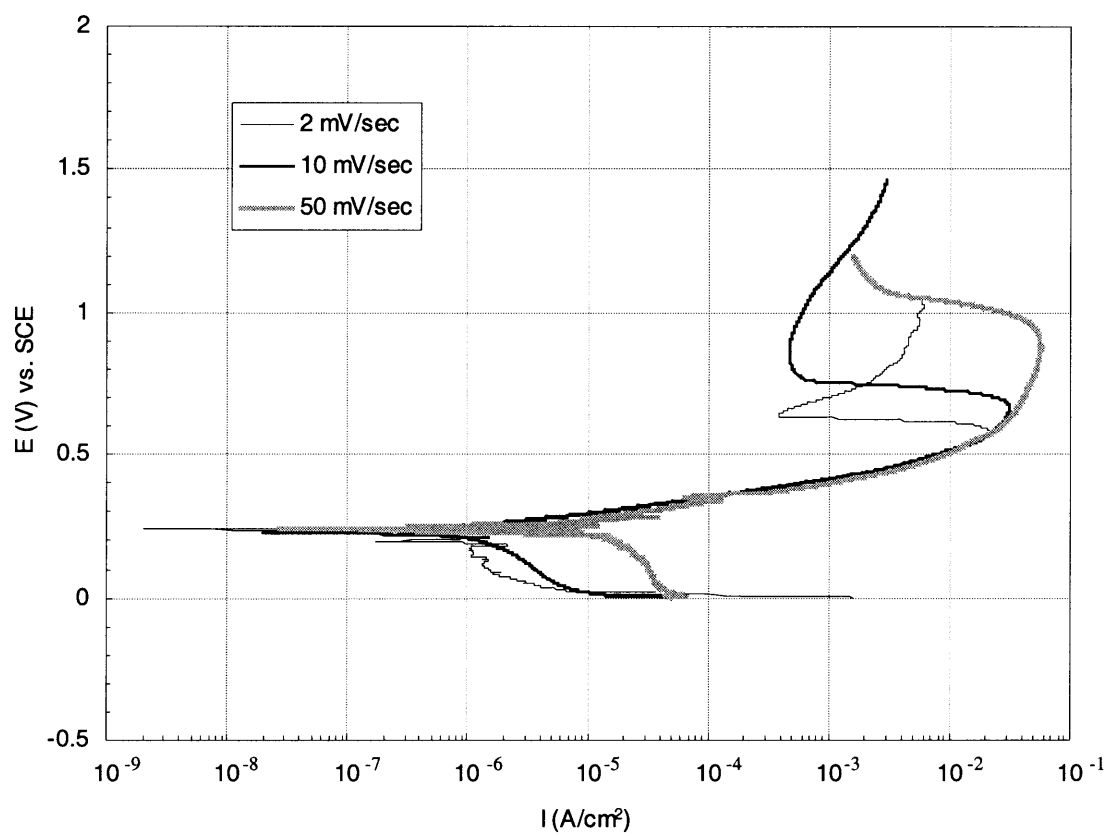Scan rate: 2 mV/sec.

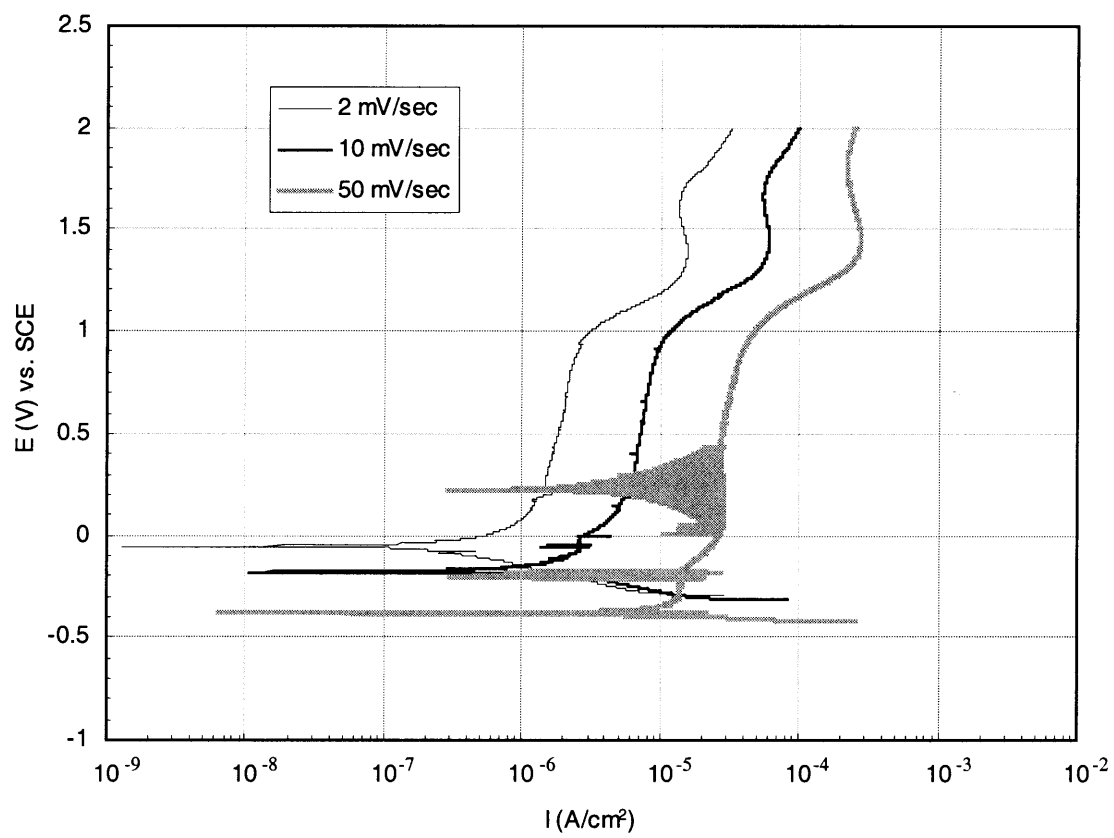Figure 4.1.1.4b Anodic Polarization Curves for Ag in 0.1 N H_2SO_4 at different scan rates.

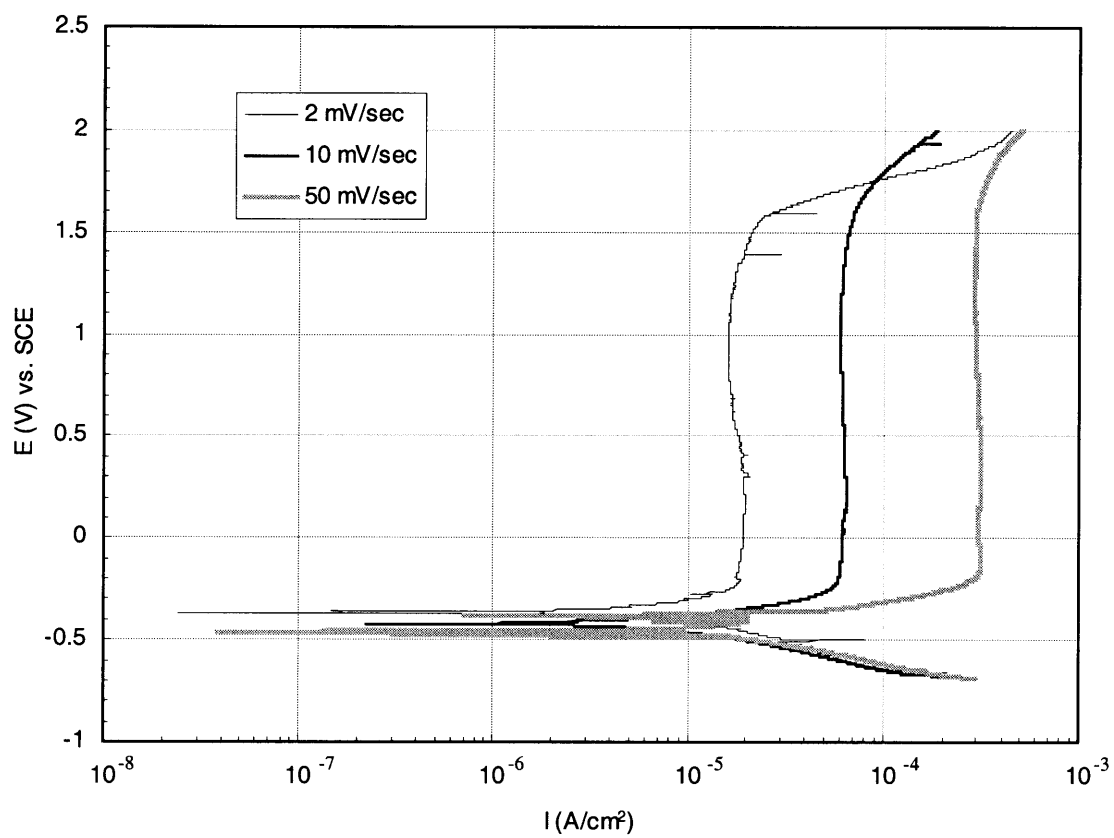Figure 4.1.1.4c Anodic Polarization Curves for TiN in 0.1 N H_2SO_4 at different scan rates.

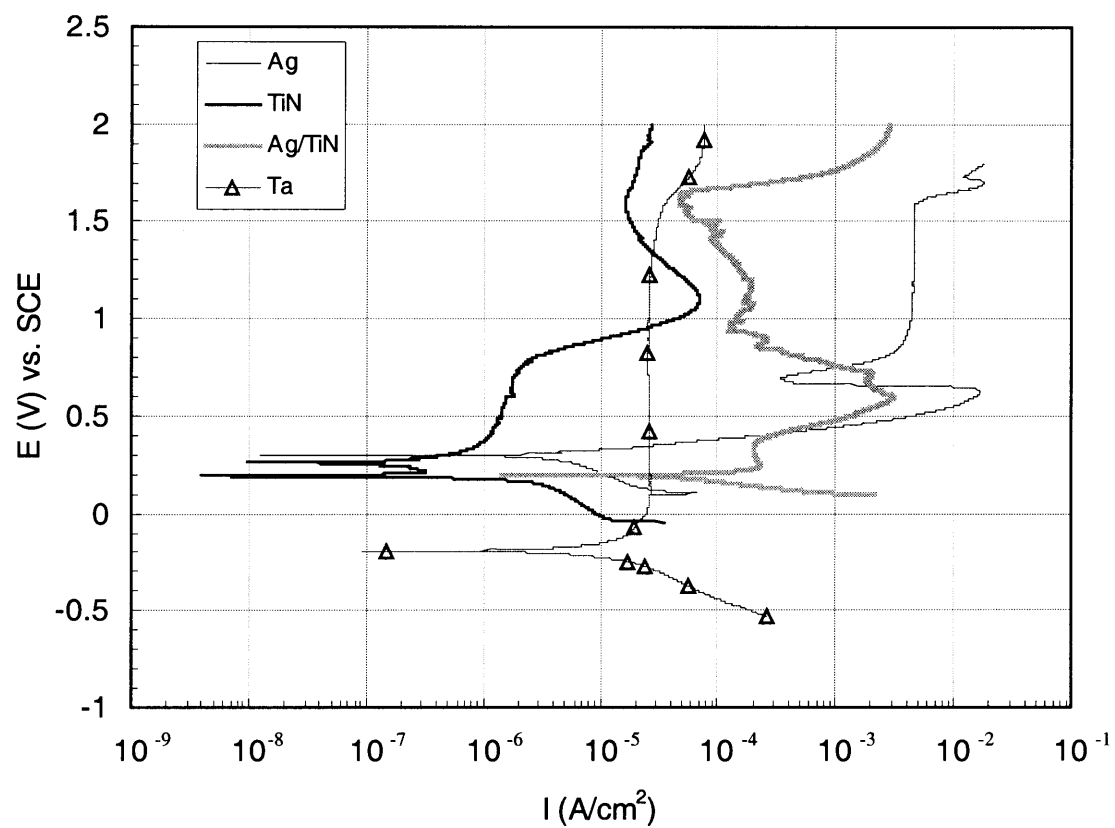Figure 4.1.1.4d Anodic Polarization Curves for Ta in 0.1 N H_2SO_4 at different scan rates.

Figure 4.1.1.5 Anodic Polarization Curves for Ag, TiN, Ag/TiN, and Ta in 0.1 N H_2SO_4 + 0.1 N H_2O_2. Scan rate: 2 mV/sec.

For TiN, the passive state starts at approximately 2 x 10^{-6} A/cm^2 and 0.5 V. An increase in current density is observed at potential values higher than 0.75 V; this behavior could be associated with the transformation of the passive film.

Ag/TiN reaches I$_{critical}$ value of 3 x 10^{-3} A/cm^2 at approximately 0.6 V. Decrease in current density is observed between 0.7 and 0.9 V, which corresponds to the active-passive behavior. Between 0.9 and 1.6 V, Ag/TiN and TiN show similar behavior.

For Ta, the passive state starts approximately at 3 x 10^{-5} A/cm^2 and 0.0 V. An increase in current density is observed at potential values higher than 1.6 V; this behavior could be associated with the transformation of the passive film.

Na$_2$B$_4$O$_7$

Figure 4.1.1.6a shows the results of anodic polarization curves for Ag, TiN, Ag/TiN, and in Ta 0.1 N Na$_2$B$_4$O$_7$. Ag shows active, active-passive, and passive behavior. TiN, Ta, and Ag/TiN do not show an active-passive state. Passive current densities increase in the order of: Ag/TiN < TiN < Ta < Ag.

For Ag, I$_{critical}$ value of 8 x 10^{-4} A/cm^2 is at 0.5 V. The current density value in the passive region is at 3 x 10^{-4} A/cm^2 in the range of potentials between 0.6 and 1.3 V.

TiN shows passive behavior at the current density value of 2 x 10^{-6} A/cm^2 approximately, and at the potentials between 0.2 and 1.0 V. An increase in current density is observed at potential values higher than 1.0 V; this behavior could be associated with the transformation of the passive film.

Ag /TiN starts its passive state at a current density value of 4 x 10^{-7} A/cm^2, and at approximately 0.4 V. The current in the passive region remains at 5 x 10^{-7} A/cm^2 in a range of potential between 0.7 and 2.0 V.
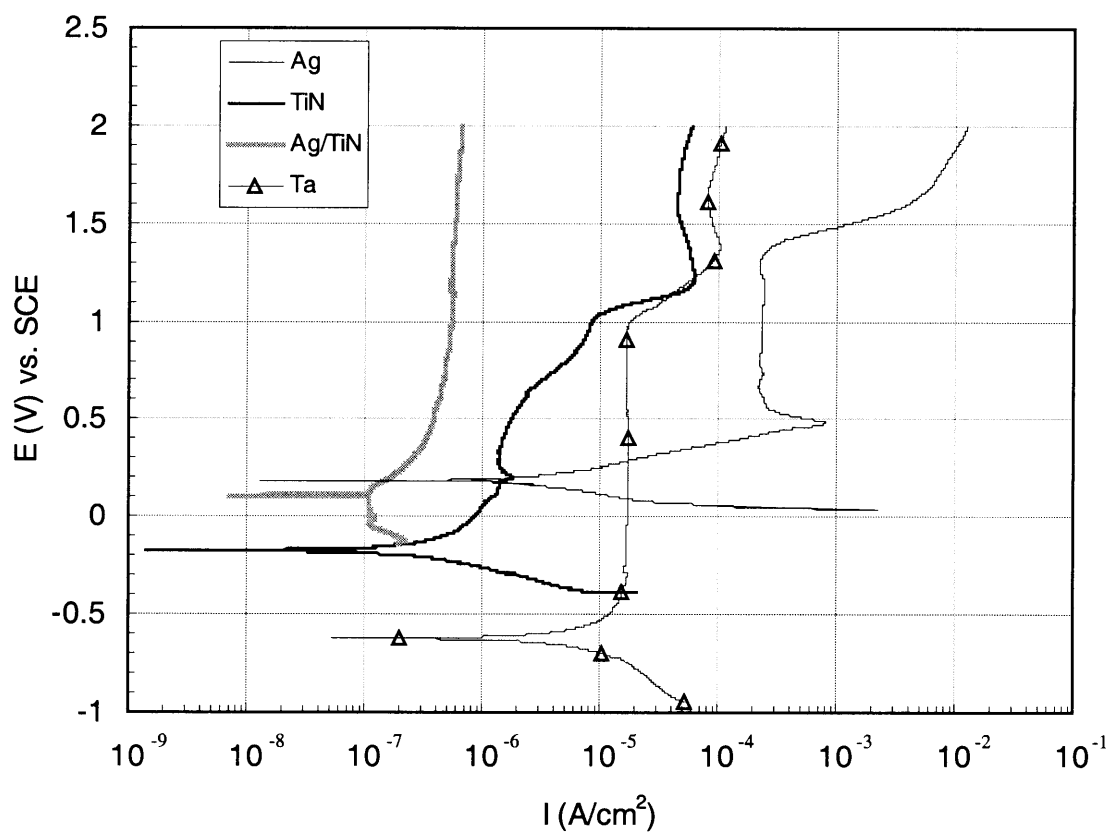
Figure 4.1.1.6a Anodic Polarization Curves for Ag, TiN, Ag/TiN, and Ta in 0.1 N
$Na_2B_4O_7$. Scan rate: 2 mV/sec.

Ta shows passive behavior between –0.4 and 1.0 V, at almost 1.2 x 10^{-5} A/cm^2. Above 1.0 V, an increase in current density is observed. This behavior could be associated with the transformation of the passive film.

Figure 4.1.1.6b shows the effect of scan rate for Ag/TiN 0.1 N Na$_2$B$_4$O$_7$. The shape of the polarization curves obtained at 2 and 10 mV/sec was similar. Surprisingly, high current values were observed at all applied potentials for the curve at the lower scan rate.

4.1.2 Aqueous Organic Solutions

Tetramethylammonium hydroxide

The anodic polarization curves for Ag, TiN, Ag/TiN, and Ta are shown in Figure 4.1.2a. The highest current values are found for Ag and the lowest for Ag/TiN. For Ag, there are two peaks present before reaching the transpassive region. The first peak is present at approximately 0.3 V and the second at approximately 0.6 V. The critical passivation current is approximately 2 x 10^{-4} A/cm^2. The maximum current for second peak is approximately 8 x 10^{-4} A/cm^2. In this solution there is no passive regions, therefore Ag is active. For the TiN specimen, active-passive behavior is observed. The critical passivation current is approximately 2 x10^{-6} A/cm^2 at 0.25 V. Before reaching the transpassive region a relatively narrow passivation region is observed. The shape of the polarization curve for Ag/TiN indicates the presence of the passive region. Also for this material, the current values at all applied potential are lower than those observed for Ag and TiN. This may indicate that Ag acts as a protective coating for the TiN substrate. Ta shows passive behavior between –0.5 and 0.6 V at 1.5 x 10^{-5}. An increase in potential is observed at potential values higher than 0.6 V, which could be associated with the transformation of the passive film.
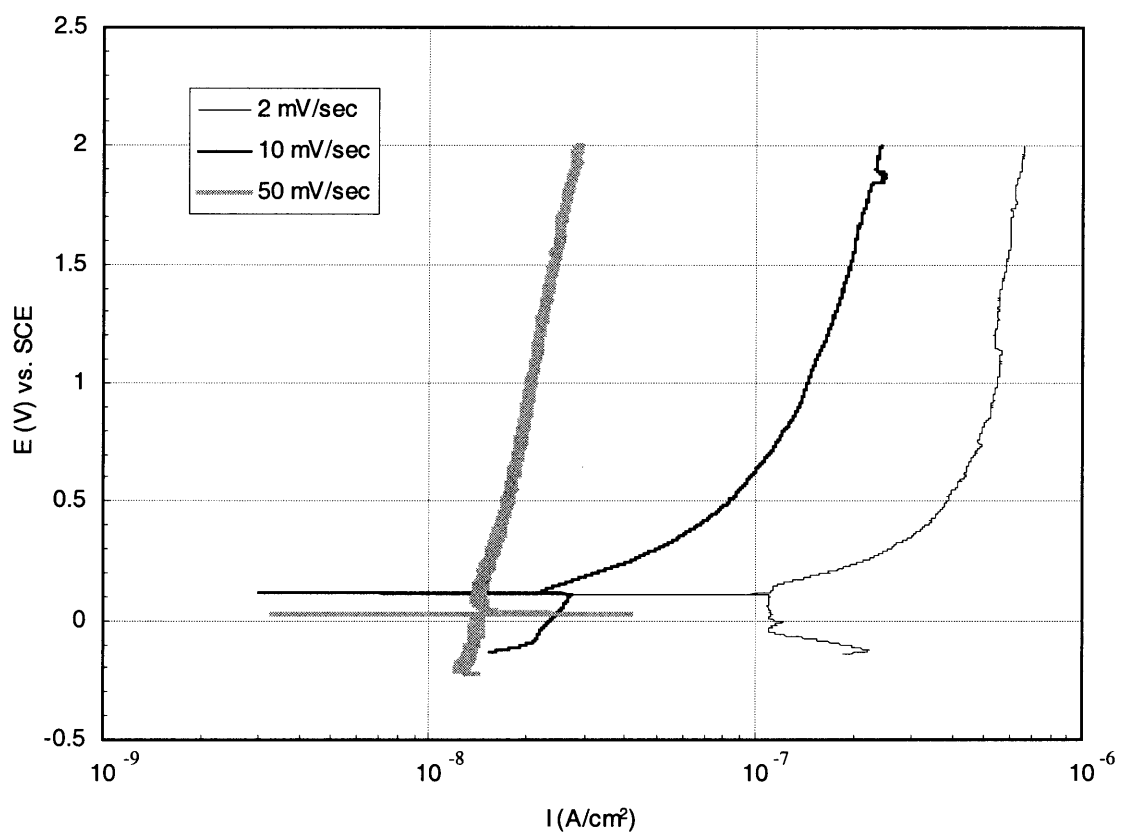
Figure 4.1.1.6b Anodic Polarization Curves for Ag/TiN in 0.1 N $Na_2B_4O_7$ at different scan rates.
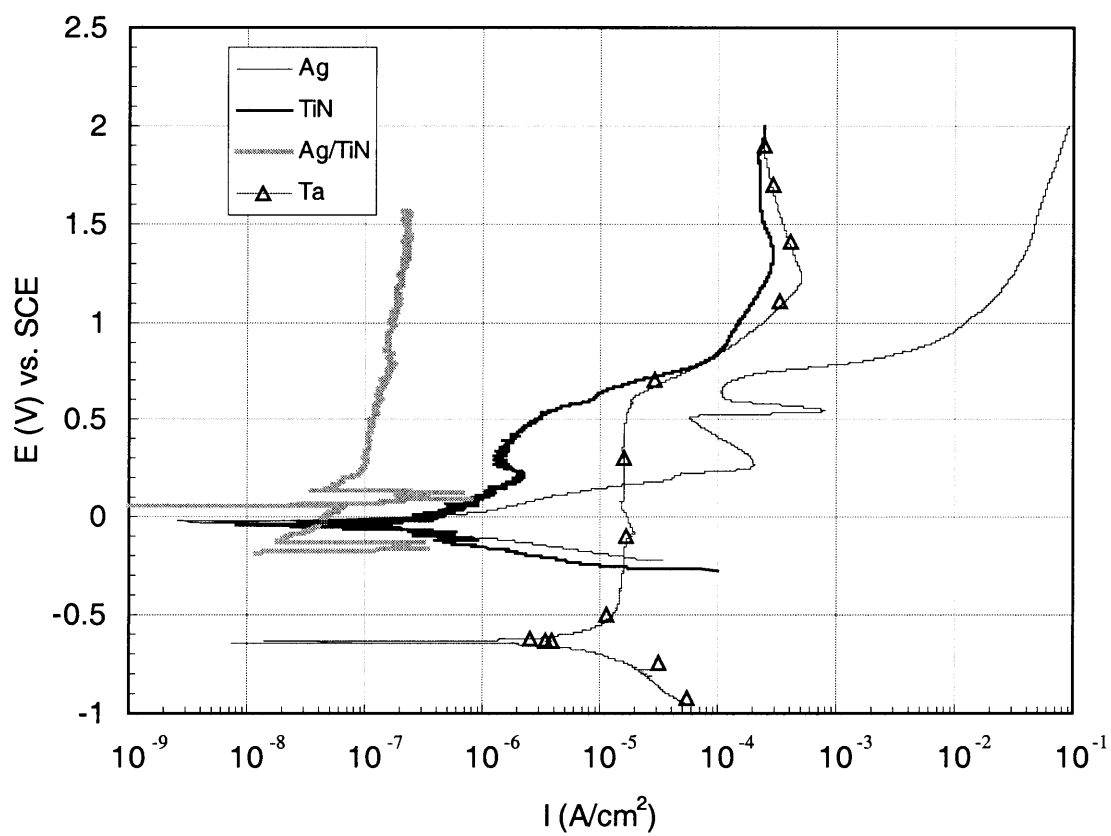
Figure 4.1.2a Anodic Polarization Curves for Ag, TiN, Ag/TiN, and Ta in 0.1 N $(CH_3)_4NOH$. Scan rate: 2 mV/sec.

The anodic polarization curves obtained for Ag at different scan rates are shown in Figure 4.1.2b. The highest current is observed at 50 mV/s. Slightly lower currents are obtained at 2 and 10 mV/s. This may indicates that the corrosion processes in this system are controlled by the activation polarization.

4.2 Potentiostatic Experiments for Silver, TiN, Silver Thin Films on TiN, and Ta

4.2.1 Aqueous Inorganic Solutions

HCl

Figure 4.2.1.1 shows the results of the potentiostatic experiment for the Ag electrode in 0.1 N HCl. The highest current is observed at the potential value of 1.8 V and the lowest at 0.2 V. The shape of the I-t curves at 0.2, 1.0, and 1.8 V, are similar to each other. For the curve obtained at 1.0 V a slight increase in current is at approximately 10 sec. The curves indicates that Ag is passive at 0.2, 1.0, and 1.8 V. This passivation is associated with the formation of AgCl on the specimen surface.

For the TiN electrode, the results of the potentiostatic experiment in 0.1 N HCl are shown in Figure 4.2.1.2. The highest current is observed at the potential value of 1.4 V, and the lowest at 0.1 V. The shape of the I-t curves at the applied potentials are similar. These curves show a decrease in current with increasing time. This indicates that TiN is passive at 0.1, 0.2, 0.7, and 1.4 V.

Figure 4.2.1.3 shows the results of the potentiostatic experiment for Ag/TiN in 0.1 N HCl. The highest current is observed at the potential value of 0.25 V and the lowest at 0.06 V. The shape of the I-t curves at 0.17, 0.25, and 1.0 V, are similar to each other. For the curve at 1.0 V a significant decrease in current is observed at approximately 3 sec. For the curves obtained at 0.17 and 0.25 V a decrease in current is observed after 10 sec. For the curve obtained at 0.06 V a slight increase in current is observed with increasing
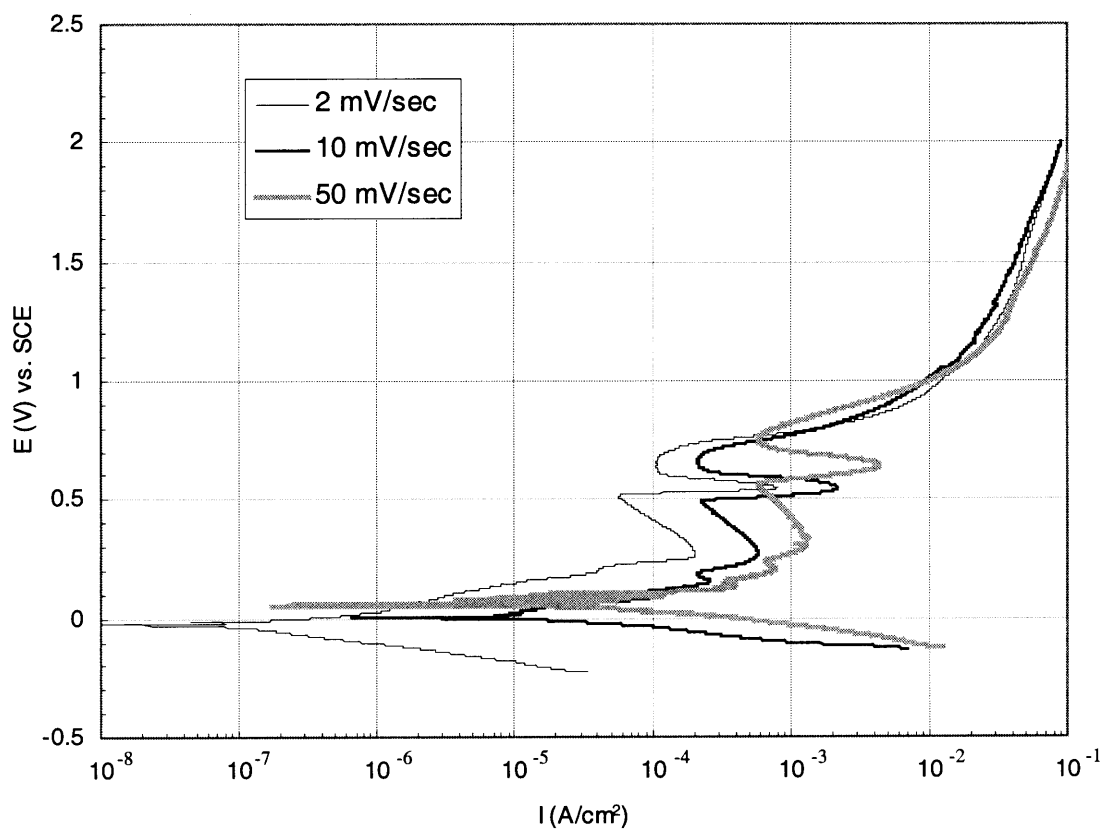
Figure 4.1.2b Anodic Polarization Curves for Ag in 0.1 N (CH₃)₄NOH at different scan rates
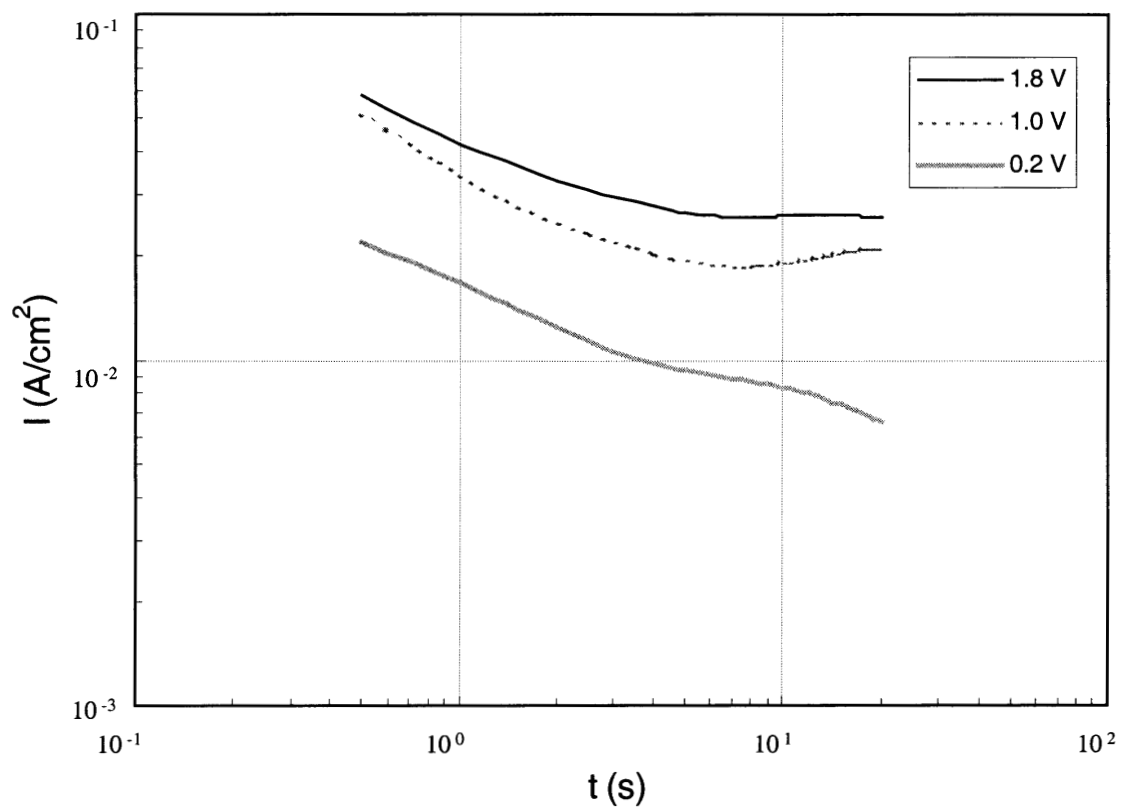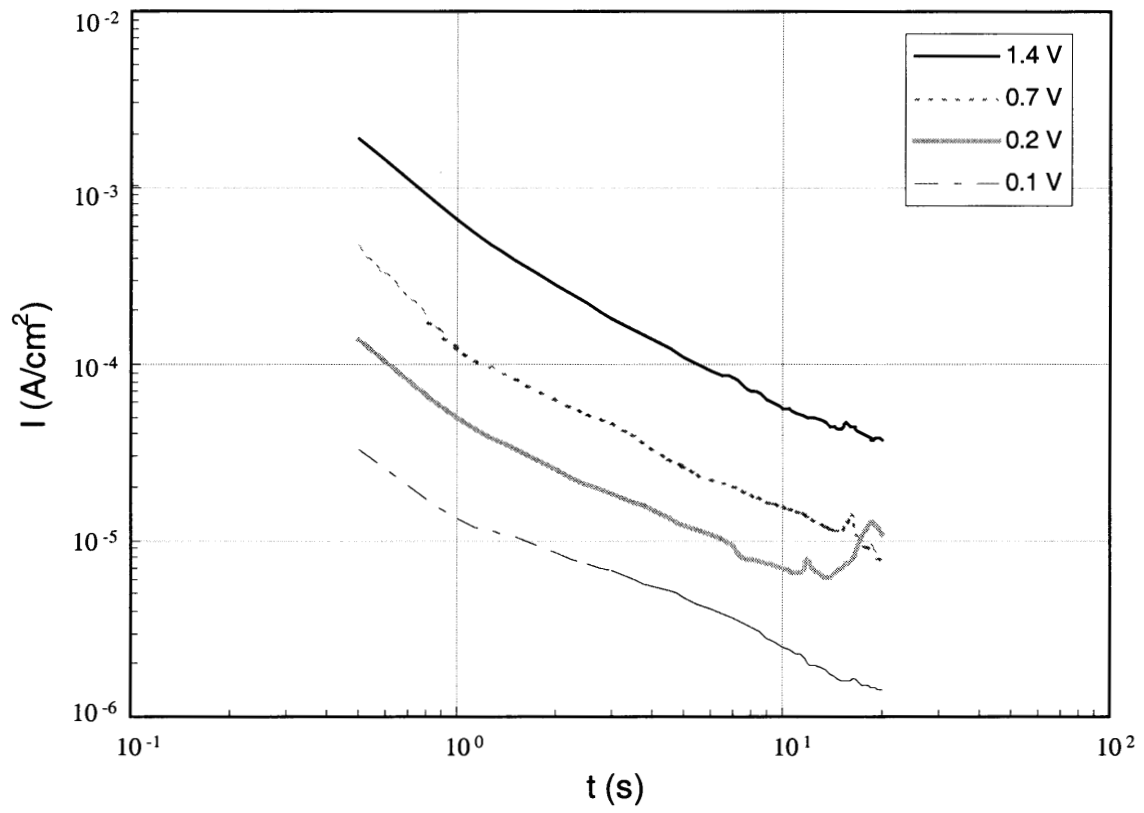
Figure 4.2.1.1 Current-Time Curves for Ag in 0.1 N HCl

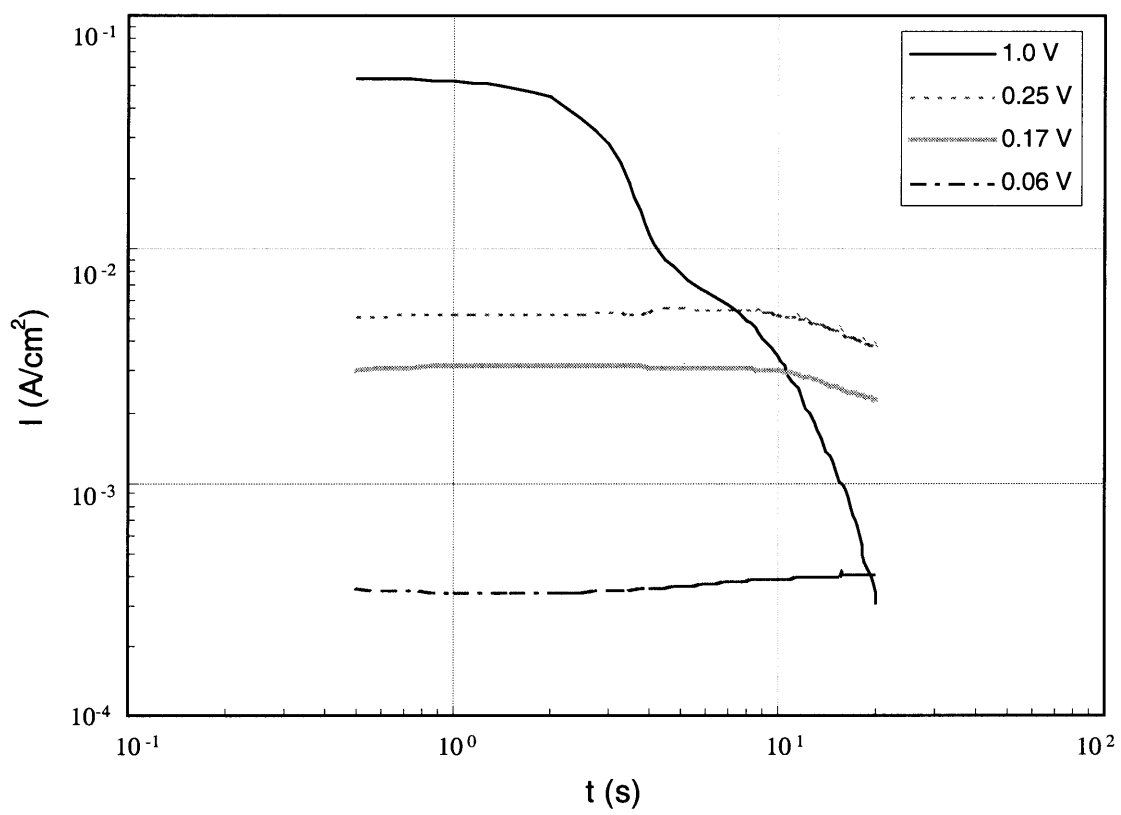Figure 4.2.1.2 Current-Time Curves for TiN in 0.1 N HCl

Figure 4.2.1.3 Current-Time Curves for Ag/TiN in 0.1 N HCl

time. This indicates that Ag/TiN is active at 0.06 V and is passive at 0.17, 0.25 and 1.0 V. This passivation is associated with the formation of AgCl on the specimen surface.

The results of the potentiostatic experiment for Ta in 0.1 N HCl are shown in Figure 4.2.1.4. The highest current is observed at the potential value of 1.8 V and the lowest at 0.0 V. These curves show a decrease in current with increasing time. For the curve obtained at 1.8 V a significant decrease in current is observed for the first second, and a slight decrease in current is observed for the rest of the experiment. The curves indicates that Ta is passive at 0.0, 1.0, and 1.8 V.

H₃PO₄

Figure 4.2.1.5 shows the results of the potentiostatic experiment for Ag in 0.1 N H₃PO₄. The highest current is observed at the potential value of 0.7 V and the lowest at 0.8 V. Initially, the values of current density are high for experiments at 0.8, 1.0 and 1.5 V, but these values decrease at 12, 8 and 3 seconds, respectively. For the curve obtained at 0.7 V a slight decrease in current is observed at 14 sec. For the curve obtained at 0.6 V, a slight increase in current is observed at 4 sec This indicates that Ag is active at 0.6 V and is passive at 0.7, 0.8, 1.0 and 1.5 V. This passivation is associated with the formation of AgPO₄ on the specimen surface.

Figure 4.2.1.6 shows the results of the potentiostatic experiment for TiN in 0.1 N H₃PO₄. The highest current is observed at the potential value of 1.3 V and the lowest at 0.2 V. These curves show a decrease in current with increasing time. This indicates that TiN is passive at 0.2, 0.7, and 1.3 V.

Figure 4.2.1.7 shows the results of the potentiostatic experiment for Ag/TiN immersed in 0.1 N H₃PO₄. For the curve at 2.0 V a significant decrease in current is observed at approximately 3 sec. The curve at 1.4 V shows a decrease in current at approximately 15 sec. The shape of the I-t curves at 0.75, 0.36, and 0.15, are similar to
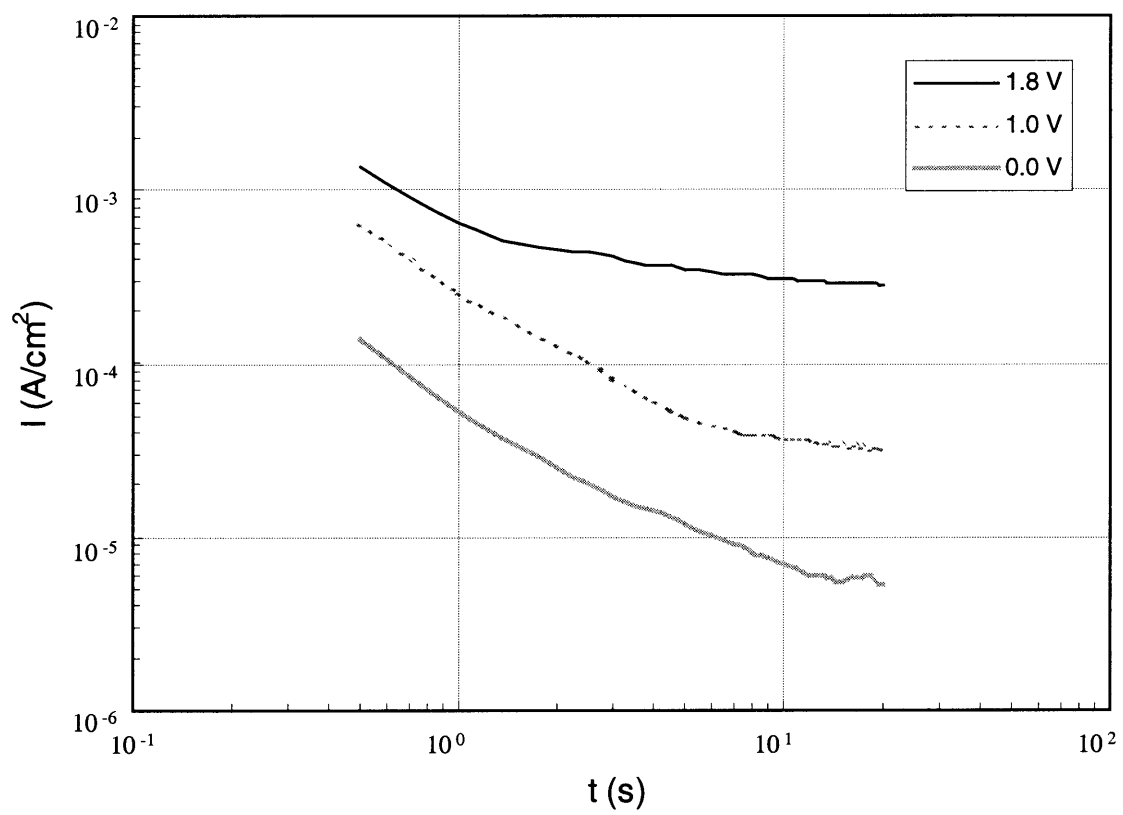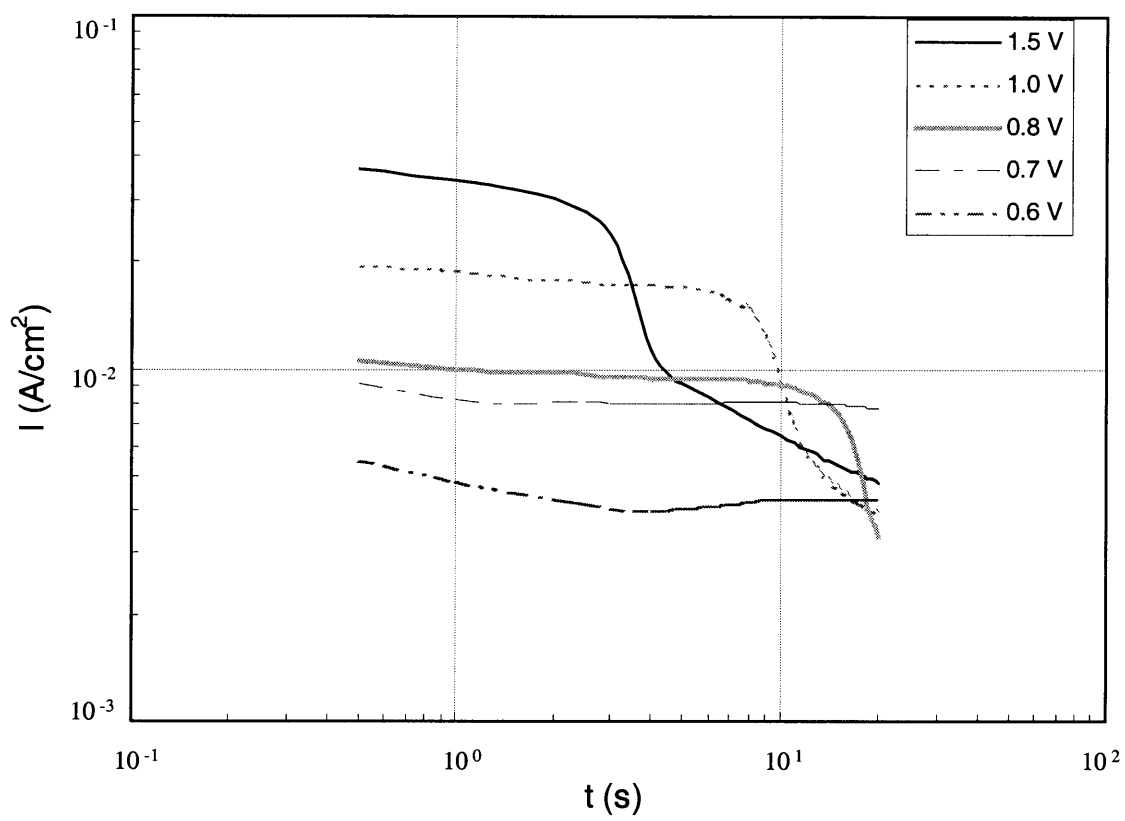
4.2.1.4 Current-Time Curves for Ta in 0.1 N HCl

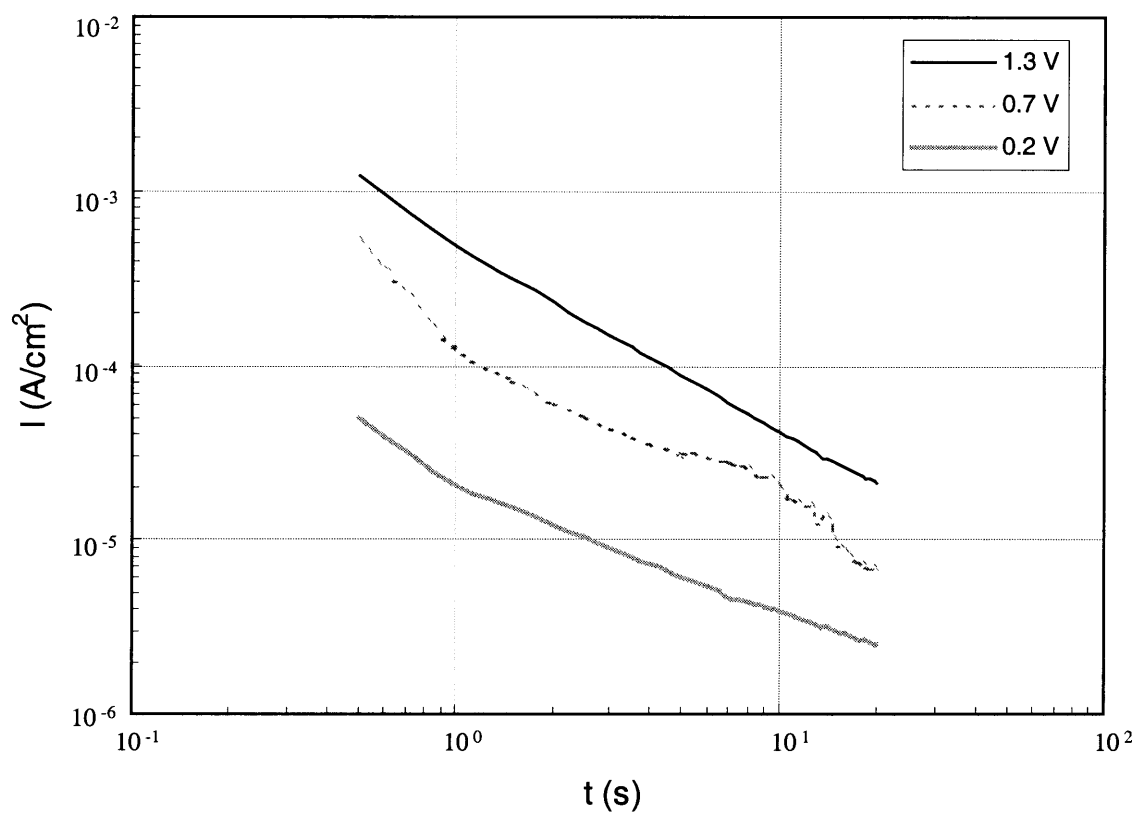Figure 4.2.1.5 Current-Time Curves for Ag in 0.1 N H_3PO_4
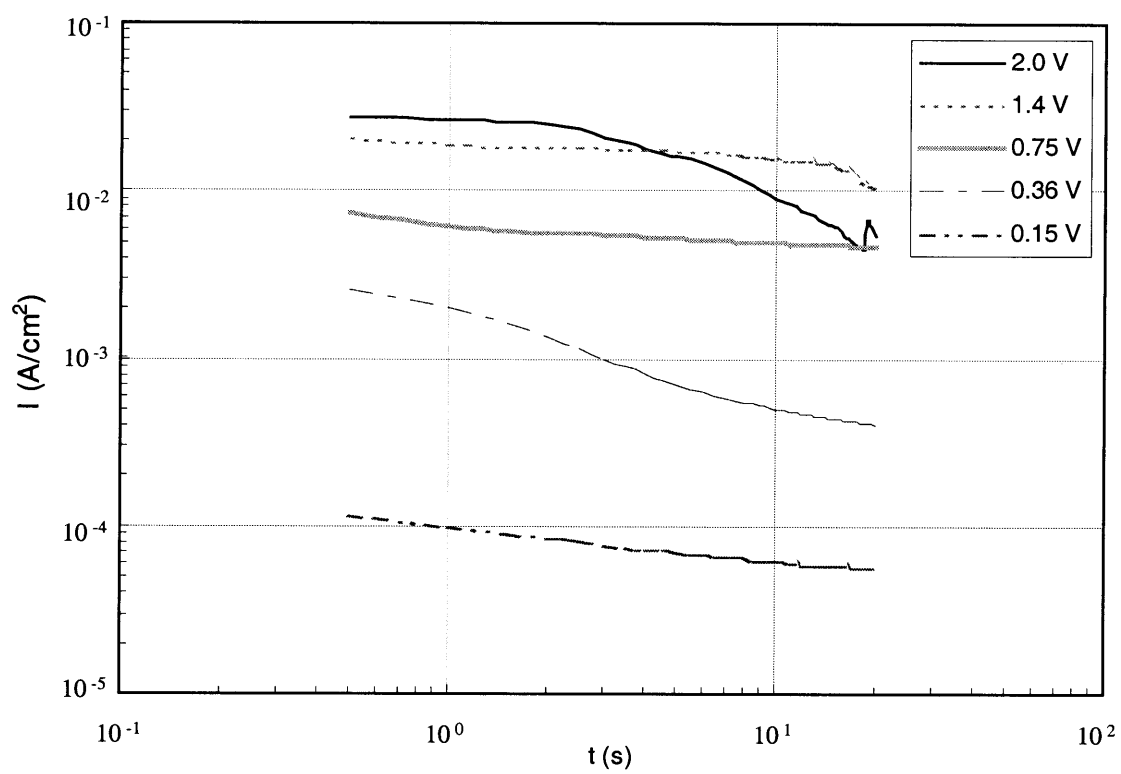
Figure 4.2.1.6 Current-Time Curves for TiN in 0.1 N H_3PO_4

Figure 4.2.1.7 Current-Time Curves for Ag/TiN in 0.1 N H_3PO_4

each other, but for the curve at 0.36 V a significant decrease in current is observed with increasing time. These results indicate that Ag/TiN is active at 0.15 V and passivates at 0.36, 0.75, 1.4, and 2.0 V. This passivation of Ag/TiN in H_3PO_4 is associated with the formation of Ag_3PO_4 on the specimen surface.

The results of the potentiostatic experiment for Ta in 0.1 N H_3PO_4 are shown in Figure 4.2.1.8. The highest current is observed at the potential value of 1.8 V and the lowest at 0.0 V. These curves show a decrease in current with increasing time. A slight decrease in current is observed for the curve obtained at 1.8 V after the first two seconds. The curves indicates that Ta is passive at 0.0, 1.0, and 1.8 V.

H_2SO_4

Figure 4.2.1.9 shows the results of the potentiostatic experiment for Ag in 0.1 N H_2SO_4. The highest current is observed at a potential value of 0.6 V and the lowest at 1.5 V. At the beginning of the experiments at 0.7, 1.0 and 1.5 V, the values of current density are higher than at 0.6 V, but these values significantly decrease at 18, 6 and 3 seconds, respectively. For the curve obtained at 0.7 V a slight decrease in current occurs with increasing time. This indicates that Ag is passive at 0.6, 0.7, 0.8, 1.0 and 1.5 V. This passivation is associated with the formation of $AgSO_4$ on the specimen surface.

For the TiN electrode, the results of the potentiostatic experiments in 0.1 N H_2SO_4 are shown in Figure 4.2.1.10. The highest current is observed at the potential value of 1.6 V and the lowest at 0.5 V. These curves show a decrease in current with increasing time. This indicates that TiN is passive at 0.5, 1.3, and 1.6 V.

Figure 4.2.1.11 shows the results of the potentiostatic experiment for Ag/TiN in 0.1 N H_2SO_4. The highest current is observed at the potential value of 0.62 V and the lowest at 0.24 V. At 1.6 V, values of current density values are higher than that for 0.6 V, but these values significantly decrease at 2 V. The shape of the I-t curves at 0.62 and 0.34
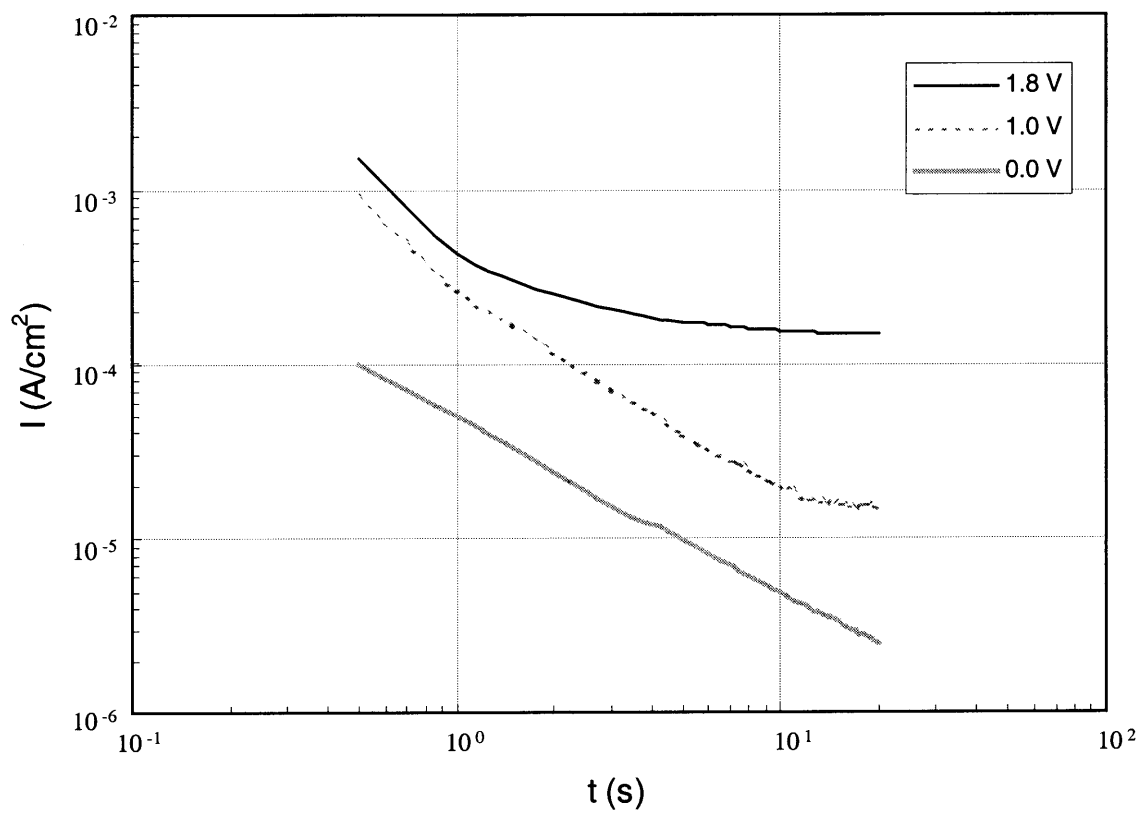
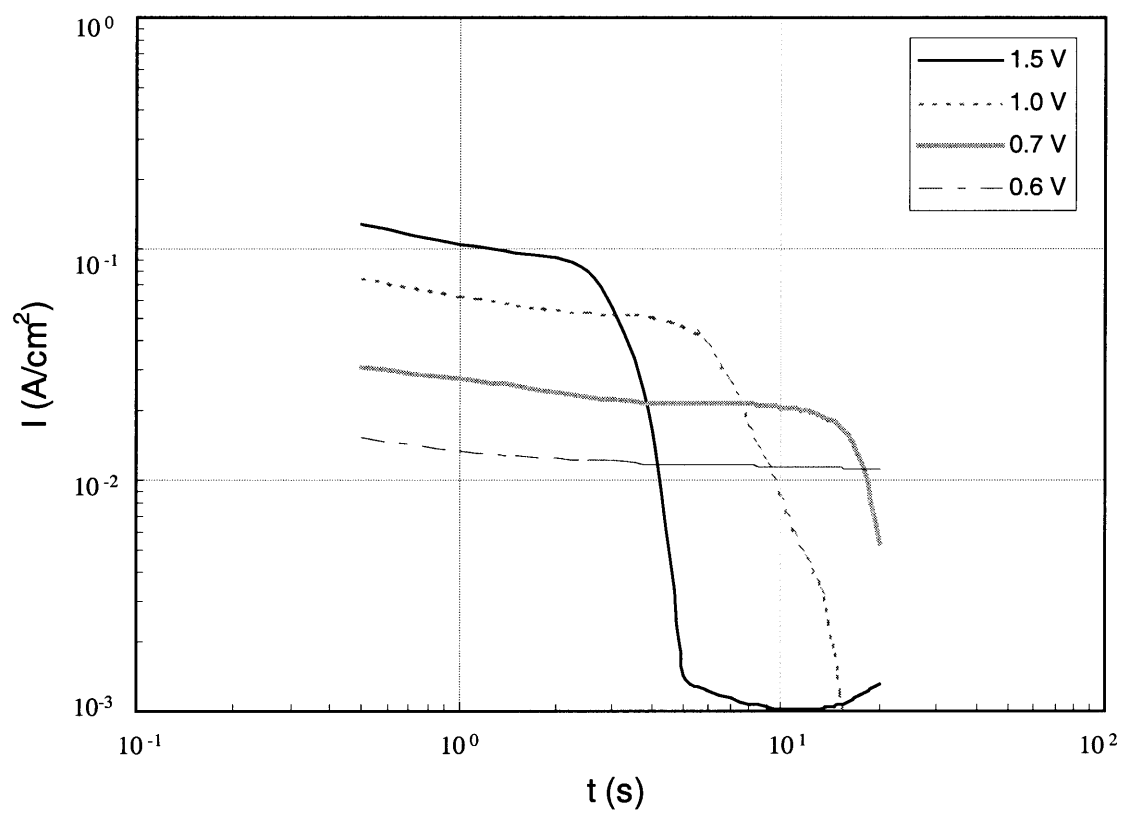4.2.1.8 Current-Time Curves for Ta in 0.1 N H₃PO₄
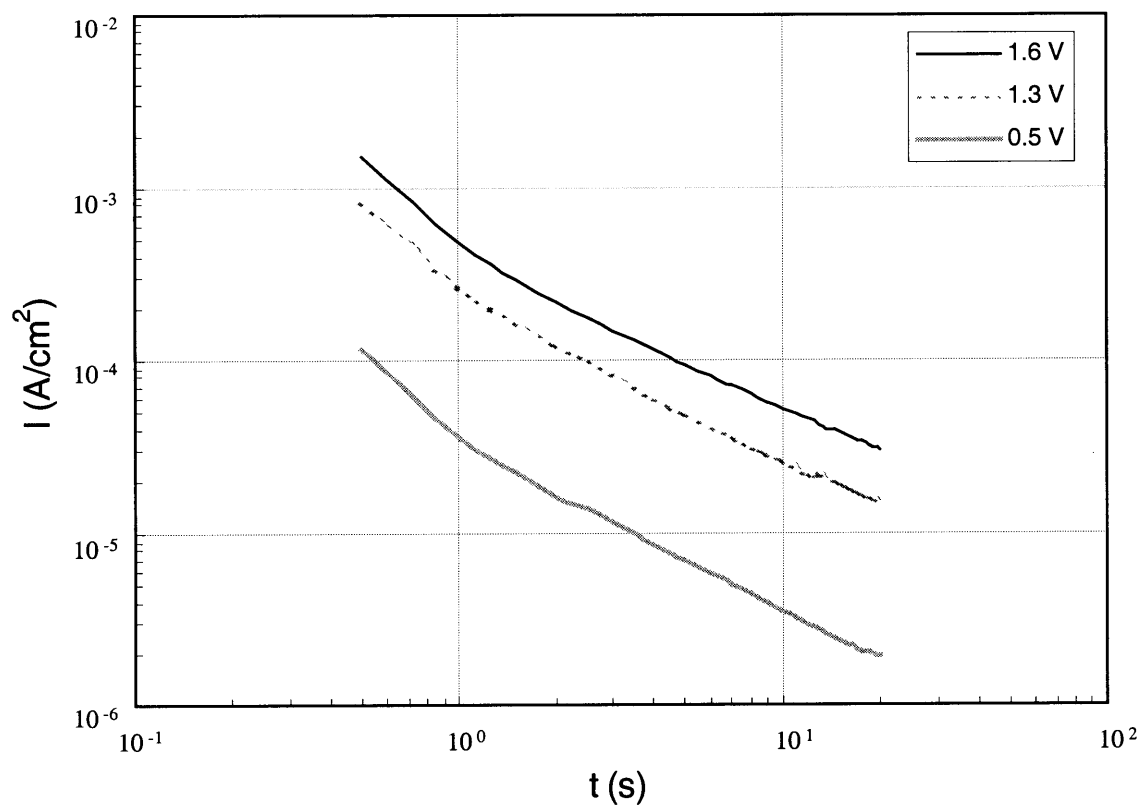
Figure 4.2.1.9 Current-Time Curves for Ag in 0.1 N H_2SO_4

Figure 4.2.1.10 Current-Time Curves for TiN in 0.1 N H_2SO_4
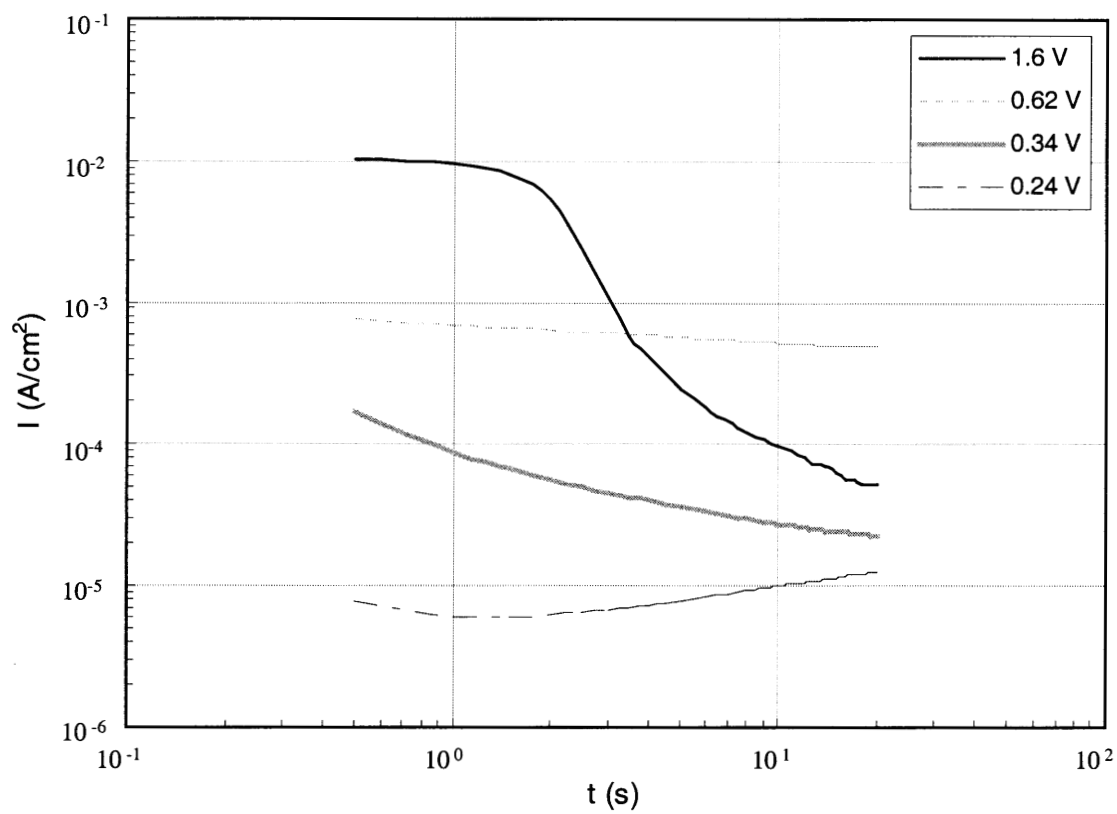
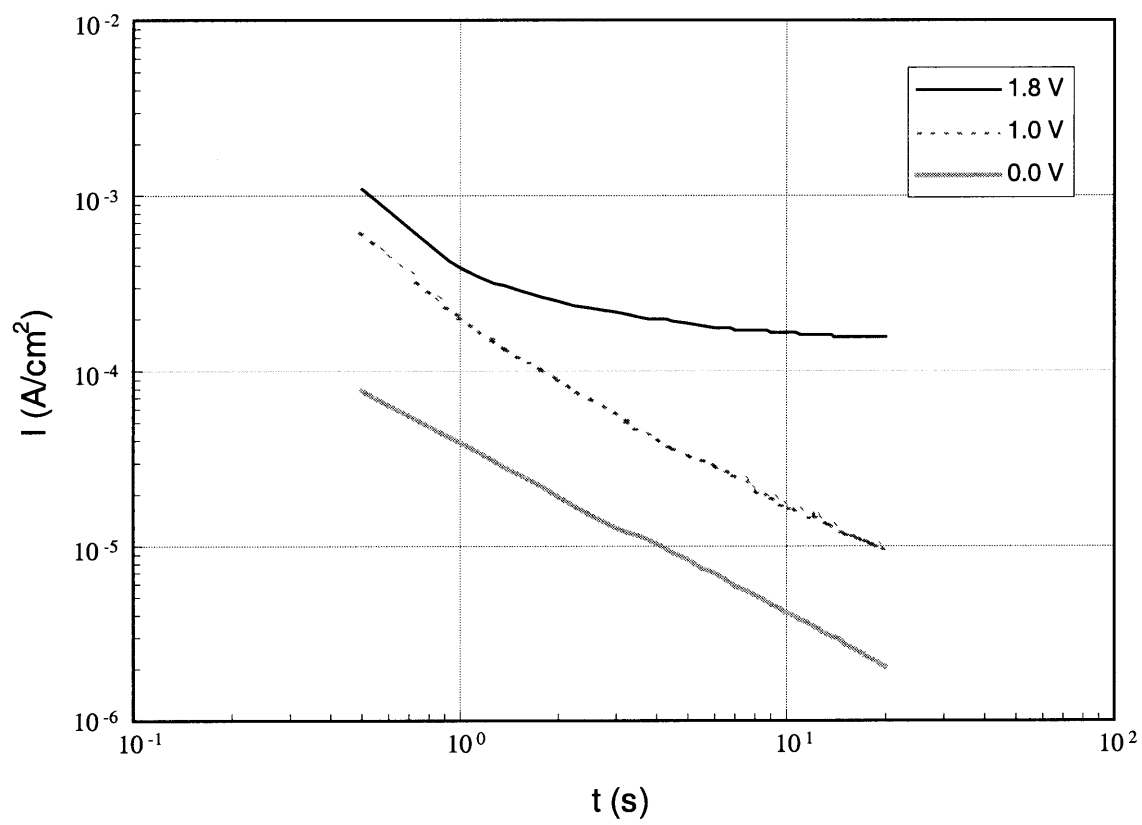Figure 4.2.1.11 Current-Time Curves for Ag/TiN in 0.1 N H_2SO_4

V are similar to each other, but for the curve at 0.34 V a significant decrease in current is observed with increasing time. For the curve obtained at 0.24 V, a slight increase in current is observed with increasing time. This indicates that Ag/TiN is active at 0.24 V and is passive at 0.34, 0.62 and 1.6 V. This passivation is associated with the formation of $AgSO_4$ on the specimen surface.

The results of the potentiostatic experiment for Ta in 0.1 N H_2SO_4 are shown in Figure 4.2.1.12. The highest current is observed at the potential value of 1.8 V and the lowest at 0.0 V. For the curve obtained at 1.8 V a significant decrease in current is observed for 1 second, and a slight decrease in current is observed for the rest of the experiment. These curves show a decrease in current with increasing time. This indicates that Ta is passive at 0.0, 1.0, and 1.8 V.

$H_2SO_4 + H_2O_2$

The results of the potentiostatic experiment for Ag in 0.1 N H_2SO_4 + 0.1 N H_2O_2 are shown in Figure 4.2.1.13. The highest current is observed at the potential value of 0.6 V and the lowest at 1.5 V. The shape of the I-t curves at 1.7 and 1.5 V, are similar to each other. In both curves a significant decrease in current is observed at approximately 1 sec, and a steady state is reached at 2 sec. Also, the shape of the I-t curves at 0.7 and 0.6 V, are similar to each other; both curves show a slight decrease in current with increasing time. This indicates that Ag is active at 0.6 and 0.7 V, and is passive at 1.7 and 1.5 V. This passivation is associated with the formation of $AgSO_4$ on the specimen surface.

For TiN, Figure 4.2.1.14 shows the results of the potentiostatic experiment in 0.1 N H_2SO_4 + 0.1 N H_2O_2. The highest current is observed at the potential value of 1.5 V and the lowest at 0.5 V. These curves show a decrease in current with increasing time. This indicates that TiN is passive at 0.5, 1.1, and 1.5 V.
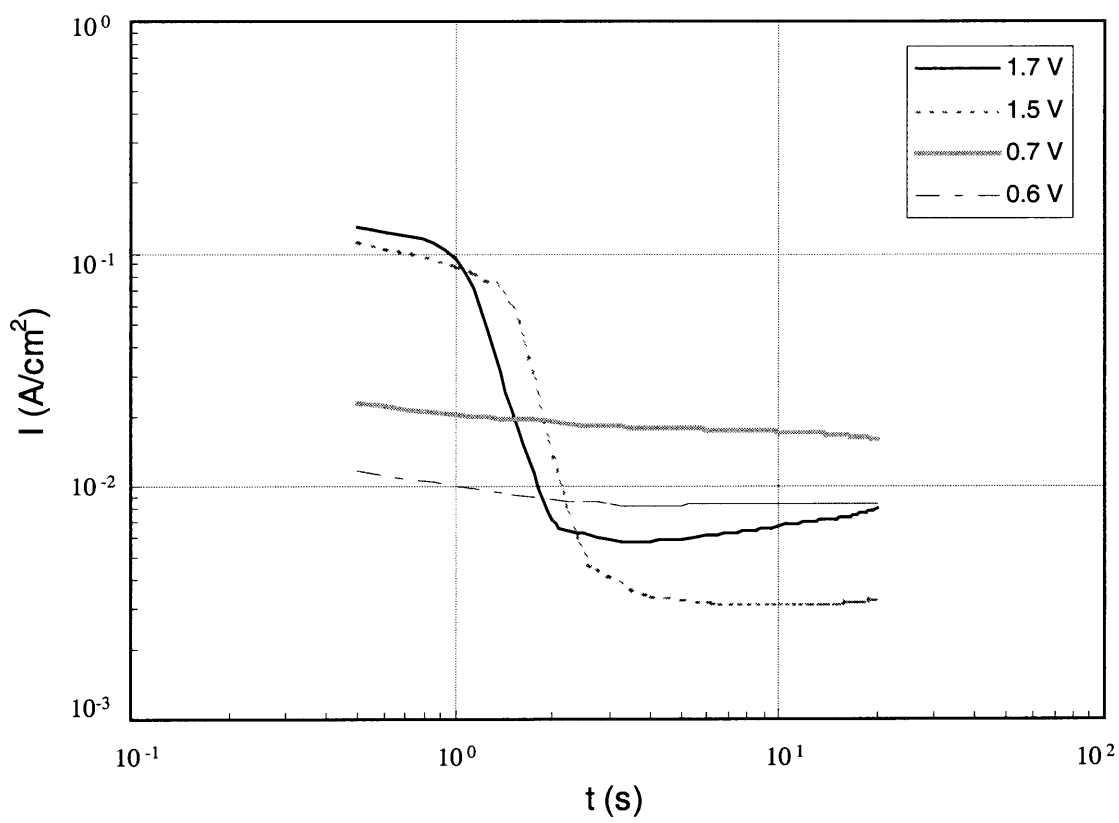
4.2.1.12 Current-Time Curves for Ta in 0.1 N H_2SO_4
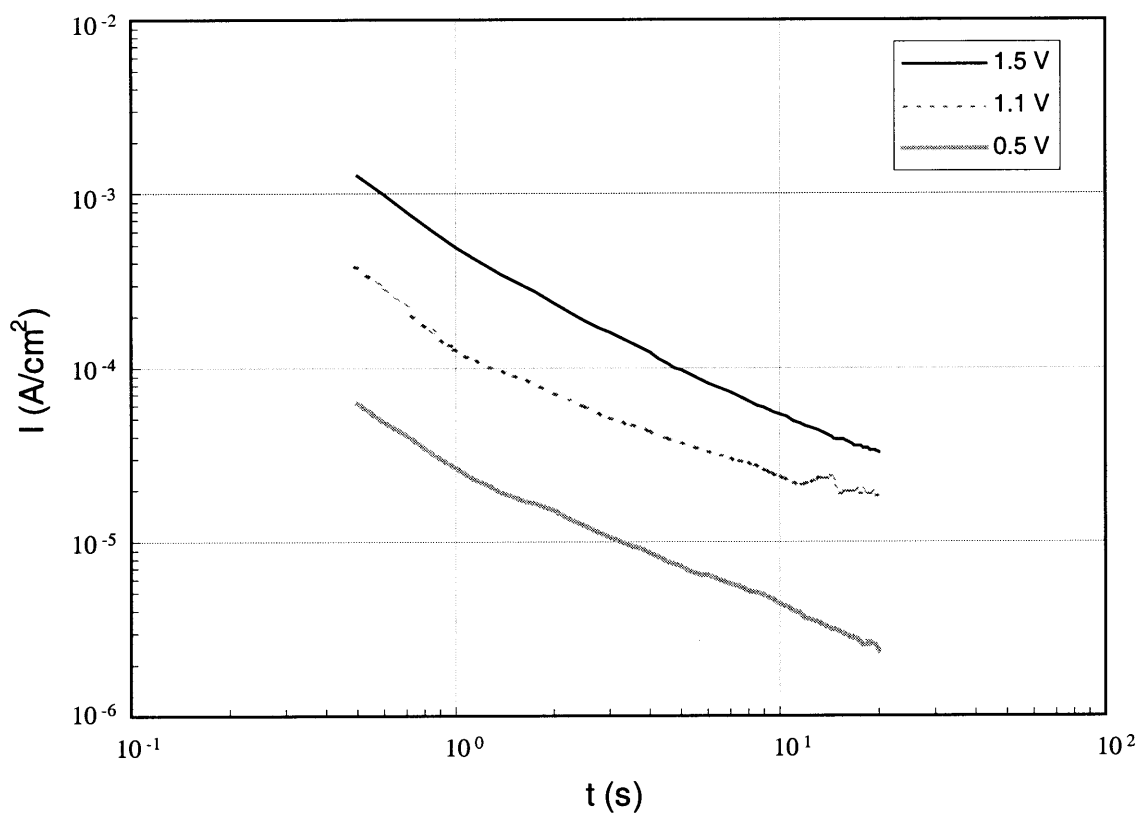
Figure 4.2.1.13 Current-Time Curves for Ag in 0.1 N H_2SO_4 + 0.1 N H_2O_2

Figure 4.2.1.14 Current-Time Curves for TiN in 0.1 N H_2SO_4 + 0.1 N H_2O_2

Figure 4.2.1.15 shows the results of the potentiostatic experiment for Ag/TiN in 0.1 N H_2SO_4 + H_2O_2. The highest current is observed at the potential value of 1.4 V and the lowest at 0.4 V. For the curve at 2.0 V a significant decrease in current is observed at approximately 4 sec. For the curve obtained at 1.4 V a decrease in current is observed after 16 sec. For the curve obtained at 0.06 V a slight decrease in current is observed with increasing time. This indicates that Ag/TiN is passive at 0.4, 0.6, 1.4, and 2.0 V. This passivation is associated with the formation of $AgSO_4$ on the specimen surface.

The results of the potentiostatic experiment for Ta in 0.1 N H_2SO_4 + H_2O_2 are shown in Figure 4.2.1.16. The highest current is observed at the potential value of 1.8 V and the lowest at 0.0 V. These curves show a decrease in current with increasing time. A slight decrease in current is observed for the curve obtained at 1.8 V after the first second. For the curve obtained at 0.0 V a slight decrease in current is observed for the first two seconds, and a significant decrease in current is observed for the rest of the experiment. The curves indicates that Ta is passive at 0.0, 1.0, and 1.8 V.

$Na_2B_4O_7$

For the Ag electrode, the results of the potentiostatic experiment in 0.1 N $Na_2B_4O_7$ are shown in Figure 4.2.1.17. The highest current is observed at the potential value of 1.5 V, and the lowest at 0.5 V. For the curves obtained at 1.5 and 1.0 V, a significant decrease in current is observed for the first second, and a slight decrease in current is observed for the rest of the experiment. For the curve obtained at 0.5 V, a decrease in current is observed at 3 sec. This indicates that Ag is passive at 0.5, 1.0, and 1.5 V.

Figure 4.2.1.18 shows the results of the potentiostatic experiment for TiN in 0.1 N $Na_2B_4O_7$. The highest current is observed at 1.3 V and the lowest at 0.2 V. These curves show a decrease in current with increasing time. This indicates that TiN is passive at 0.2, 0.7, and 1.3 V.
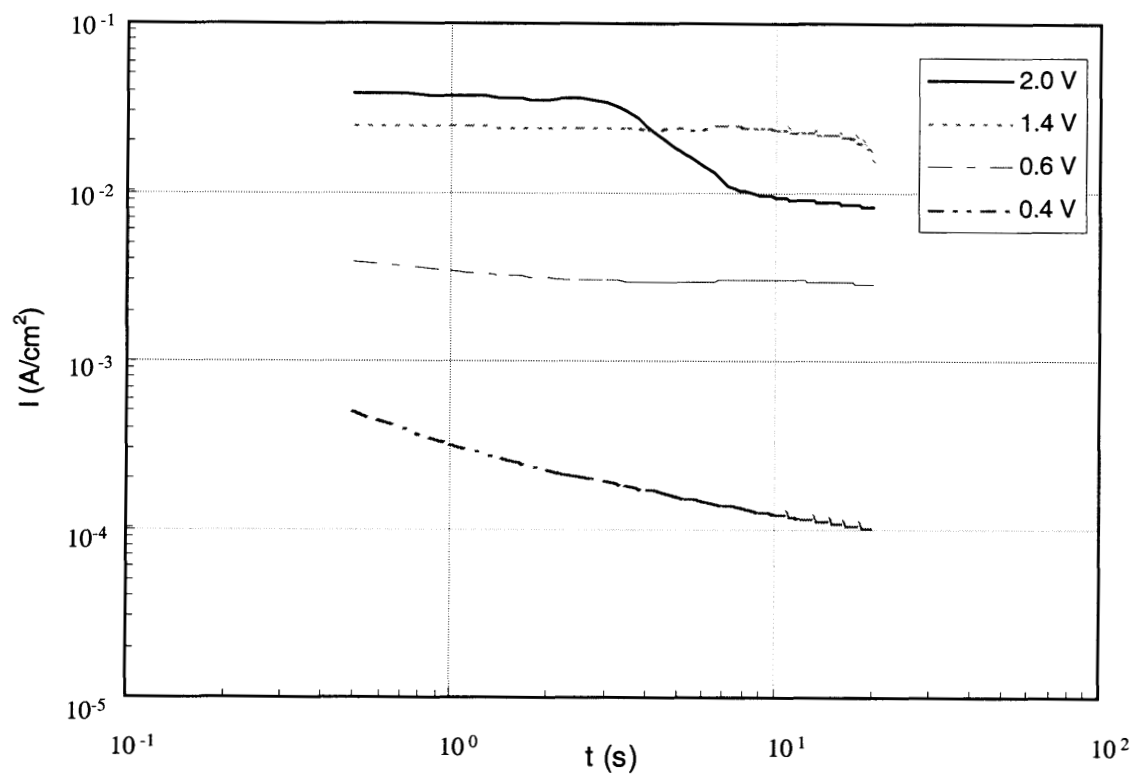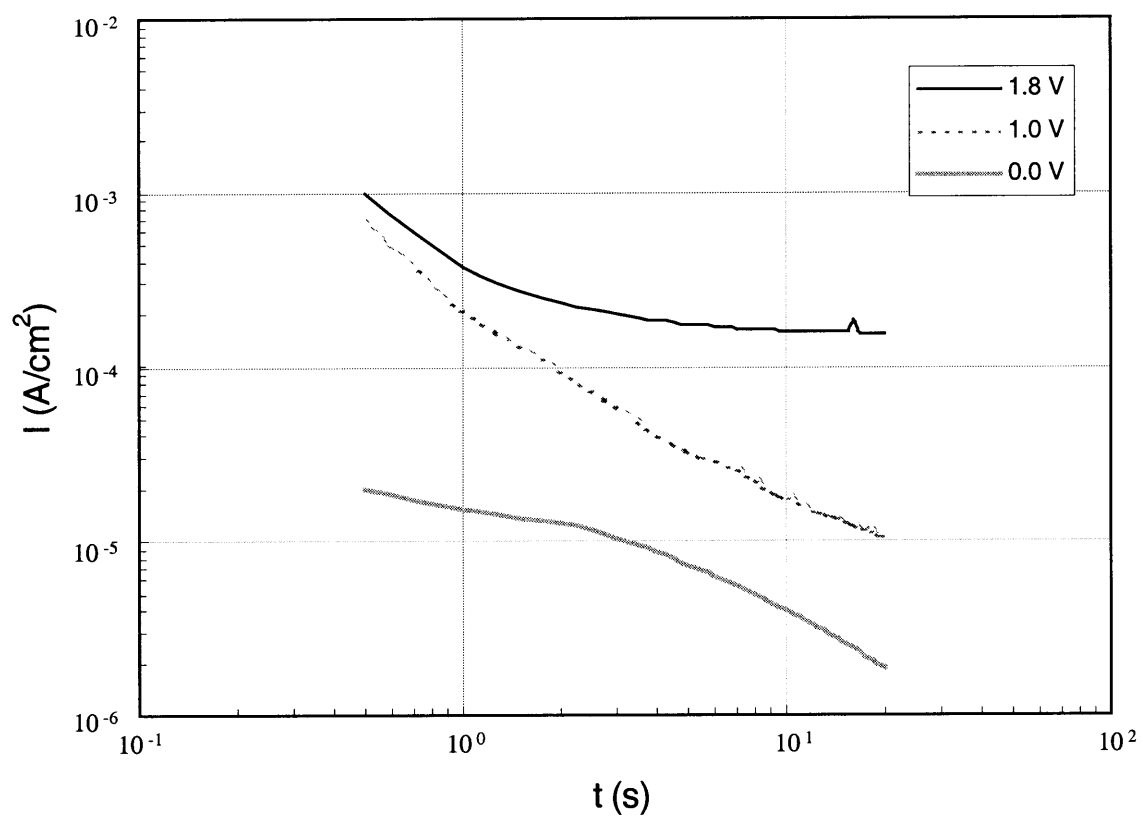
Figure 4.2.1.15 Current-Time Curves for Ag/TiN in 0.1 N H_2SO_4 + 0.1 N H_2O_2
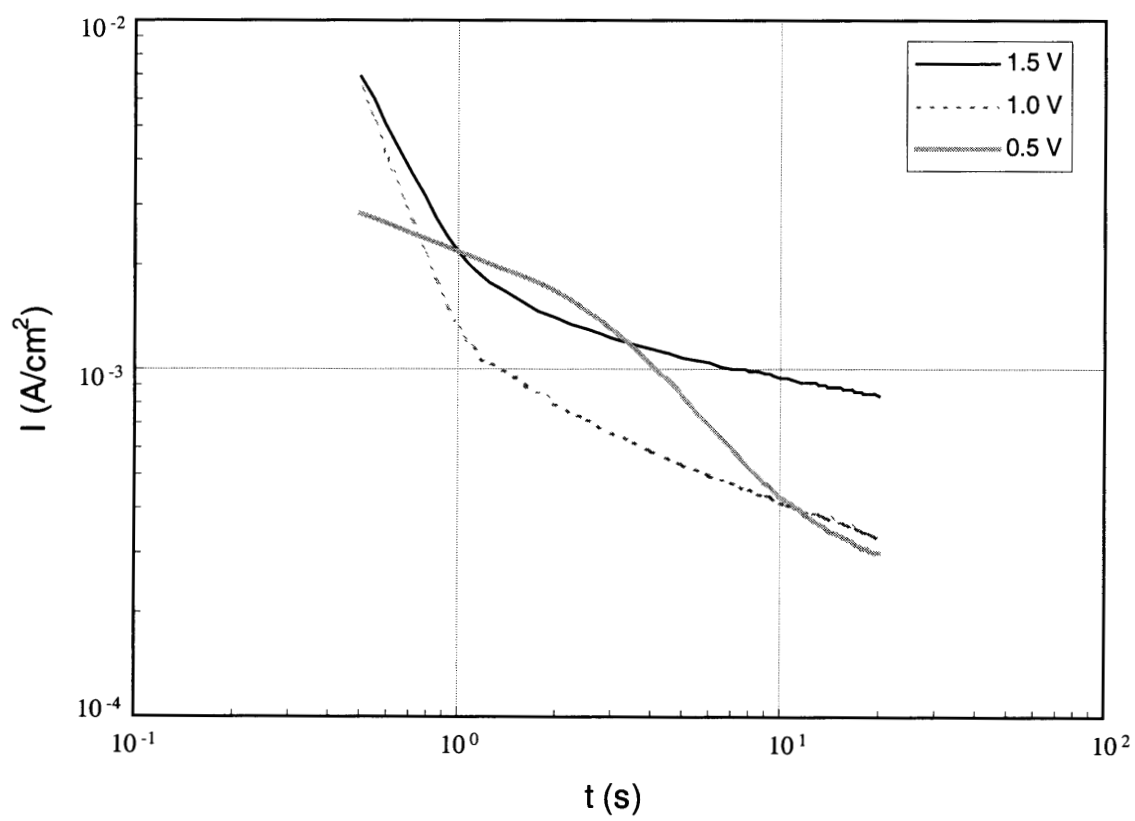
4.2.1.16 Current-Time Curves for Ta in 0.1 N H_2SO_4 + 0.1 N H_2O_2

Figure 4.2.1.17 Current-Time Curves for Ag in 0.1 N $Na_2B_4O_7$
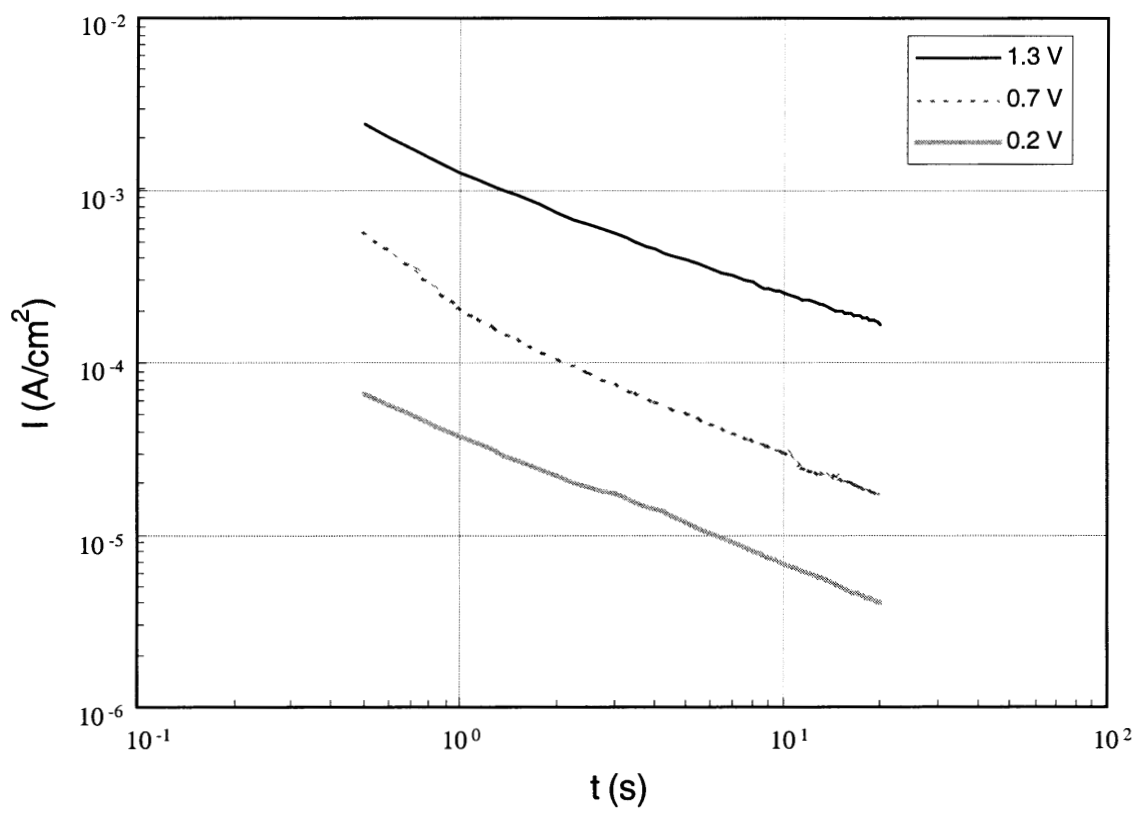
Figure 4.2.1.18 Current-Time Curves for TiN in 0.1 N $Na_2B_4O_7$

The results of the potentiostatic experiment for Ag/TiN in 0.1 N $Na_2B_4O_7$ are shown in Figure 4.2.1.19. The shape of the I-t curves at 0.2, 0.55, 1.0, and 1.5 V, are similar to each other. These curves show an increase in current with increasing time, which indicates that Ag/TiN is active at the applied potentials.

The results of the potentiostatic experiment for Ta in 0.1 N $Na_2B_4O_7$ are shown in Figure 4.2.1.20. The highest current is observed at the potential value of 1.4 V and the lowest at 0.0 V. These curves show a decrease in current with increasing time. The shape of the I-t curves at 0.0, 0.7, and 1.4 V are similar to each other. This indicates that Ta is passive at this values of potential.

4.2.2 Aqueous Organic Solutions

Tetramethylammonium hydroxide

For the Ag electrode, Figure 4.2.2.1 shows the results of the potentiostatic experiment when it is immersed in 0.1 N $(CH_3)_4NOH$. The highest current value is observed at 0.54 and the lowest at 0.5 V. The curve obtained at 0.54 V shows three zones. In the first zone (the first 2 seconds) a decrease in current occurs. For the second zone (between 2 and 10 seconds), an increase in current occurs until a maximum current of 1.5 x 10^{-3} A/cm^2. In the third zone (time > 10 seconds), the current decreases. The shape of the I-t curves at 0.28, 0.50, and 0.65 V, are similar to each other, and indicates that Ag is passive at these potentials.

The results of the potentiostatic experiment for TiN in 0.1 N $(CH_3)_4NOH$ are shown in Figure 4.2.2.2. The highest current is observed at 1.3 V and the lowest at 0.2 V. These curves show a decrease in current with increasing time. This indicates that TiN is passive at 0.2, 0.7, and 1.3 V.
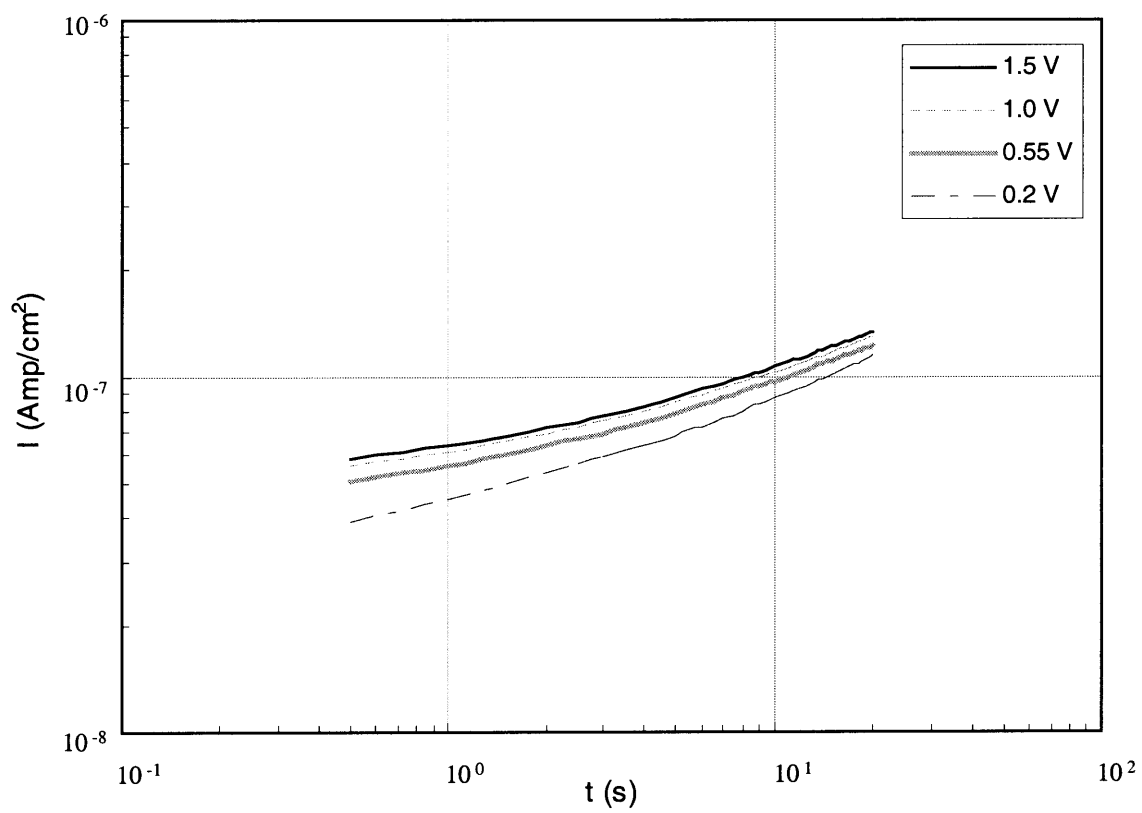
Figure 4.2.1.19 Current-Time Curves for Ag/TiN in 0.1 N $Na_2B_4O_7$
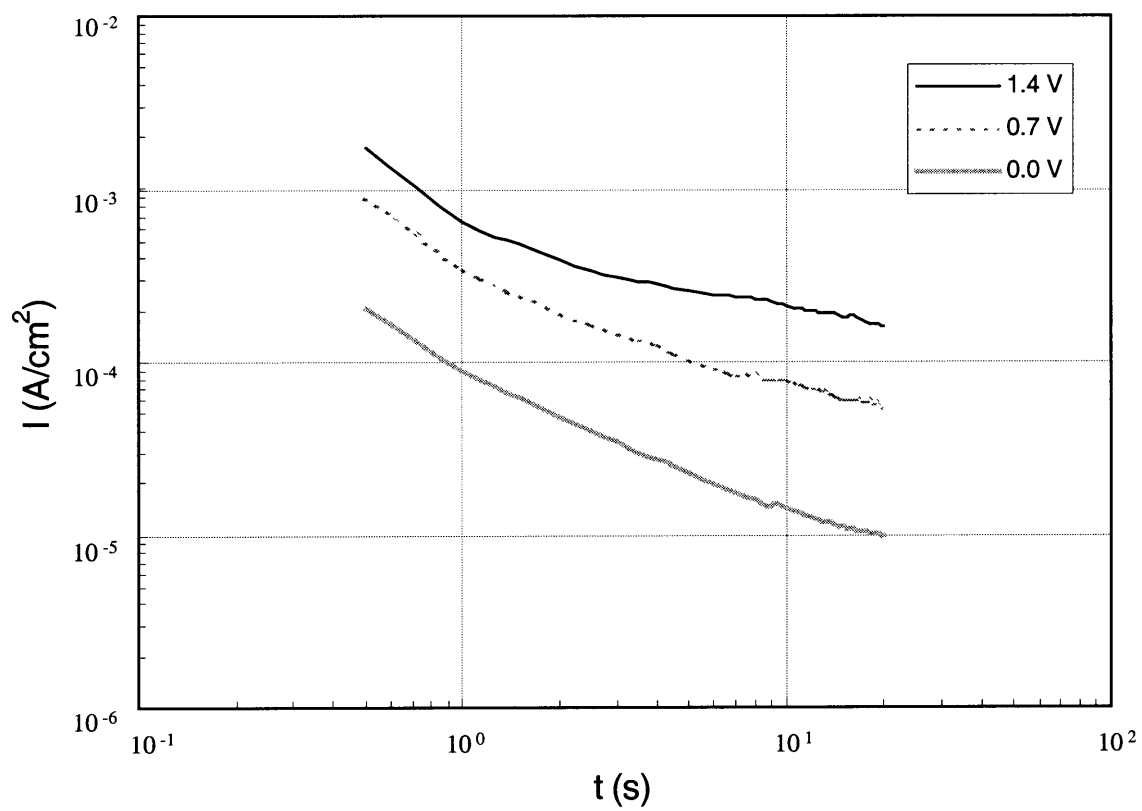
4.2.1.20 Current-Time Curves for Ta in 0.1 N $Na_2B_4O_7$
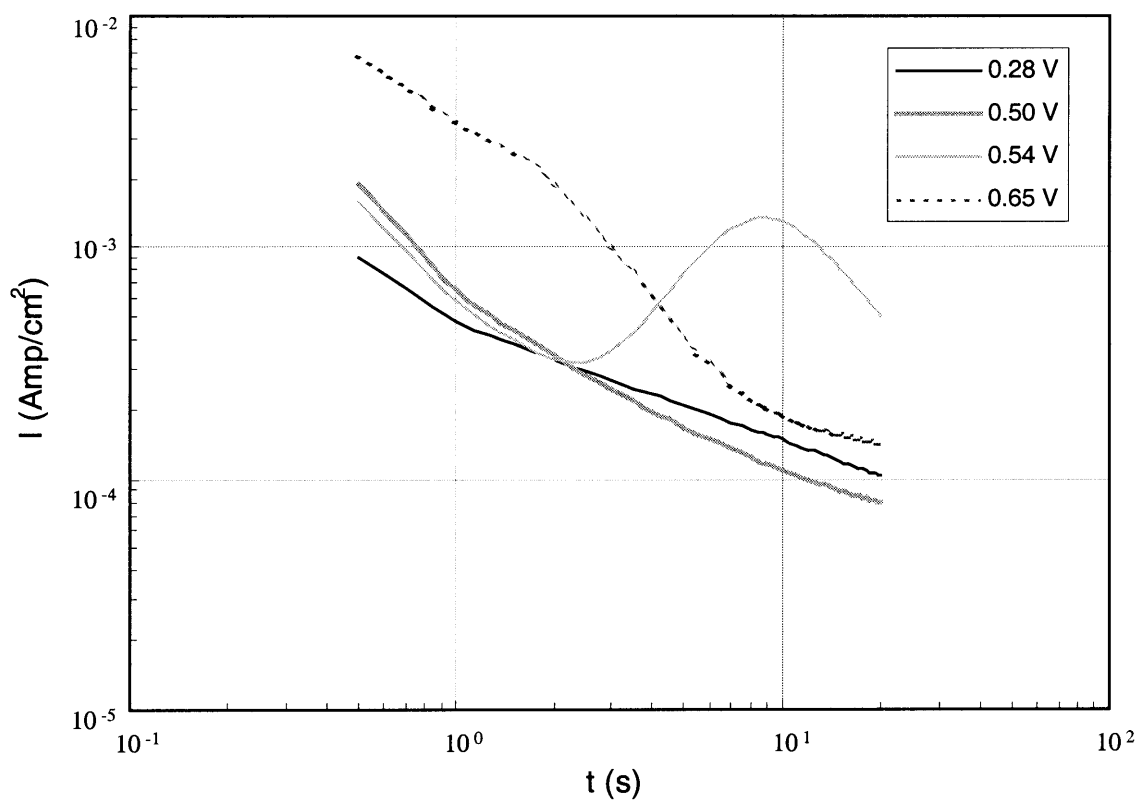
Figure 4.2.2.1 Current-Time Curves for Ag in 0.1 N $(CH_3)_4NOH$
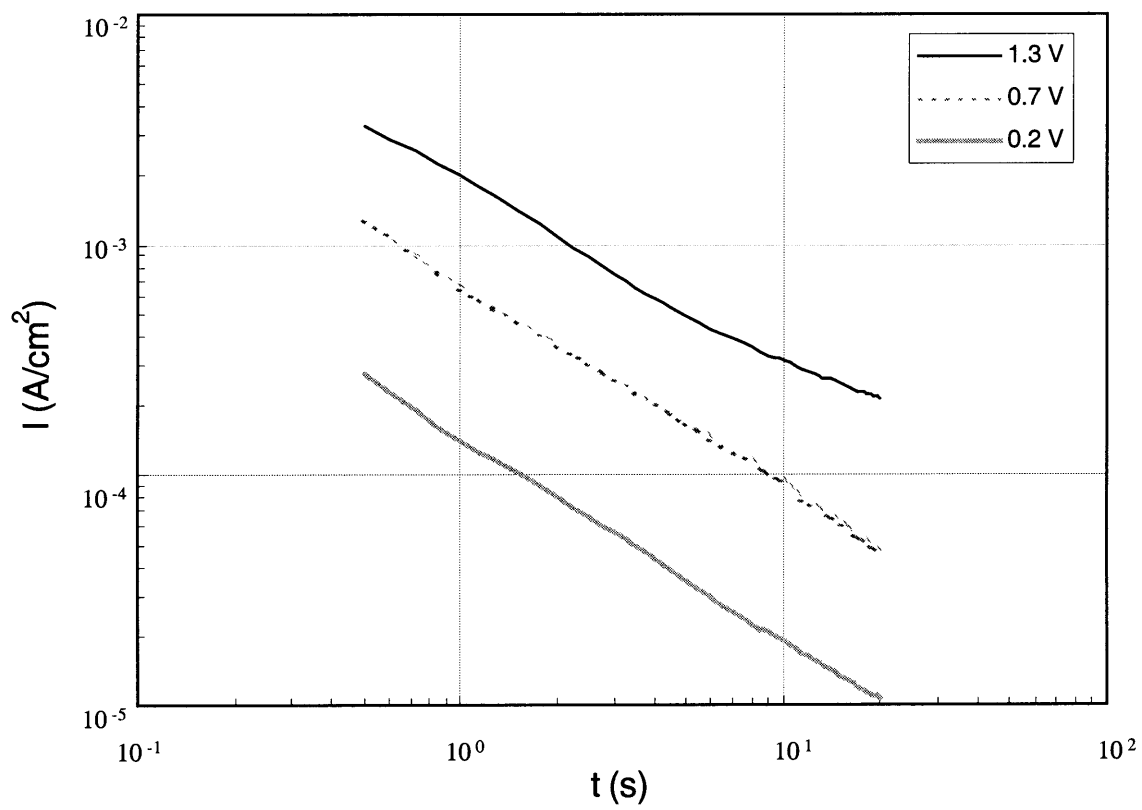
Figure 4.2.2.2 Current-Time Curves for TiN in 0.1 N $(CH_3)_4NOH$

Figure 4.2.2.3 shows the results of the potentiostatic experiment for Ag/TiN in 0.1 N $(CH_3)_4NOH$. The shape of the I-t curves at 0.4, 0.8, 1.2, 1.6, and 2.0 V are similar to each other. These curves show an increase in current with increasing time, which indicates that Ag/TiN is active at the applied potentials.

The results of the potentiostatic experiment for Ta in 0.1 N $(CH_3)_4NOH$ are shown in Figure 4.2.2.4. The highest current is observed at the potential value of 1.3 V and the lowest at 0.0 V. These curves show a decrease in current with increasing time. The curves indicates that Ta is passive at 0.0, 0.5, and 1.3 V.

4.3 Open Circuit Potentials Measurements

4.3.1 Ag

The open circuit potentials values for Ag in HCl, H_3PO_4, H_2SO_4, $H_2SO_4 + H_2O_2$, $Na_2B_4O_7$, and $(CH_3)_4NOH$ are shown in Figures 4.3.1a. In each solution, the potential values appear not to change with increasing time. After 6 hours of exposure, Ag shows the lowest potential value in HCl and $(CH_3)_4NOH$ and the highest in H_2SO_4 and $H_2SO_4 + H_2O_2$. In H_3PO_4, Ag had a slightly higher potential value in $Na_2B_4O_7$. All the measured potential values are between 26 mV and 180 mV, as shown in Figure 4.3.1b.

4.3.2 TiN

Figure 4.3.2a shows the open circuit potentials values for TiN in HCl, H_3PO_4, H_2SO_4, $H_2SO_4 + H_2O_2$, $Na_2B_4O_7$, and (CH_3). After 6 hours of exposure, TiN shows the lowest potential value in HCl and $(CH_3)_4NOH$ and the highest in $H_2SO_4 + H_2O_2$. In H_2SO_4, TiN had an increment in potential in 200 mV. Also, TiN shows similar potential values in $Na_2B_4O_7$ and H_3PO_4. All the measured potential values are between −180 mV and 390 mV, as shown in Figure 4.3.2b.
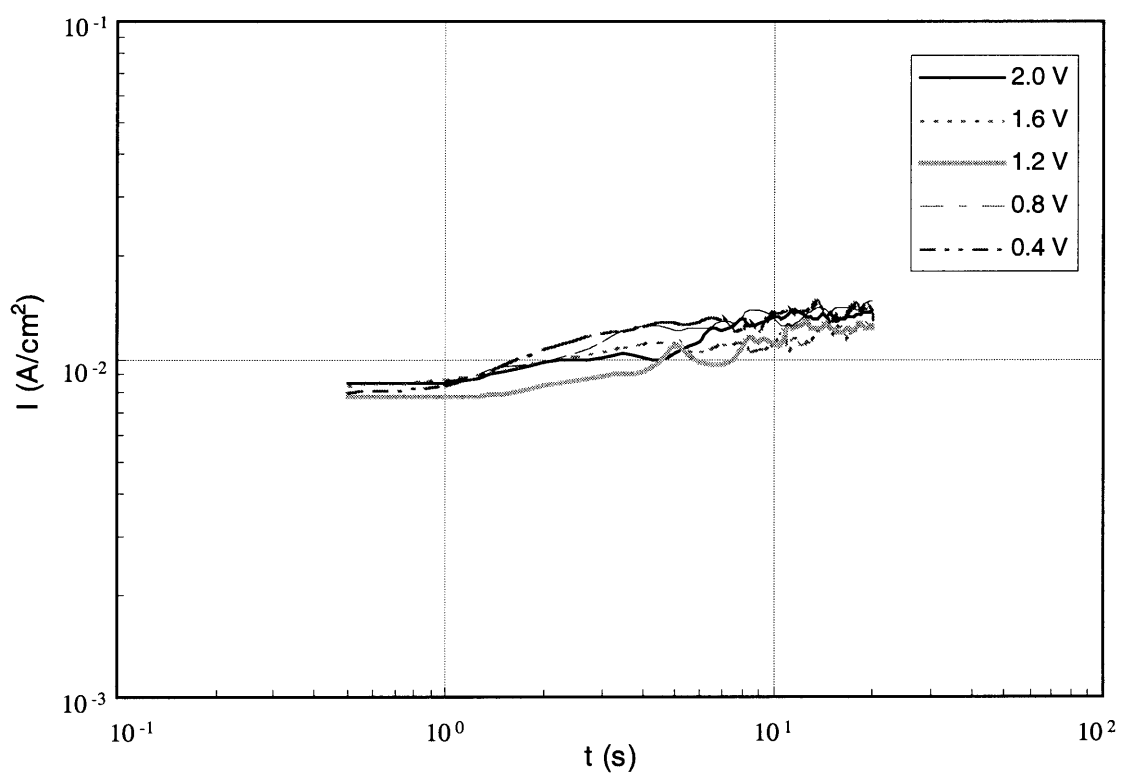
Figure 4.2.2.3 Current-Time Curves for Ag/TiN in 0.1 N $(CH_3)_4NOH$
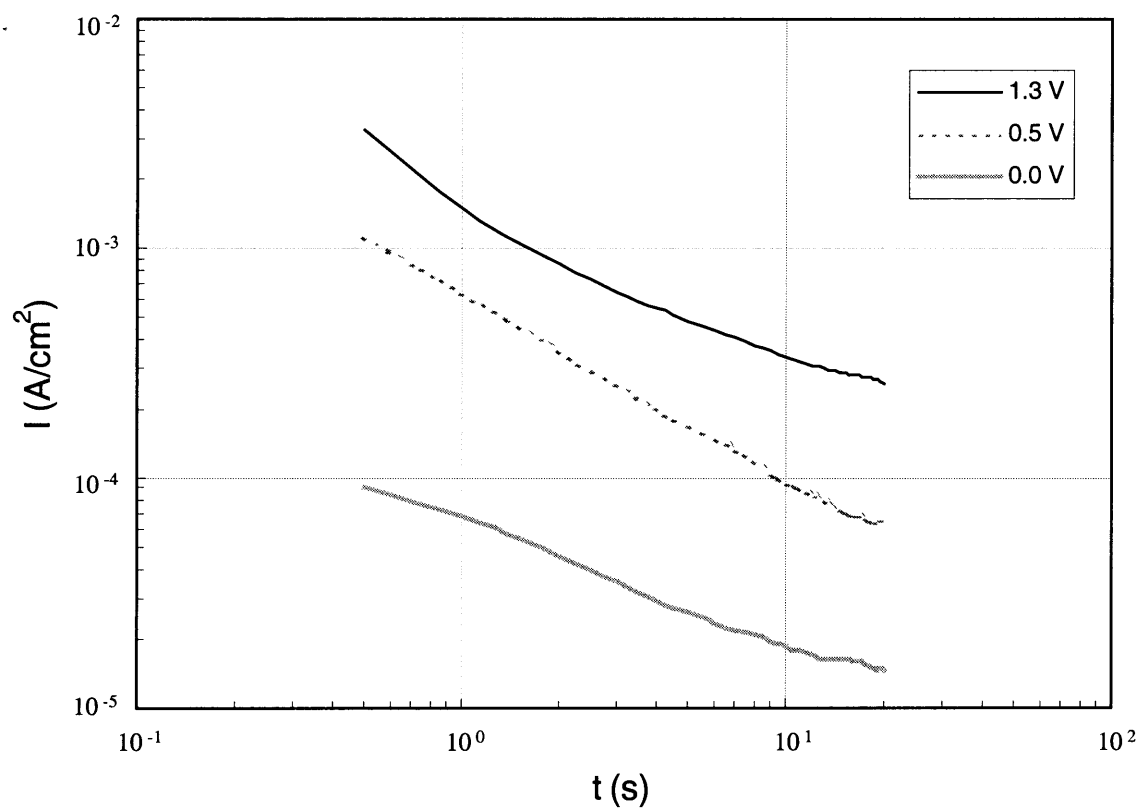
4.2.2.4 Current-Time Curves for Ta in 0.1 N $(CH_3)_4NOH$

Figure 4.3.1a Open circuit potential values for Ag in HCl, H_3PO_4, H_2SO_4, $H_2SO_4 + H_2O_2$, $Na_2B_4O_7$, and $(CH_3)_4NOH$

Figure 4.3.1b Potential values for Ag in HCl, H_3PO_4, H_2SO_4, $H_2SO_4 + H_2O_2$, $Na_2B_4O_7$, and $(CH_3)_4NOH$

	0.1 N HCl	0.1 N H_3PO_4	0.1 N H_2SO_4	0.1 N H_2SO_4 + 0.1 N H_2O_2	0.1 N $Na_2B_4O_7$	0.1 N $(CH_3)_4NOH$
■ Ag	0.026	0.116	0.18	0.18	0.104	0.045
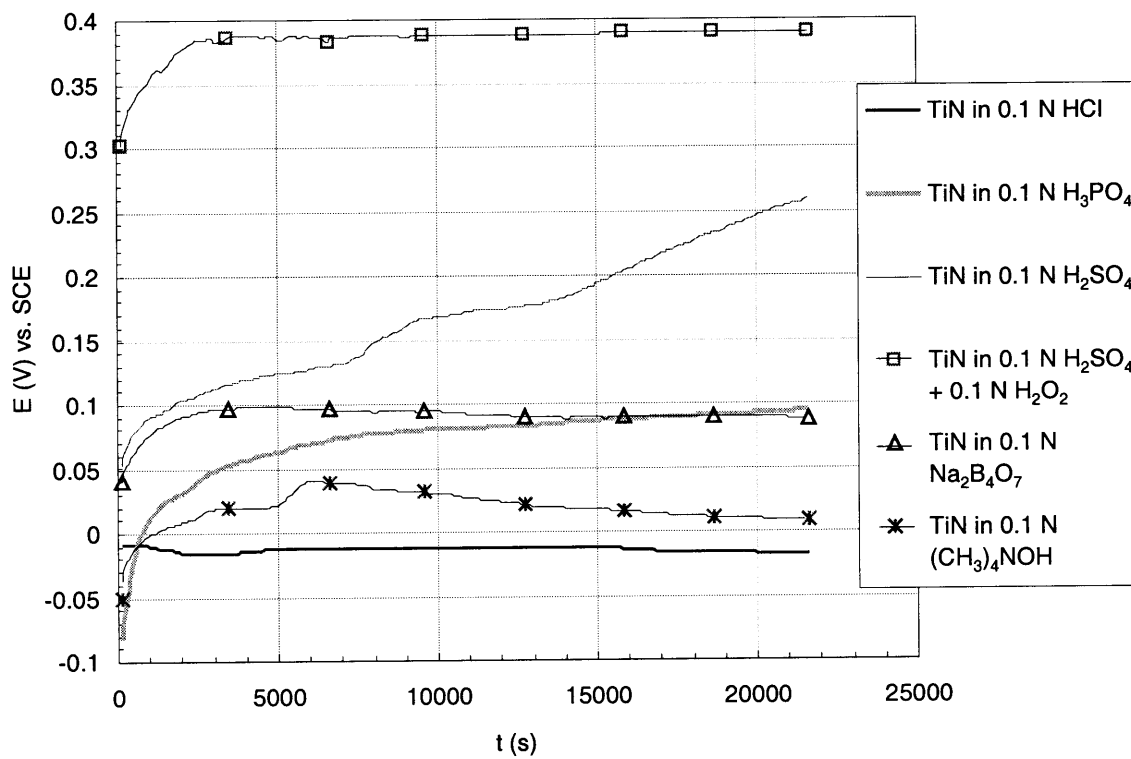
Figure 4.3.2a Open circuit potential values for TiN in HCl, H_3PO_4, H_2SO_4, H_2SO_4 + H_2O_2, $Na_2B_4O_7$, and $(CH_3)_4NOH$

🔲 TiN	0.1 N HCl	0.1 N H₃PO₄	0.1 N H₂SO₄	0.1 N H₂SO₄ + 0.1 N H₂O₂	0.1 N Na₂B₄O₇	0.1 N (CH₃)₄NOH
	-0.18	0.1	0.25	0.39	0.09	0.008

Figure 4.3.2b Potential values for TiN in HCl, H_3PO_4, H_2SO_4, $H_2SO_4 + H_2O_2$, $Na_2B_4O_7$, and $(CH_3)_4NOH$

4.3.3 Ag/TiN

For Ag/TiN, open circuit potentials values in HCl, H_3PO_4, H_2SO_4, $H_2SO_4 + H_2O_2$, $Na_2B_4O_7$, and $(CH_3)_4NOH$ are shown in Figures 4.3.3a. In each solution, the potential values appear not to change with increasing time. The lowest potential value for Ag/TiN after 6 hours of exposure is observed in HCl and $(CH_3)_4NOH$, and the highest in $H_2SO_4 + H_2O_2$. In H_3PO_4. All the measured potential values are between 24 mV and 190 mV, as shown in Figure 4.3.3b.

4.3.4 Ta

The open circuit potentials values for Ta in HCl, H_3PO_4, H_2SO_4, $H_2SO_4 + H_2O_2$, $Na_2B_4O_7$, and $(CH_3)_4NOH$ are shown in Figures 4.3.4a. After 6 hours of exposure, Ta shows the lowest potential value in HCl, $(CH_3)_4NOH$, and $Na_2B_4O_7$. The highest value of potential is observed in H_2SO_4 and $H_2SO_4 + H_2O_2$. All the measured potential values are between -472 mV and 20 mV, as shown in Figure 4.3.4b.

4.4. Solution Corrosivity

4.4.1 Ag

Figure 4.4.1a shows the anodic polarization curves of Ag immersed in oxidizing solutions, like 0.1 N H_2SO_4 and in 0.1 N H_2SO_4 + 0.1 N H_2O_2. In both solutions, Ag shows active, active-passive, and passive behavior. Current density in the passive region starts at 2 x 10^{-3} A/cm^2 in H_2SO_4 and 5 x 10^{-3} A/cm^2 in $H_2SO_4 + H_2O_2$, at a potential value of 0.8 V, on both curves.

Figure 4.4.1b shows the anodic polarization curves of Ag immersed in non-oxidizing solutions, like 0.1 N HCl, 0.1 N H_3PO_4, 0.1 N $Na_2B_4O_7$, and 0.1 N $(CH_3)_4NOH$.
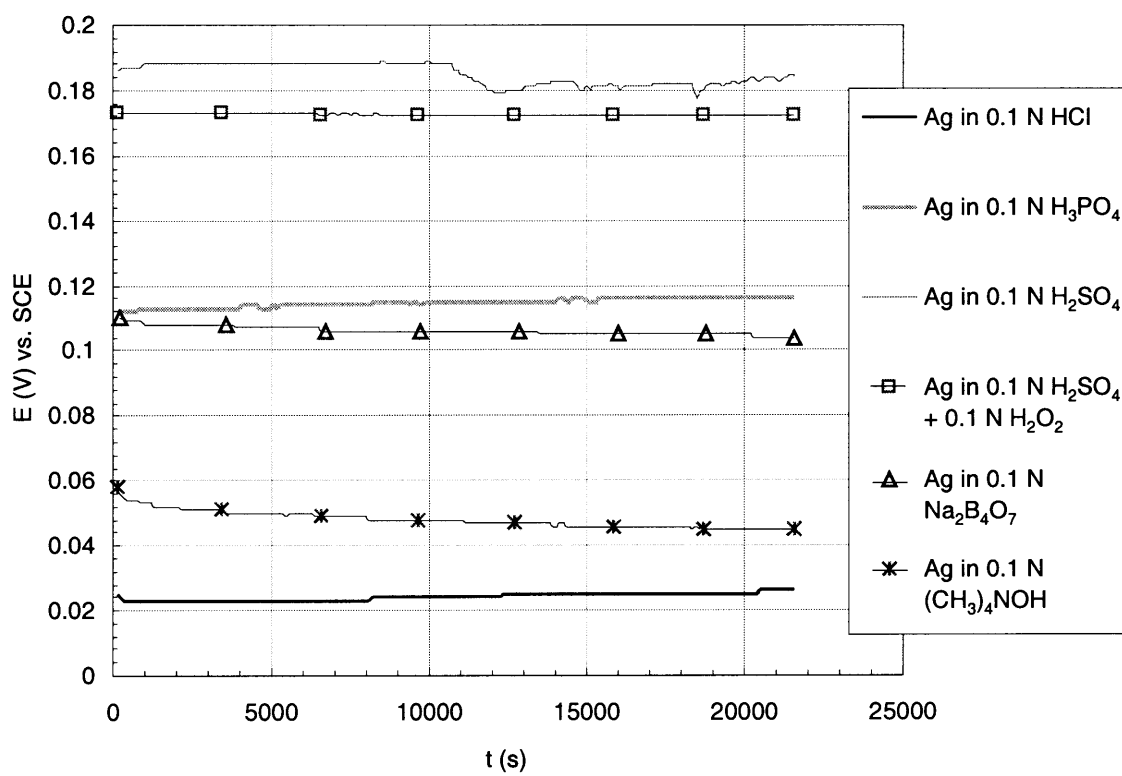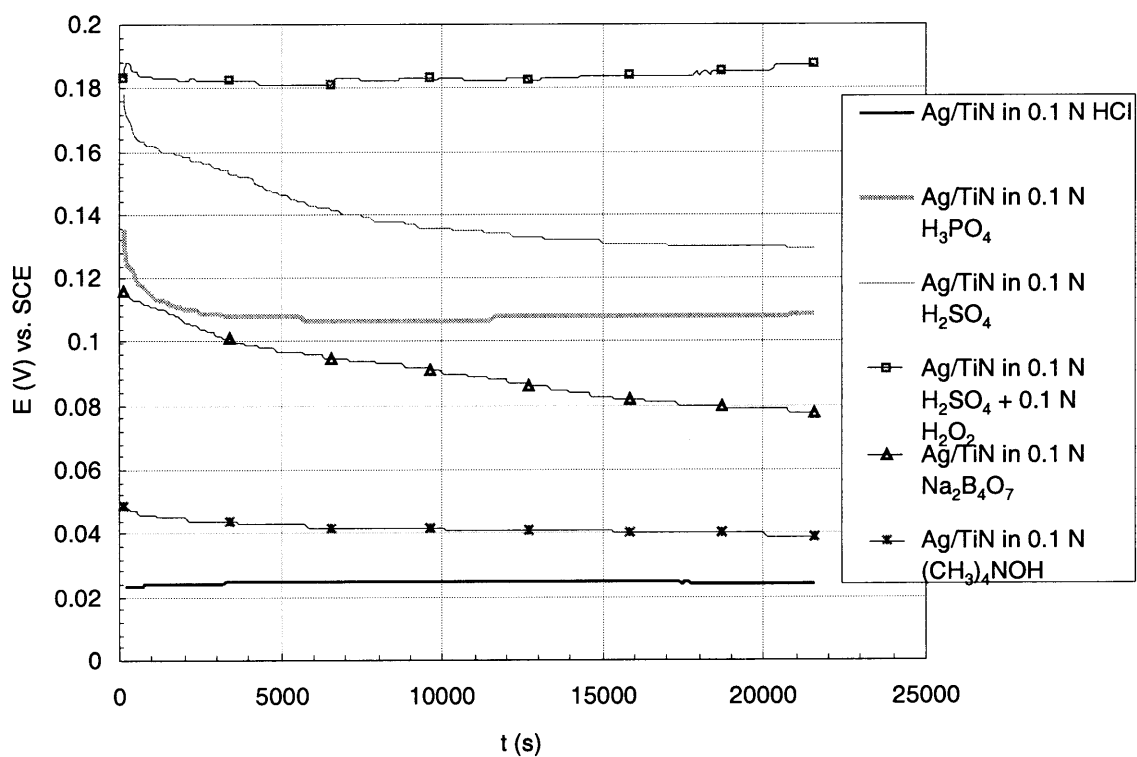
Figure 4.3.3a Open circuit potential values for Ag/TiN in HCl, H₃PO₄, H₂SO₄, H₂SO₄ + H₂O₂, Na₂B₄O₇, and (CH₃)₄NOH
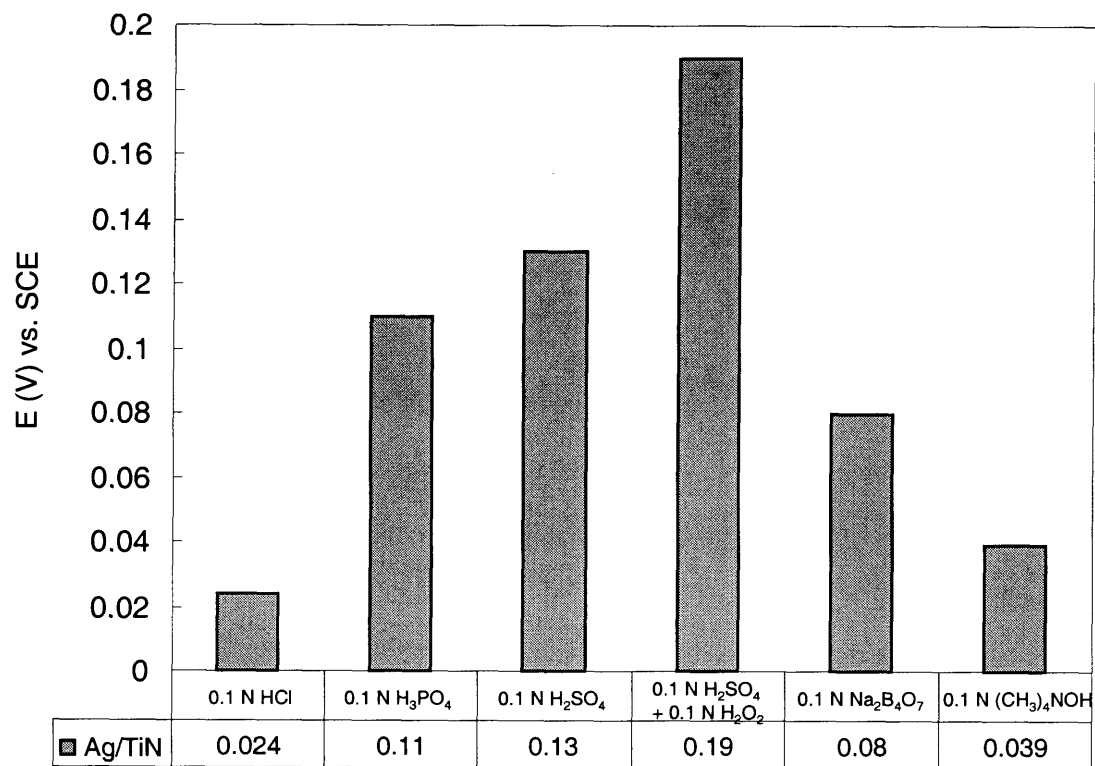
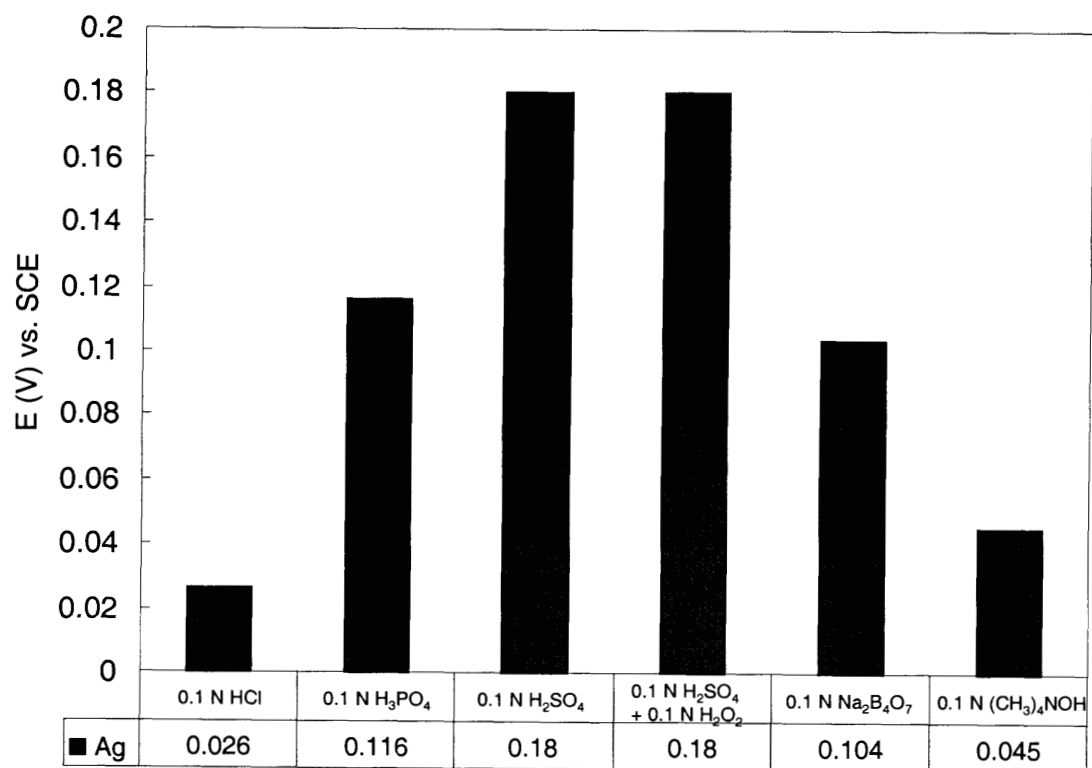Figure 4.3.3b Potential values for Ag/TiN in HCl, H_3PO_4, H_2SO_4, $H_2SO_4 + H_2O_2$, $Na_2B_4O_7$, and $(CH_3)_4NOH$
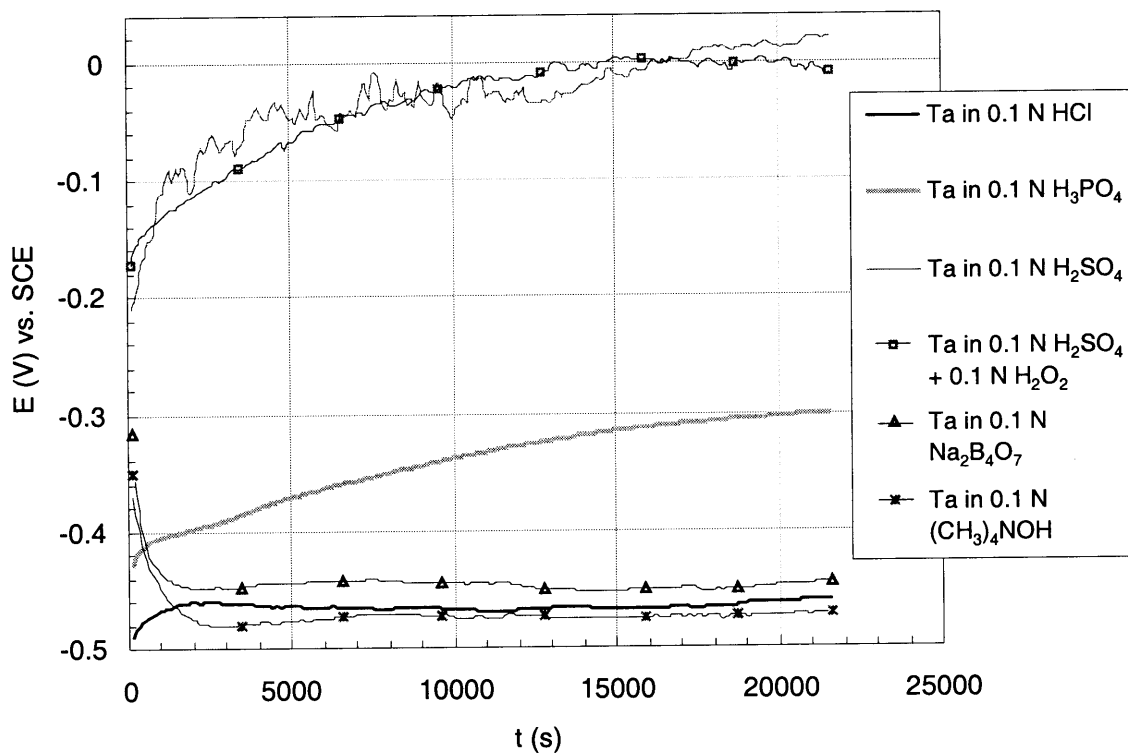
Figure 4.3.4a Open circuit potential values for Ta in HCl, H_3PO_4, H_2SO_4, $H_2SO_4 + H_2O_2$, $Na_2B_4O_7$, and $(CH_3)_4NOH$
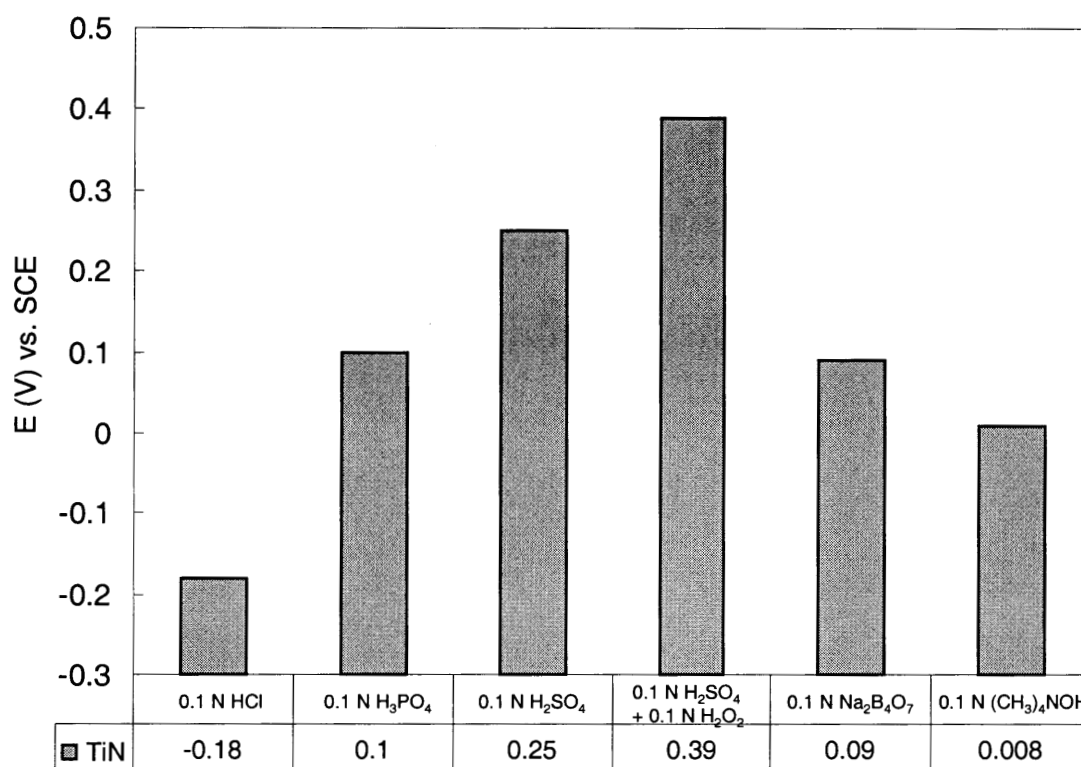
	0.1 N HCl	0.1 N H$_3$PO$_4$	0.1 N H$_2$SO$_4$	0.1 N H$_2$SO$_4$ + 0.1 N H$_2$O$_2$	0.1 N Na$_2$B$_4$O$_7$	0.1 N (CH$_3$)$_4$NOH
Ta	-0.459	-0.3	0.02	-0.009	-0.444	-0.472
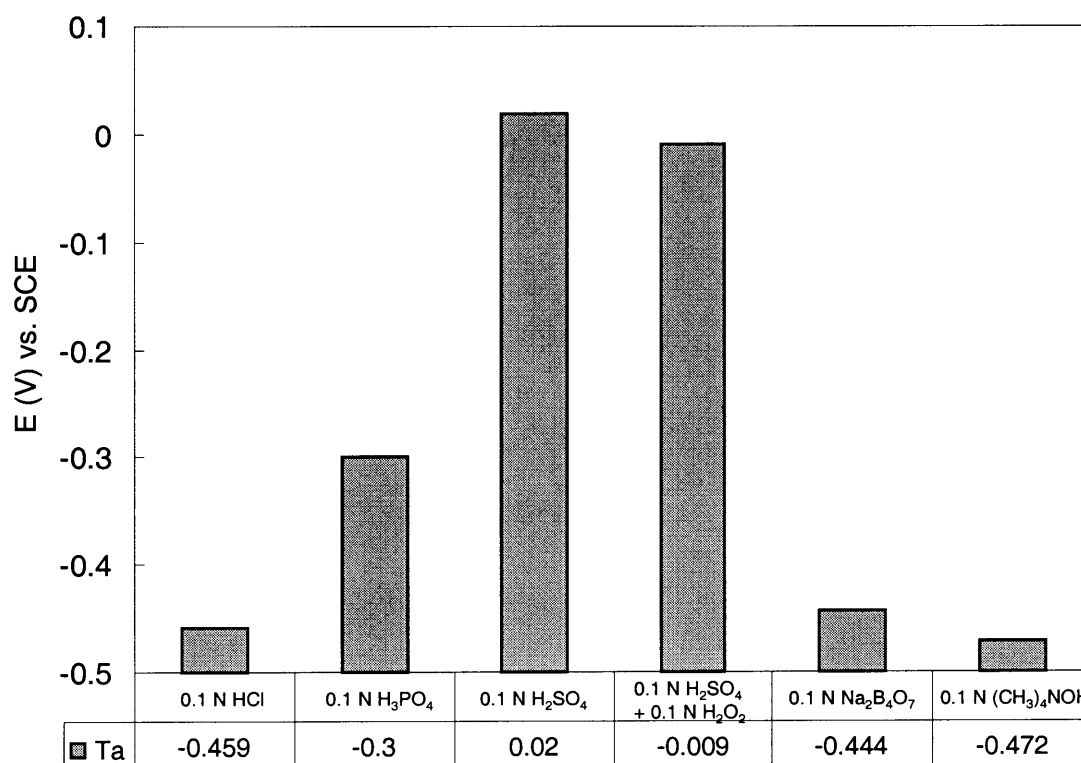
Figure 4.3.4b Potential values for Ta in HCl, H$_3$PO$_4$, H$_2$SO$_4$, H$_2$SO$_4$ + H$_2$O$_2$, Na$_2$B$_4$O$_7$, and (CH$_3$)$_4$NOH
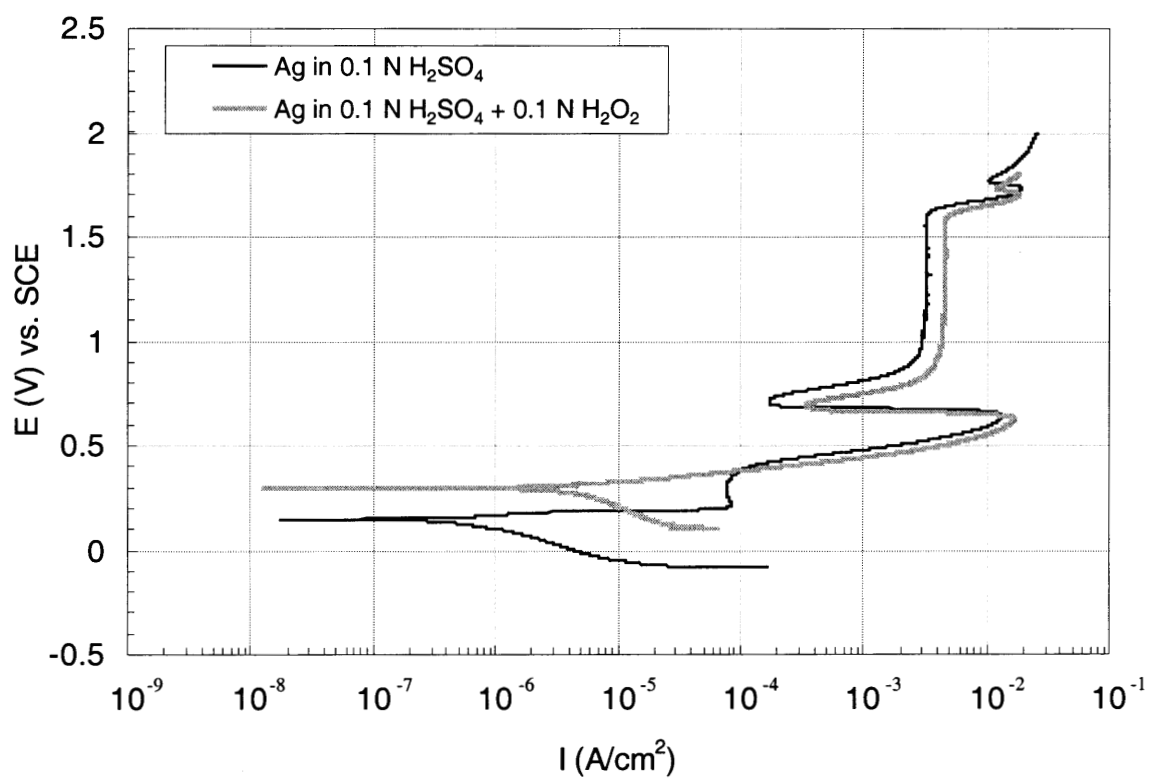
Figure 4.4.1a Effect of oxidizer solutions on Ag electrode
Scan rate: 2 mV/sec
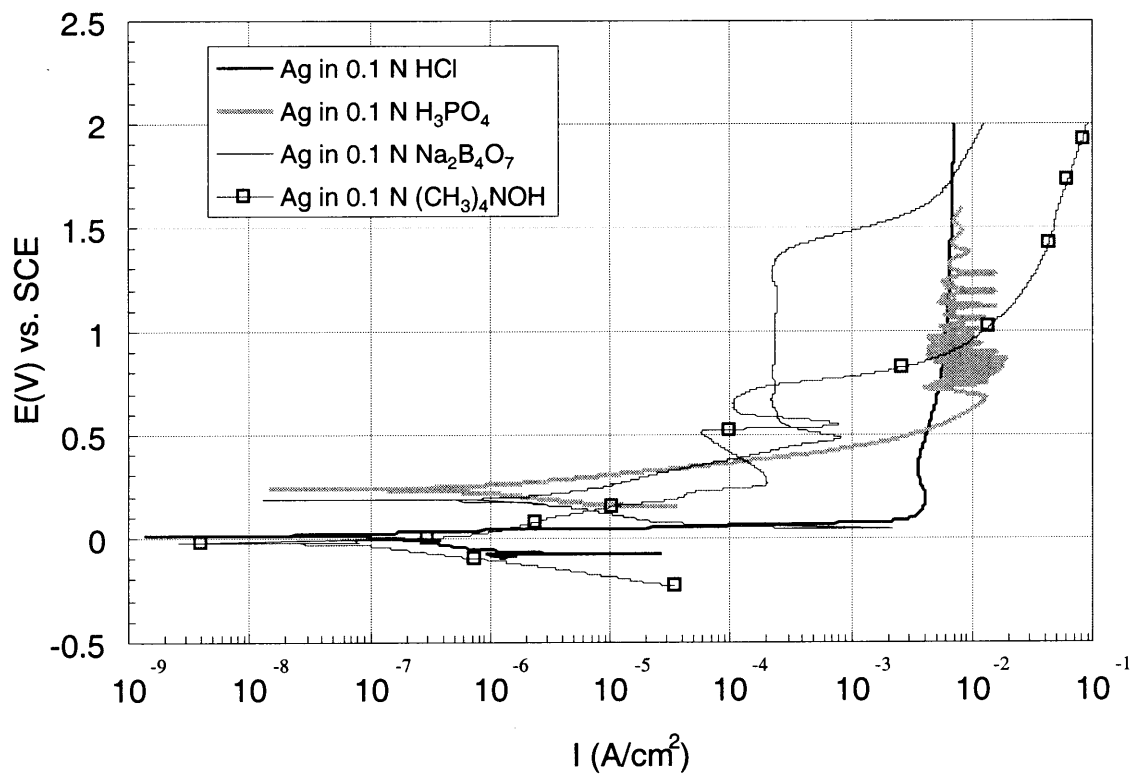
Figure 4.4.1b Effect of non-oxidizer solutions on Ag electrode
Scan rate: 2mV/sec

In these solutions, Ag shows active, active-passive, and passive behavior. In HCl, Ag reaches $I_{critical}$ of 5 x 10^{-2} A/cm^2 at 0.2 V. The active-passive behavior is observed between 0.2 and 3.5 V. In H_3PO_4, oscillations are observed above 0.75 V in the passive region. In $Na_2B_4O_7$, the current density value in the passive region is at 3 x 10^{-4} A/cm^2 in the range of potentials between 0.6 and 1.3 V. In $(CH_3)_4NOH$, there are two peaks present before reaching the transpassive region. However, there is no passive region present, therefore Ag is active.

4.4.2 TiN

Figure 4.4.2a shows the anodic polarization curves of TiN immersed 0.1 N H_2SO_4 and in 0.1 N H_2SO_4 + 0.1 N H_2O_2. The behavior of TiN in both solutions is similar to each other. In both curves, the passive state start at approximately 2 x 10^{-6} A/cm^2, but in a range of potentials between 0.2 and 1.0 V for H_2SO_4, and 0.5 to 0.75 V for H_2SO_4 + H_2O_2.

Figure 4.4.2b shows the anodic polarization curves of TiN immersed in 0.1 N HCl, 0.1 N H_3PO_4, 0.1 N $Na_2B_4O_7$, and 0.1 N $(CH_3)_4NOH$. TiN reaches $I_{critical}$ of 3 x 10^{-5} A/cm^2 at 0.15 V. In HCl, the current in the passive region starts at 3 x 10^{-5} A/cm^2 and at a potential value of 0.25 V. In H_3PO_4, $I_{critical}$ is 8 x 10^{-6} A/cm^2 at 0.2 V. The current in the passive region is approximately 3 x 10^{-6} A/cm^2 at the potential value of 0.3 V. In $Na_2B_4O_7$, TiN shows passive behavior at the current density value of 2 x 10^{-6} A/cm^2. In $(CH_3)_4NOH$, active-passive behavior is observed. The critical passivation current is approximately 2 x10^{-6} A/cm^2 at 0.25 V. Before reaching the transpassive region a relatively narrow passivation region is observed.

Figure 4.4.2a Effect of oxidizer solutions on TiN electrode
Scan rate: 2mV/sec

Figure 4.4.2b Effect of non-oxidizer solutions on TiN electrode
Scan rate: 2mV/sec

4.4.3 Ag/TiN

Figure 4.4.3a shows the anodic polarization curves of Ag/TiN immersed in 0.1 N H_2SO_4 and in 0.1 N H_2SO_4 + 0.1 N H_2O_2. Ag/TiN reaches $I_{critical}$ value of 3 x 10^{-3} A/cm^2 for H_2SO_4 and 7 x 10^{-3} A/cm^2 for H_2SO_4 + H_2O_2, at approximately 0.6 V for both curves. A decrease in current density is observed between 0.7 and 0.9 V, which corresponds to the active-passive behavior in both cases.

Figure 4.4.3b shows the anodic polarization curves of Ag/TiN immersed in 0.1 N HCl, 0.1 N H_3PO_4, 0.1 N $Na_2B_4O_7$, and 0.1 N $(CH_3)_4NOH$. In 0.1 N HCl a decrease in current density is observed between 0.3 and 0.9 V, which corresponds to the active-passive behavior. similar situation is observed for H_3PO_4. In $Na_2B_4O_7$, Ag /TiN starts its passive behavior at the current density value of 4 x 10^{-7} A/cm^2, and at approximately 0.4 V. In $(CH_3)_4NOH$, the shape of the polarization curve for Ag/TiN indicates the presence of the passive region.

4.4.4 Ta

Figure 4.4.4a shows the anodic polarization curves of Ta immersed 0.1 N H_2SO_4 and in 0.1 N H_2SO_4 + 0.1 N H_2O_2. The passive current remains in 2 x 10^{-5} A/cm^2, for a wide range of potentials between –0.2 to 1.6 V for H_2SO_4 and 0 to 1.6 V for H_2SO_4 + H_2O_2.

Figure 4.4.4b shows the anodic polarization curves of Ta in 0.1 N HCl, 0.1 N H_3PO_4, 0.1 N $Na_2B_4O_7$, and 0.1 N $(CH_3)_4NOH$. The values for the passive current density for all the solutions in this graph are between 10^{-4} and 10^{-5} A/cm^2. A region that could be associated with the transformation of the passive film is reached at high values of potential for HCl and H_3PO_4, while this zone start at approximately 1.0 V for $Na_2B_4O_7$ and 0.6 V for $(CH_3)_4NOH$.
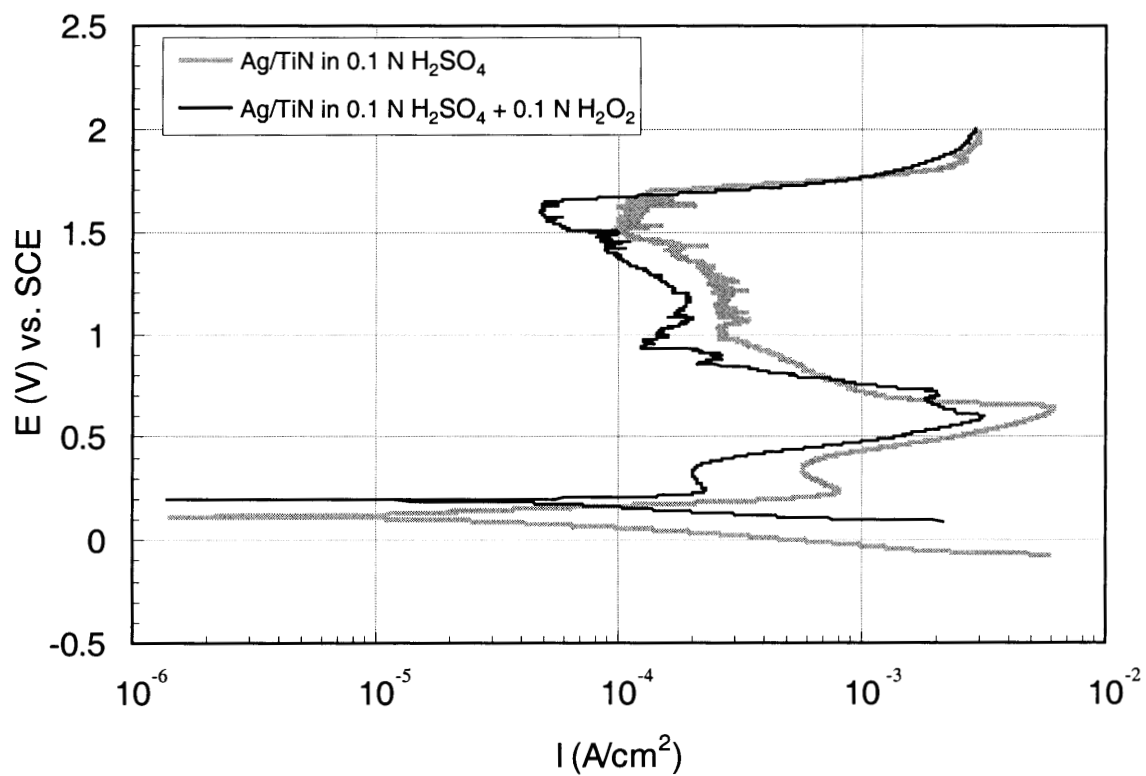
Figure 4.4.3a Effect of oxidizer solutions on Ag/TiN electrode
Scan rate: 2 mV/sec

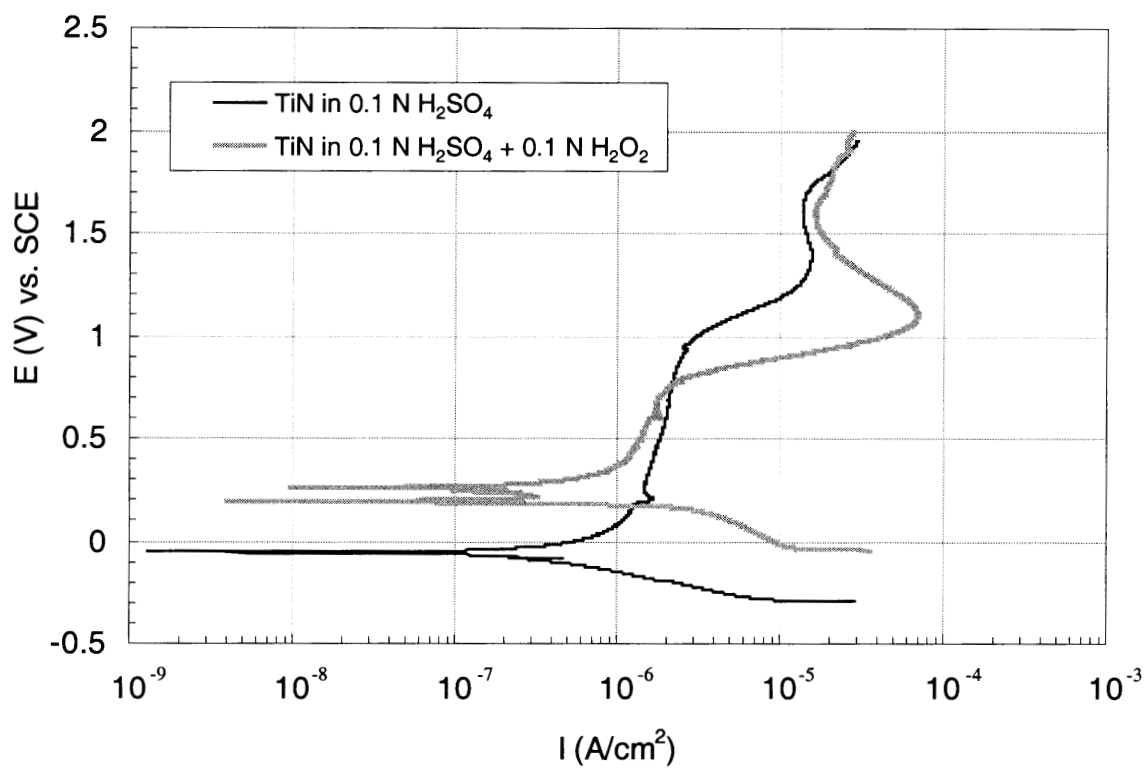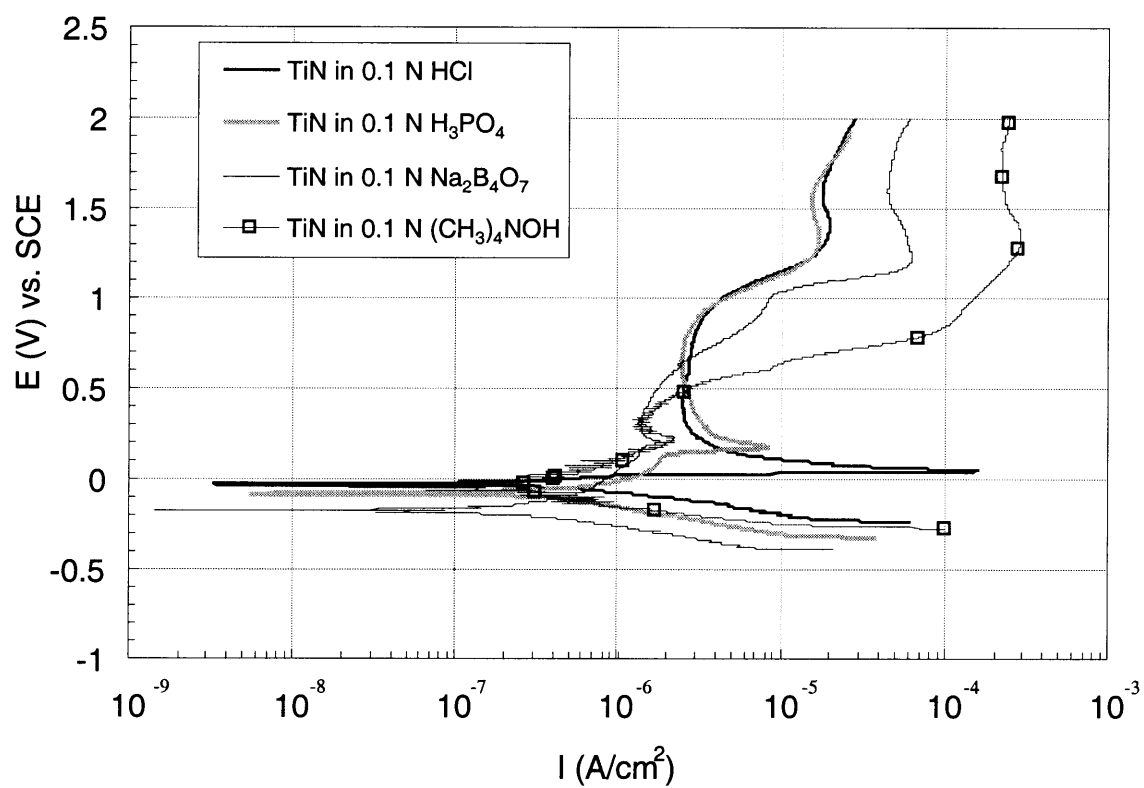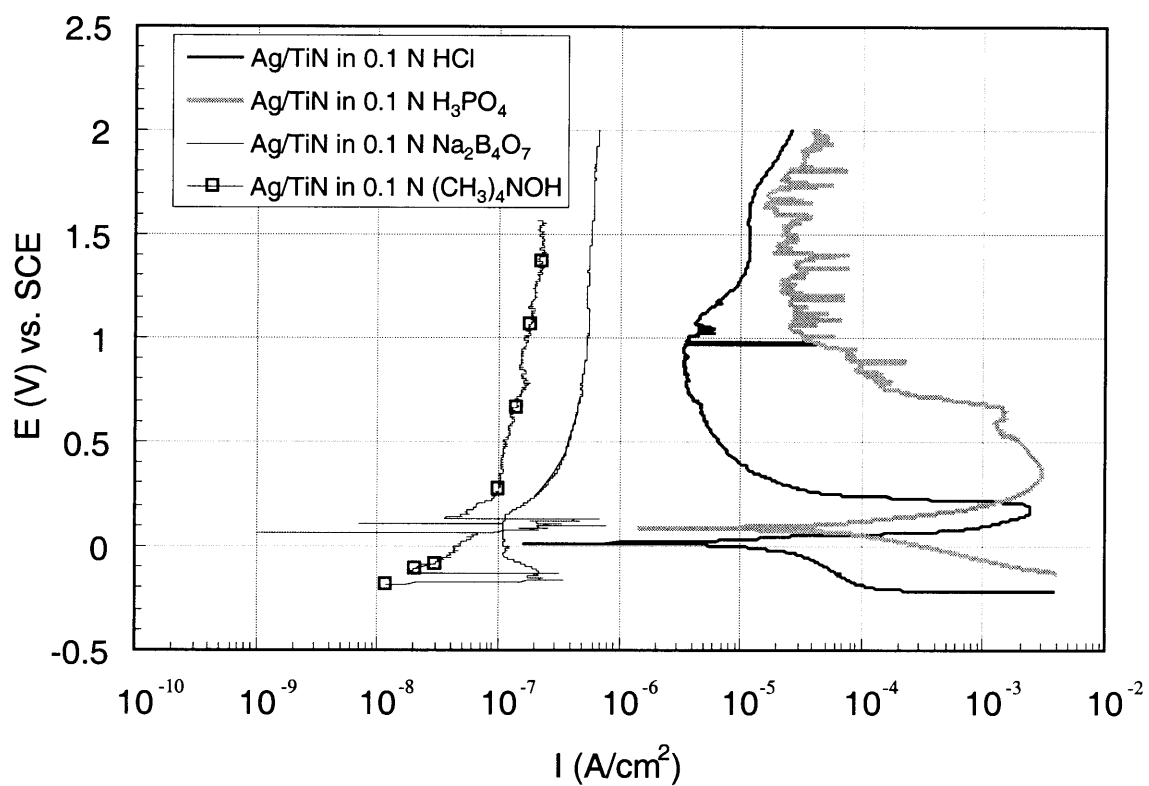Figure 4.4.3b Effect of non-oxidizer solutions on Ag/TiN electrode
Scan rate: 2 mV/sec
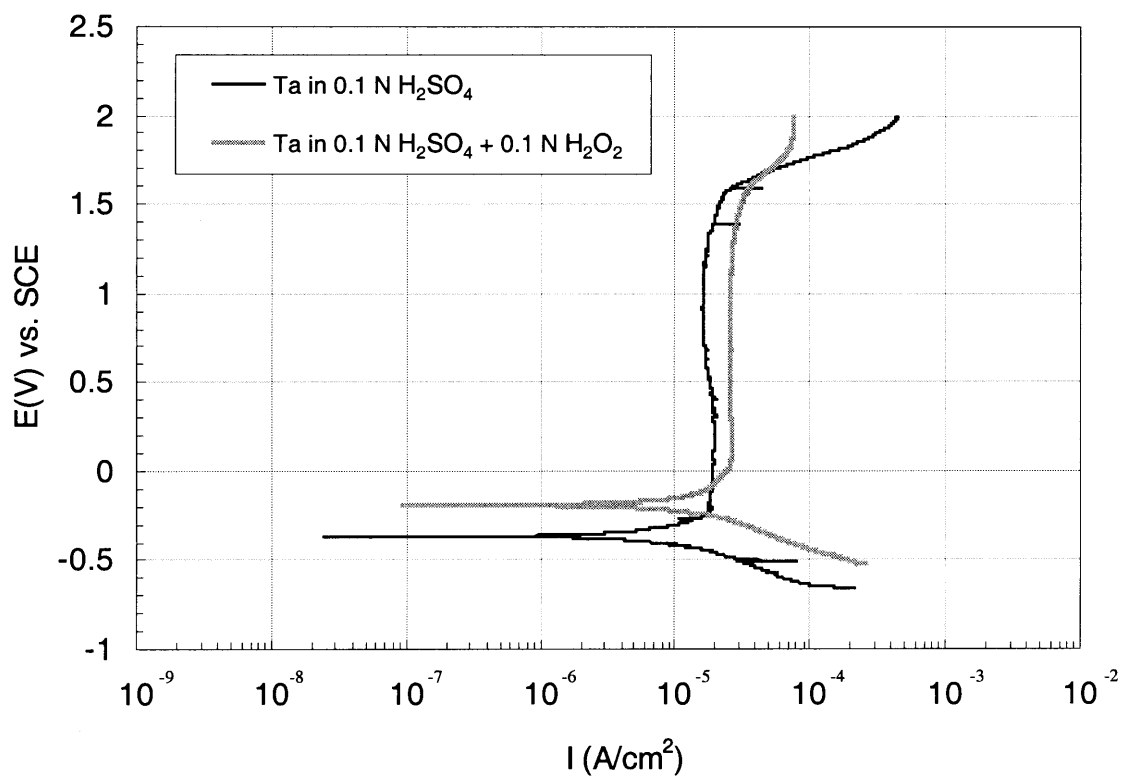
Figure 4.4.4a Effect of oxidizer solutions on Ta electrode
Scan rate: 2 mV/sec
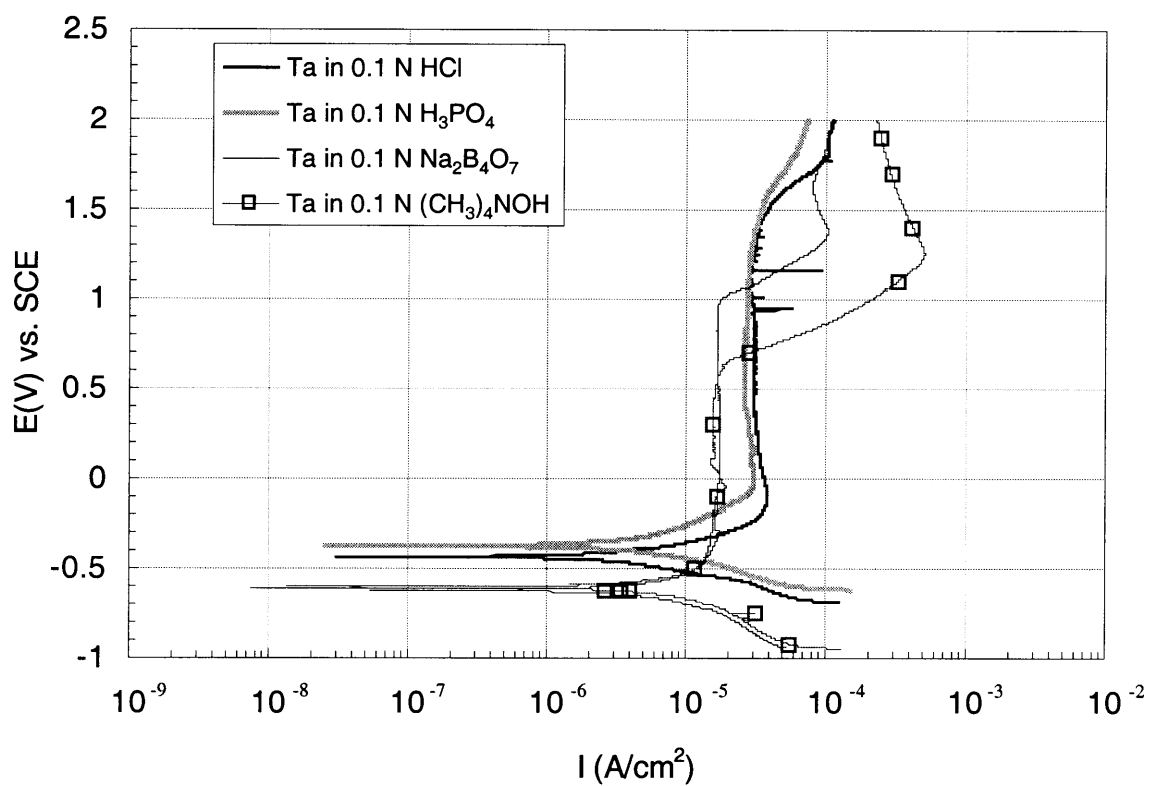
Figure 4.4.4b Effect of non-oxidizer solutions on Ta electrode
Scan rate: 2 mV/sec

4.5 Corrosion Rate Measurements

Corrosion rates, in terms of penetration, were determine from the Tafel slopes of the polarization curves (Figures 4.1.1.1, 4.1.1.2a, 4.1.1.3a, 4.1.1.4a, 4.1.1.4b, 4.1.1.4c, 4.1.1.4d, 4.1.1.5, 4.1.1.6a). The following equation was used to calculate corrosion rate in A/cm^2:

$$r = \frac{I_{corr} \cdot a}{n \cdot F}$$

where

r = corrosion rate

I_{corr} = corrosion current

a = atomic weight

n = number of equivalents exchanged

F = Faraday's constant

For corrosion rates in mils per year (mpy) the equation listed below was used:

$$r = 0.129 \times \frac{I_{corr} \cdot a}{n \cdot D}$$

where

D = density

Table 4.5 shows the corrosion rate values for Ag, TiN, Ag/TiN and Ta in 0.01 N HCl, 0.1 N HCl, 0.1 N H_3PO_4, 0.1 N H_2SO_4, 0.1 N H_2SO_4 + 0.1 N H_2O_2, 0.1 N $Na_2B_4O_7$, and 0.1 N $(CH_3)_4NOH$.

Table 4.1 Corrosion rates for Ag, TiN, Ag/TiN, and Ta in HCl, H_3PO_4, H_2SO_4, H_2SO_4 + H_2O_2, $Na_2B_4O_7$, and $(CH_3)_4NOH$.

Electrode	Solution	I_{corr} (A/cm^2)	I_{corr} (mpy)
Ag	0.01 N HCl	2.8 x 10^{-7}	332.1
TiN	0.01 N HCl	6.6 x 10^{-11}	0.16
Ta	0.01 N HCl	5.2 x 10^{-10}	0.39
Ag/TiN	0.01 N HCl	2.6 x 10^{-8}	30.4
Ag	0.1 N HCl	3.4 x 10^{-10}	0.41
TiN	0.1 N HCl	1.1 x 10^{-10}	0.26
Ta	0.1 N HCl	3.9 x 10^{-10}	0.29
Ag/TiN	0.1 N HCl	1.3 x 10^{-8}	15.8
Ag	0.1 N H_3PO_4	1.3 x 10^{-9}	1.57
TiN	0.1 N H_3PO_4	6.6 x 10^{-11}	0.16
Ta	0.1 N H_3PO_4	3.9 x 10^{-10}	0.29
Ag/TiN	0.1 N H_3PO_4	9.2 x 10^{-8}	109.7
Ag	0.1 N H_2SO_4	6.4 x 10^{-10}	0.76
TiN	0.1 N H_2SO_4	5.1 x 10^{-11}	0.12
Ta	0.1 N H_2SO_4	6.3 x 10^{-10}	0.47
Ag/TiN	0.1 N H_2SO_4	1.4 x 10^{-7}	161.55
Ag	0.1 N H_2SO_4 + 0.1 N H_2O_2	7.1 x 10^{-9}	8.39
TiN	0.1 N H_2SO_4 + 0.1 N H_2O_2	7.7 x 10^{-11}	0.18
Ta	0.1 N H_2SO_4 + 0.1 N H_2O_2	1.6 x 10^{-9}	1.21
Ag/TiN	0.1 N H_2SO_4 + 0.1 N H_2O_2	7.5 x 10^{-8}	89.0
Ag	0.1 N $Na_2B_4O_7$	6.1 x 10^{-9}	7.28
TiN	0.1 N $Na_2B_4O_7$	3.4 x 10^{-11}	0.08
Ta	0.1 N $Na_2B_4O_7$	4.3 x 10^{-10}	0.32
Ag/TiN	0.1 N $Na_2B_4O_7$	2.5 x 10^{-10}	0.30
Ag	0.1 N $(CH_3)_4NOH$	6.3 x 10^{-10}	0.75
TiN	0.1 N $(CH_3)_4NOH$	2.2 x 10^{-10}	0.52
Ta	0.1 N $(CH_3)_4NOH$	5.1 x 10^{-10}	0.38
Ag/TiN	0.1 N $(CH_3)_4NOH$	2.3 x 10^{-10}	0.27

The highest corrosion rate was found for Ag in 0.01 N HCl, indicating unacceptable corrosion resistance of this metal [24]. Also, Ag/TiN has relatively high corrosion rates in 0.01 N HCl, 0.1 N HCl, 0.1 N H_3PO_4, 0.1 N H_2SO_4, and 0.1 N H_2SO_4 + 0.1 N H_2O_2, indicating poor corrosion resistance of this thin film in the above solutions. However, Ag and Ag/TiN have relatively low corrosion rates in 0.1 N $Na_2B_4O_7$ and 0.1 N $(CH_3)_4NOH$. This could be associated with the formation of a protective passive film on the specimen surfaces. According to the Pourbaix diagram for Ag, at pH between 9.5 and 14 Ag is immune or forms Ag_2O. TiN and Ta have low values of corrosion rate in all the investigated solutions. This indicates that TiN and Ta exhibit good corrosion resistance. According to the Pourbaix diagrams for Ta and Ti [11], these metals show a wide region of passivity. Therefore, the thermodynamic data may explain why Ta and TiN show a good corrosion resistance.

Chapter 5
Conclusions

:

- Based on the potentiodynamic experiments, Ag thin films dissolve in HCl, H_3PO_4, H_2SO_4, and $H_2SO_4 + H_2O_2$. These results indicate that Ag thin films are active.

- Ag thin films in $Na_2B_4O_7$ and in $(CH_3)_4NOH$ passivate. Indicating their corrosion resistance in these solutions.

- The shape of the anodic polarization curves for Ag in H_2SO_4, and in $H_2SO_4 + H_2O_2$ are similar to each other. This indicates that there is no effect of H_2O_2 on the corrosion behavior of Ag in H_2SO_4.

- Ag shows relatively high current values in the passive region in HCl and in H_3PO_4. This indicates mechanical passivation of Ag.

- In $Na_2B_4O_7$ current values of Ag are low in the passive region. This indicates good resistivity of Ag in this solution.

Chapter 6

References

1. Manepalli R., Kohl P.A. and Bidstrup-Allen S. A., High conductivity silver metallization for advanced interconnects. *Electrochemical Society Proceedings*. Vol. 97-31, pp. 211-217, 1997.

2. Schaffer J. P., Saxena A., Antolovich S. D., Sanders T. H. and Warner S. B., *The Science and Design of Engineering Materials*. McGraw-Hill, 2nd Edition, 1999.

3. Harper C. A. and Sampson R. M., *Electronic Materials and Processes Handbook*. McGraw-Hill, 2nd Edition, pp. 5.17-5.20, 1994.

4. Kirk Othmer, *Encyclopedia of Chemical Technology*. John Wiley & Sons, 3rd Edition, 1984.

5. Sneed M. C., Maynard J. L. and Brasted R. C., *Comprehensive Inorganic Chemistry*. D. Van Nostrand Company, Inc., Vol. 2, pp. 115-183, 1973.

6. *The New Encyclopedia Britannica*. Encyclopedia Britannica, 15th Edition, 1990.

7. Comprehensive Inorganic Chemistry. Pergamon Press Ltd., Vol. 3, 1st Edition, 1973.

8. *CRC Handbook of Chemistry and Physics*. CRC Press, 71st Edition, 1991.

9. Heslop R. B. & Jones K., *Inorganic Chemistry*. Elsevier Scientific Publishing Co., p. 725, 1976.

10. Graedel T. E., Corrosion mechanisms for silver exposed to the atmosphere, *Journal of the Electrochemical Society*. Vol. 139 (7), pp. 1963-1970, 1992.

11. Pourbaix *M., Atlas of Electrochemical Equilibria in Aqueous Solution*. Pergamon Press. 1966.

12. Wang S., Raaijmakers I., Burrow B. J., Suthar S., Redkar S., and Kim K., Reactively sputtered TiN as a diffusion barrier between Cu and Si. *Journal of Electrochemical Society.* Vol. 68 (11), pp. 5176-5187, 1990.

13. *CRC Handbook of Metal Etchants.* CRC Press, 71st Edition, 1991.

14. Chatterjee S., Sudarshan T. S., and Chandrashekhar S., Modelling and experimental studies of properties of TiN coatings. *Journal of Materials Science.* Vol. 27, pp. 1989-2006, 1993.

15. Powel R. A., and Rossnagel S., *PVD for Microelectronics: Sputter Deposition Applied to Semiconductor Manufacturing.* Academic Press, p. 313-323, 1999.

16. Kodas T.T. and Hampden-Smith M. J., *The Chemistry of Metal CVD.* VCH Publishers Inc., pp. 24-338, 1994.

17. Wang M. T., Lin Y. C., and Chen M. C., Barrier properties of very thin Ta and TaN layers against copper diffusion. *Journal of Electrochemical Society.* Vol. 145 (7), pp. 2538-2545, 1998.

18. Chang C. Y. and Sze S. M., *ULSI Technology.* McGraw-Hill Co. Inc., pp. 389-393, 1996.

19. Lee M. K., Wang H. D., and Wang J. J., A Cu seed layer for Cu deposition on silicon, *Solid-State Electronics.* Vol. 41, pp. 695-702, 1997.

20. Dubin V. M., Shacham-Diamand Y., Zhao B., Vasudev P. K., and Ting C. H., Selective and blanket electroless copper deposition for ultra-large scale integration. *Journal of Electrochemical Society.* Vol 144 (7), pp. 898-908, 1997.

21. Brewster R. Q., *Organic Chemistry.* Prentice Hall, Inc., 2nd Edition, 1969.

22. Jones D. A., *Principles and Prevention of Corrosion*, Prentice Hall, Inc., 2nd Edition, 1996.

23. Wranglen, G. *An Introduction to Corrosion and Protection of Metals.* Chapman and Hall, 1985.

24. Fontana M. G., *Corrosion Engineering.* McGraw-Hill, 3rd Edition, 1986.